MASTER

Enhanced Heat Transfer by Adaptive Flow Reorientation Using a Feedback Control Strategy

van der Struijk, Anton A.L.M.

Award date:
2022

EINDHOVEN UNIVERSITY OF TECHNOLOGY
Department of Mechanical Engineering
Dynamics and Control Section

Enhanced Heat Transfer by Adaptive Flow Reorientation Using a Feedback Control Strategy

Master thesis

A.A.L.M. van der Struijk (1257528)

DC 2022.096

Coaches:
dr. ir. E. Steur
dr. ir. M.F.M. Speetjens
ir. R. Lensvelt

Supervisor:
prof. dr. ir. N. van de Wouw

Additional MSc Committee members:
dr. D.J. Guerreiro Tomé Antunes

This report was made in accordance with the TU/e Code of Scientific Conduct for the Master thesis.

Eindhoven, December 7, 2022

Abstract

Fast transport of heat in a fluid to achieve thermal homogenization is desired in a large variety of industries, such as food processing and geothermal sites. Conventional approaches to obtain a homogeneous temperature field rely on periodic reorientation schemes, which are specifically designed for efficient fluid mixing. However, efficient mixing does not automatically yield optimal heat transfer. In the case of heat transfer, it is required to find the optimal balance between fast increase of the total energy content and fast homogenization of the internal temperature distribution. The 2D Rotated Arc Mixer (RAM) is adopted to study heat transfer governed by advective and diffusive heat transfer. Different stirring motions can be introduced in the 2D RAM to generate advection and enhance heat transfer.

A prior numerical study reveals that an adaptive reorientation scheme can substantially accelerate the heating compared to conventional time-periodic reorientation designed for efficient mixing. In this thesis, the development of control strategies to accomplish a homogeneous temperature field as fast as possible is continued. Simulations are performed to investigate the effect of the cost function, activation time, and horizon on the performance of an MPC controller. From the simulations, it follows that the cost function is essential for a good performance of the MPC algorithm. When only one circulation direction is possible in the RAM, the L1-norm of the temperature would be the best option for the cost function, whereas the L2-norm of the temperature would be the best cost function when two directions of rotation are possible. The optimal activation time depends on several parameters and cannot be determined for a specific case. Moreover, the simulations show that it is beneficial to use a large horizon in the MPC controller since a homogeneous temperature field is obtained faster using a larger horizon. Simulations also show the potential of using other methods to further improve the performance of the algorithm. However, further experimental research is required to elaborate on these methods and to draw conclusions from them.

Preface

This master thesis marks the last step in my life as a Mechanical Engineering student at the Eindhoven University of Technology. In the last year, I got the opportunity to work on the development of a feedback control strategy for improving heat transfer, which is relevant to several engineering applications. First, I want to thank the people that helped me to get to the final results.

During the project, there were many moments I got stuck or needed help. Ruud Lensvelt was luckily often available to answer questions via e-mail or in a short Teams meeting. His support helped me to improve the quality of the project. Once in two weeks, also Erik Steur and Michel Speetjens were present to help me and discuss the progress of my project. You provided me with useful feedback and new ideas in these meetings, which kept me motivated to improve my work. Moreover, your criticism showed me different points of view, which encouraged me to critically look at my work. In addition, I would like to thank Nathan van de Wouw for his support during the meetings we had every six weeks. Your insights were very helpful for the project.

Despite working on my own research and gaining a lot of knowledge, it was a challenging and hard period for me. When following regular courses, you have a lot of contact with fellow students. When working on your graduation project, on the other hand, you are really working on your own project without much contact with others. Working on my thesis in the library and in SEL/SOL kept me motivated. Moreover, this study showed me that research is accompanied by setbacks. You have to take those setbacks as opportunities to grow as an engineer.

Last but not least, I want to thank my family and friends. They were always willing to listen to me and help me when needed. Without their support, I could not have delivered this work.

Anton van der Struijk
Boxtel, November 2022

Contents

Nomenclature

Abbreviations

ADE	Advection-diffusion equation
CEC	Certainty equivalent control
FDM	Finite difference method
FEM	Finite element method
FVM	Finite volume method
MPC	Model predictive control
RAM	Rotated arc mixer

Groups, algebras, and sets

$\mathbb{R}$	The set of real numbers
W	Convex set

Roman symbols

$\mathbf{A}$	Discrete matrix approximation of the advection-diffusion operator
A	Area
$A_{T\sigma}$	Performance indicator
$\mathbf{B}$	Input matrix
c	Control horizon
c_p	Specific heat capacity
E	Energy
$\mathbf{e}_\theta$	Unit vector in azimuthal direction
$\mathbf{F}$	State matrix
H	Horizon
J	Cost function
k	Aperture number
M	Number of modes on the computational grid
m	Specific eigenmode
N	Number of apertures
N_r	Number of elements in radial direction
N_θ	Number of elements in angular direction
$\mathbf{n}$	Normal vector
n	Discrete time step
P	Pressure
p	Prediction horizon
Pe	Péclet number

$\mathbf{Q}$	State cost matrix
Q	Amount of modes after truncation
Q_f	Final state cost matrix
$\mathbf{R}$	Rotation matrix on the computational grid
r	Radial direction in polar coordinates
Re	Real number
Re	Reynolds number
s	Number of subsystems
Sr	Strouhal number
T	Temperature
$\mathbf{T}$	Nodal temperature value vector
T_0	Initial temperature
T_∞	Boundary temperature
$\hat{T}$	Temperature approximation
$\bar{T}$	Average temperature
$\tilde{T}$	Transient temperature
T^*	Average dimensionless temperature
T'	Temperature heterogeneity
t	Global time
t_ϵ	Transient time
$\mathbf{U}$	Evolution matrix
U	Azimuthal velocity of the apertures
u	Discrete control action
$\mathbf{V}$	Eigenvector matrix
V	Volume
$\mathbf{v}$	Fluid velocity
w	Time-varying vector
$\mathbf{X}$	Computational grid
$\mathbf{x}$	Position/state vector
$\mathbf{z}$	Control input

Greek symbols

α	Thermal diffusivity
$\boldsymbol{\alpha}_m$	Expansion coefficient mapped on computational grid
α_m	Expansion coefficient
β	Performance indicator
Γ	Boundary of the fluid domain of the 2D RAM
γ	Weighting factor
Δ	Arc length
Δt	Difference in t
ϵ	Cost
ζ	Performance indicator
Θ	Angular offset
θ	Angular direction in polar coordinates
κ	Performance indicator
Λ	Eigenvalue matrix
λ	Eigenvalue
μ	Weighting factor
ν	Kinematic viscosity

$\boldsymbol{\xi}$	Co-state
ρ	Density
σ	Standard deviation of fluid temperature
τ	Aperture activation time
τ_m	Characteristic time scale
τ_v	Viscous time scale
ϕ	Eigenvector
χ	Performance indicator
Ω	Angular velocity
ω	Circulation direction

Other symbols

$\mathcal{D}$	Circular domain of the 2D RAM
$\partial\mathcal{D}$	Boundary of the fluid domain of the 2D RAM
$\mathcal{R}$	Rotation matrix
$\mathcal{U}$	Reorientation scheme
$\mathcal{W}$	Input set

Subscripts and superscripts

$\hat{(\cdot)}$	Approximate variable
$\bar{(\cdot)}$	Mean value
$\tilde{(\cdot)}$	Transient value
$\check{(\cdot)}$	Normalized value
$(\cdot)^\top$	Transpose

Chapter 1

Introduction

1.1 Fluid stirring and heating

Stirring and mixing of scalars (e.g., heat or chemicals) by fluid flow plays an important role in many industrial applications of sizes extending from micrometers to hundreds of kilometers [1]. One application can be found in the thermal management of power electronics to maintain optimal operating temperatures. Cooling of computer hardware has been one of the central issues concerning computer technologies for many decades, since it is often the limiting constraint for performance [2, 3]. Successful flow control can prove beneficial to improve heat transfer, thereby allowing further improvements in speed, efficiency, and reliability in electronics. Furthermore, several applications can be found in microfluidic systems. For example, applications in the field of biomedical diagnostics and drug development, which are widely used in the food and chemical industries [4, 5]. In the field of subsurface engineering, some practical applications include the extraction of geothermal energy or minerals [6], remediation of contaminated groundwater [7], and localization of pollutants for in-situ remediation and recovery [8]. Other relevant engineering applications can be found in polymer extrusion, glass manufacturing, tailings, and paper-making [9, 10].

Some examples in nature include magma transport in the Earth's mantle and dispersion of hydrocarbons within fractured rock [1]. An intriguing aspect of natural flows is their wide range of scales, both in space and time. At the large end of the scale are huge weather systems and the oceanic conveyor belt, both tens of thousands of kilometers in size [11]. Figure 1.1 shows some areas of application.

Enhancing transport of scalars to improve the mixing/heating rate will be beneficial to a large variety of industries. As for fluid flows, an important area of research is the so-called laminar regime, which is characterized by its ordered stream and deterministic nature. Laminar conditions preclude mixing by turbulence. Under these conditions mixing of scalars may be accomplished through chaotic advection [1]. To achieve chaotic advection, scalar transport is influenced by repetitive changes, often periodic reorientations, to the flow based on mixing principles described in [12]. Conventional approaches to obtain a homogeneous scalar field rely on these periodic reorientation schemes, which are specifically designed for efficient fluid mixing. In the case of heat transfer, the common assumption in practice is that applying the conventional mixing approach automatically yields optimal heat transfer. This assumption does not necessarily hold, since diffusion can also play an important role in scalar transport (characterized by the Péclet number Pe). First, the relationship between fluid motion and thermal transport is highly non-trivial for heat transport by an interplay of

convection and diffusion. Moreover, heat transport will often involve exchange across system boundaries, in contrast to fluid mixing, which generically only involves transport within the system boundaries. The temperature gradient between fluid and system boundary will drive the heat transfer. It is important to refresh material near heat transfer boundaries, otherwise the temperature gradients at those boundaries lessen and heat transfer slows down [13]. Therefore, it is required to find the optimal balance between fast increase of the total energy content and fast homogenization of the internal temperature distribution. Efficient fluid mixing, on the other hand, only relies on the rapid homogenization of the scalar field. As a result, fluid mixing schemes may create a sub-optimal or even counter-productive condition for accelerated heat transfer, at least in the vicinity of the boundary [14]. The main objective of this research is therefore to develop a feedback control strategy to accomplish a homogeneous temperature field as fast as possible, considering both energizing and homogenization of the internal temperature.

1.2 Existing methods for efficient fluid mixing and heating

Recent research is directed towards improving mixing and heating further. The amount of literature about mixing is quite extensive, in contrast to the available literature about stirring and mixing of scalars. A good overview of the different techniques is given in [1] and [15]. Most techniques require detailed information about the velocity field or fluid motion. In [16], an aperiodic mixing protocol has been advocated that destroys the symmetries in the phase space by preventing the formation of unmixed zones due to island formation to achieve mixing throughout the fluid. Knowledge of these symmetries provides a basis for systematic methods for destroying islands. Moreover, from [17] it follows that aperiodicity can enhance mixing enormously. To achieve complete mixing for a flow, regular motions must be removed; procedures that achieve global chaos are therefore highly desirable. Aperiodic perturbations generate widespread chaos under conditions where periodic flows generate regular motions.

Another method to tackle the problem of efficient fluid mixing is using (approximate) dynamic programming from a switched system perspective [18]. A switched linear system is typically characterized by a finite set of linear subsystems in which the switching among

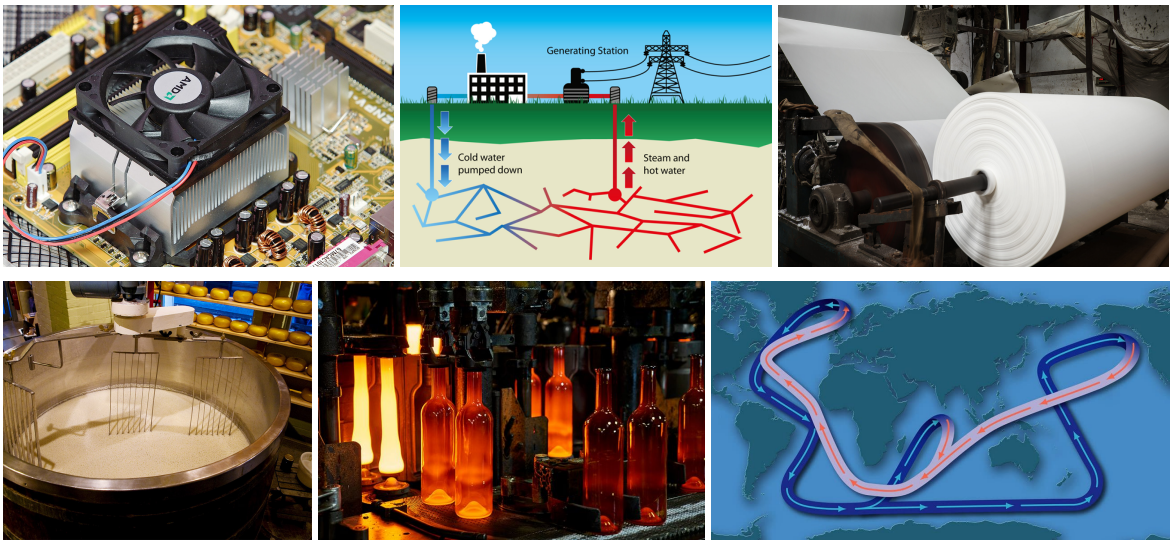

Figure 1.1: Relevant areas of application for stirring and mixing of scalars.

these subsystems is governed by a state- and/or time-dependent switching protocol. As a first step, temporal and spatial discretization is used by means of the cell-mapping method on the original infinite-dimensional fluid models to make the control problem tractable. The original mixing problem can then be formulated as an optimal control problem for a linear discrete-time switched system. A novel feedback law for mixing fluids is proposed based on suboptimal rollout policies in dynamic programming contexts. Finally, it follows that this feedback law guarantees a performance improvement over any given (open-loop) periodic mixing control.

In contrast to control strategies for mixing, literature on control strategies for maximizing heat transfer is scarce. The majority of the research on this topic is focused on scalar transport only by (chaotic) advection and is frequently limited to highly idealized configurations and/or forcing techniques with few practical applications. Several studies show that control laws and measures intended for advective transport (i.e., limit $Pe \to \infty$) may still be effective for finite Pe, addressing the effect of diffusion. For example, in [19] flow forcing optimized for advective transport worked well for $Pe \geq 10^4$, and in [20] the mix-norm was successfully applied for $Pe \sim \mathcal{O}(10^3)$. Most optimal-control approaches in existing research, however, still have two major shortcomings: limited robustness to unforeseen disturbances and omission of diffusive transport both internally and across non-adiabatic boundaries. This again motivates the development of specialized control strategies to improve advective-diffusive scalar transport in realistic flow systems with non-adiabatic boundaries.

In [21], the heat transfer enhancement within a two-rod stirring device is numerically investigated. The fluid is heated by the walls (a cylindrical tank and the rods), which are maintained at a constant temperature. Different stirring protocols are analyzed, from which it is concluded that the use of discontinuous wall rotations is necessary to promote heat transfer by chaotic advection. Thus, the stirring rods and the cylinder tank should move alternately. In this way, hot spots in the vicinity of walls are avoided. However, only open-loop control has been used in this research.

Another control strategy is adaptive reorientation of the flow by interval-wise selection of the reorientation that is predicted to yield optimal scalar transport for a future time horizon [14]. In this research, a compact model based on the spectral decomposition of the scalar evolution in the base flow is used to enable fast predictions. The study reveals that the adaptive reorientation scheme can substantially accelerate the heating compared to conventional time-periodic reorientation designed for efficient mixing. The compact model predicts the temperature one step forward in time, after which the reorientation is selected which yields optimal heat transfer. This approach can be seen as an MPC controller with a horizon of one time step. Further developments of control strategies are possible by, for example, extending the horizon. Moreover, currently the entire state is measured with a camera. In practice, it might only be possible to measure a part of the state by, e.g., a limited number of temperature sensors. This demonstrates the need to develop observers that can estimate the state from discrete sensor data.

The common goal in these applications essentially is accomplishment of maximum heat transfer between a domain boundary and a flow inside this domain via active manipulation of the flow. A flow can be manipulated in different ways, e.g., by rotating (a part of) the wall, stirring, letting the flow follow a geometric path, etc. One well-known example is stirring a fluid (e.g., soup) to boost heat transfer. Despite the different methods to manipulate a flow, in all cases the main goal is to find the best flow to accomplish a homogeneous temperature field as fast as possible.

Using control technology to yield optimal scalar transport by adaptive reorientation of the flow is not completely new. Although in the conventional method to accelerate scalar transport (open-loop) periodic mixing protocols are used, a first step using a closed-loop control strategy has been taken in [14]. Optimal control combined with a fast predictor can significantly accelerate thermal homogenization. In [14], the transient temperature is only predicted one step forward in time. Based on this temperature prediction, the optimal control action is determined. However, it might be more beneficial to predict the transient temperature some steps further away in time to determine the optimal control action.

Moreover, as discussed before, an adequate description of the control target is essential. In [21] and [22] first steps have been taken with regard to performance indicators for achieving a homogeneous temperature field as fast as possible. However, the optimal performance indicator for this problem has not yet been formulated.

When the transient temperature is predicted only one step ahead, the computational effort is low. However, the computational effort will increase rapidly when the temperature should be predicted multiple steps ahead in time. To regulate scalar transport in real time, the computational effort must remain low. Therefore, it might be required to use a reduced-order model.

1.3 Research objectives

This work adopts the 2D Rotated Arc Mixer (RAM), described in [23], as the representative configuration for in-depth analysis of scalar transport. The 2D RAM is visualized in Figure 1.2. The RAM has several control parameters to tune the flow conditions to achieve desired transport characteristics, making it flexible for applications and theoretical developments. In this research, it is assumed that the complete temperature field is available via measurements. The focus of this research will therefore be on developing a control strategy.

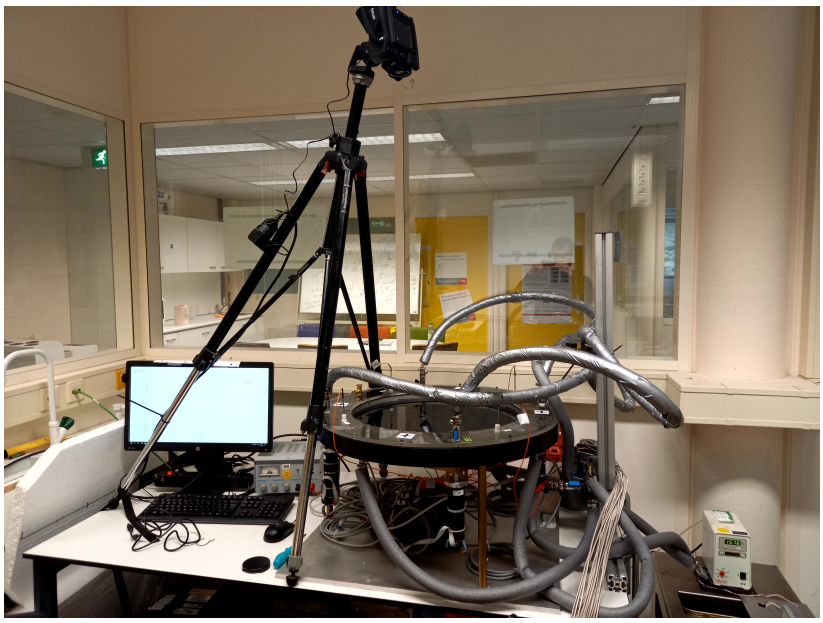

Figure 1.2: The setup with the 2D Rotated Arc Mixer. The infrared camera at the top measures the temperature field.

The main objective of this research is therefore:

Develop a full-state feedback control strategy to accomplish a homogeneous temperature field as fast as possible for the 2D RAM, in which heat transfer will take place between object and flow via controlled reorientation of the flow.

Furthermore, some subgoals have been formulated to accomplish the main goal of this research. The subgoals are discussed in the next sections.

1.3.1 Performance indicators

An adequate description of the control target is essential. It is required to find the optimal balance between fast increase of the total energy content and fast homogenization of the internal temperature distribution. The first step is to come up with a performance indicator, that reflects achieving a homogeneous temperature field as fast as possible for the 2D RAM. For example, an important question is to find the optimal error norm to minimize the error between the current temperature field and the desired temperature field. In [22], a start has been made on this subject. Relevant metrics are discussed for the global dynamics, which enables formulation of the control problem as the minimization of a dedicated cost function that naturally emerges from the dynamic analyses and adequately incorporates both processes, i.e., increasing energy content and thermal homogenization. This research builds on the work done in [21] and [22], in which several performance indicators are defined. The performance of these indicators is not yet compared in a minimization procedure of a cost function in an optimal control problem. The following subgoal is defined for development of a performance indicator:

Design a performance indicator (i.e., a cost function) that reflects attaining a homogeneous temperature field as fast as possible for the 2D RAM.

by adaptive reorientation of the flow

1.3.2 Control strategy

Conventional approaches to obtain a homogeneous temperature field rely on periodic reorientation schemes, as discussed in Section 1.1. The goal is to propose a feedback control solution that outperforms any proposed periodic protocol over a finite horizon. The adaptive reorientation scheme which maximizes heat transfer has to be found, based on intermediate temperature fields. Using this modeling perspective, suboptimal rollout policies in a dynamic programming context will be used as a starting point for the control strategy [24, 25]. Different policies will be compared, after which one policy will be chosen based on computational time and performance. In [14] a model predictive control (MPC) approach is applied using a horizon of one time step. A longer horizon will in general result in better performance, however, it also increases the computational time significantly. It is important to find a good balance between performance and computational time. The following subgoal is defined for development of the control strategy:

Design a full-state feedback controller that outperforms any proposed periodic protocol over a finite horizon.

1.3.3 Model reduction

The compact model of [14] will be used for the development of the control strategy. This model leans on the existence of a spectral decomposition of the temperature evolution into

eigenmodes, which enables simulation of the temperature evolution using matrix-vector multiplications instead of a (computationally for more expensive) time-marching scheme. The compact model in [14] reduces the computation effort dramatically, i.e., by 3-4 orders of magnitude compared to conventional time-marching.

In [14] the dedicated approach described in [26] is employed to obtain the system matrix $\mathbf{A}_1$ of the base flow and its spectral decomposition underlying the compact model. System matrix $\mathbf{A}_1$ of the base flow, however, can also be obtained using conventional FDM/FVM/FEM schemes, resulting in a more accurate system matrix of the base flow. The disadvantage of using FDM/FVM/FEM schemes is the large computational time, making it impossible to use it for the development of the control strategy.

As discussed in Section 1.3.2, it is desired to predict the temperature evolution multiple steps ahead in time. The current control scheme only requires one step ahead predictions, so the computational effort is low. However, when using an MPC approach, the number of predictions (and therefore also the computational costs) increase exponentially when more predictions are needed as illustrated in Figure 1.3. To regulate scalar transport in real time, it is important that the computational effort remains low. The required computational time, however, depends on several parameters, such as the characteristic velocity of the flow field and the radius of the domain. When using the same values as in [23], the reference time scale (i.e., the forcing period) is 625 s. However, for systems with a higher velocity and/or a smaller domain it might be required to reduce the computational costs even further.

Model reduction is a technique for obtaining a lower-dimensional approximation to a high-dimensional dynamical system. A good overview of different approximation methods is given in [27]. Gramians are important tools for system approximation and can be used to represent a quantitative measure of controllability and observability. In this research, a linear switched system is considered, which represents an important class of hybrid systems that consists of a family of linear time-invariant subsystems and a rule that orchestrates the switching between them, e.g., the adaptive reorientation scheme. Methods exist for model reduction of a hybrid system, such as LMI-based methods [28, 29], balanced truncation [30–34], and

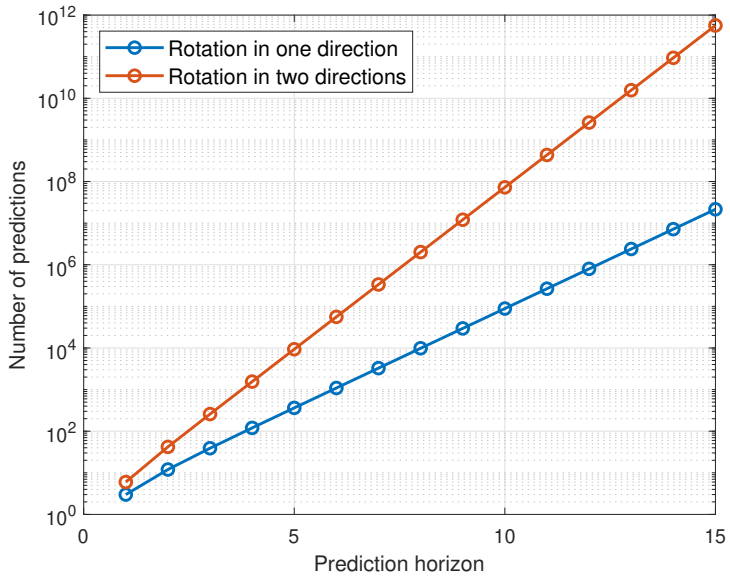

Figure 1.3: Number of predictions needed for different horizons.

moment matching [35, 36].

The following subgoal is defined for reduction of the model:

Reduce the complexity of the compact model, which approximates the dynamics of the full-order system with sufficient accuracy, to make fast predictions of the temperature evolution.

1.4 Structure of the report

This report has the following structure. The relevant background material is discussed in Chapter 2. The background material consists of the modeling of the 2D RAM, the thermal problem, switched linear systems, optimal control, and performance indicators. Chapter 3 subsequently discusses the main contributions of this research. The main contributions are the performance evaluation of the designed controller, including the effect of different performance indicators, the horizon, and the activation time on performance. In Chapter 4, some further possible improvements are proposed based on the results in Chapter 3. In this part, model reduction is discussed as well. This chapter gives motivation to further research. Finally, a conclusion and recommendations are given in Chapter 5.

Chapter 2

Mathematical preliminaries and background material

This chapter provides a review of preliminary material. Firstly, modeling of the 2D RAM is discussed. The 2D RAM can be modeled using the method described by Lensvelt *et al.* [14] and using conventional FVM schemes. The first method will be discussed in this chapter, because this model will be used for the simulations in this research. Thereafter, the control of the 2D RAM is discussed. Different types of (sub)optimal control will be elaborated upon. This will be followed by Section 2.3, in which different performance indicators are discussed and analyzed. It is essential to find a good performance indicator, which can be used as a cost function in the control algorithm. The cost function determines the choices made in the process and is crucial for good performance. Finally, the main findings of this chapter are discussed in Section 2.4.

The flow configuration in the 2D RAM, the thermal problem, and the numerical method are already extensively and well explained in the work of Lensvelt *et al.* [14], and are therefore concisely repeated in Section 2.1. Only small changes are made to these parts, which are mostly cross-references and layout-related issues.

2.1 Model of the 2D Rotated Arc Mixer

This section discusses the 2D Rotated Arc Mixer in more detail. Furthermore, the governing equations are given and it is explained how the model can be simulated numerically.

2.1.1 Flow configuration

The 2D Rotated Arc Mixer introduced in [23] will be used as the representative configuration for the analysis of heat transfer. The goal is to heat an initially cold fluid via an isothermal hot boundary by reorientating 2D flow fields.

It is assumed that the flow is laminar and incompressible. The 2D RAM consists of a disk $\mathcal{D} = \left\{(r, \theta) \in \mathbb{R}^2 \mid r \leq R, -\pi \leq \theta < \pi\right\}$ with radius R which is enclosed by a boundary $\Gamma = \partial\mathcal{D}$ as shown in Figure 2.1. Circumference Γ contains N apertures of arc length Δ which consecutively differ from each other by an angular offset $\Theta = 2\pi/N$ as illustrated in Figure 2.1a. The arc length is constrained as the apertures cannot overlap. The centerline of arc k, $1 \leq k \leq N$, is located at angle $\theta_k = (k-1)\Theta$. The flow inside the RAM can be driven by sliding wall segments along these apertures via viscous drag. Moreover, no-slip boundary

conditions assure the absence of flow at the circumference Γ. Only at an active aperture k the angular velocity ω_k drives the fluid flow inside $\mathcal{D}$ through viscous drag. These conditions can be physically realized through a motor-belt system as presented in [23]. By activating an aperture, the flow field influences heat transport through advection. This accelerates homogenization of the scalar field inside $\mathcal{D}$ compared to mere diffusive heating.

By activating the first arc (i.e., centered on the x-axis) in clockwise direction at an angular velocity Ω a steady flow $\mathbf{v}_1$ with streamline pattern following Figure 2.1b is created. This is called the *base flow* of the RAM. In this research, the 2D RAM will be simulated with a radius $R = 1$ and unit angular velocity $\Omega = 1$ without loss of generality.

The motion of the fluid can be described with the conservation laws for mass and momentum. Assuming incompressibility, laminar flow and absence of body forces other than gravity, the conservation laws can be written in non-dimensional form as

$$\boldsymbol{\nabla} \cdot \mathbf{v} = 0, \qquad Sr\frac{\partial \mathbf{v}}{\partial t} + Re\ \mathbf{v} \cdot \boldsymbol{\nabla}\mathbf{v} = -\boldsymbol{\nabla} P + \boldsymbol{\nabla}^2 \mathbf{v}, \tag{2.1}$$

with $\mathbf{v}(\mathbf{x}, t)$ the fluid velocity and $P(\mathbf{x}, t)$ the pressure in position $\mathbf{x} \in \mathcal{D}$ at time $t \geq 0$, which depends on the fluid flow. Moreover, system (2.1) is parameterized by the Strouhal number $Sr = \tau_v/\tau = R^2/\nu\tau$ and the Reynolds number $Re = UR/\nu = \Omega R^2/\nu$, with $\tau_v = R^2/\nu$ the viscous time scale, $U = \Omega R$ the azimuthal velocity of the apertures, ν the kinematic viscosity of the fluid, R the radius as in Figure 2.1a and τ the aperture activation time. The aperture activation time should not be chosen too small, since this will result in poor performance [37]. In this research, the same lower bound for τ is considered as in [22], i.e., $\tau \geq 3$. Strongly laminar conditions imply (i) a rapid response of the fluid to changes in flow forcing by the apertures (i.e., $Sr = \tau_v/\tau \ll 1$) and (ii) negligible fluid inertia (i.e., $Re \ll 1$). This implies the base flow is a steady Stokes flow symmetric about the x-axis and admitting

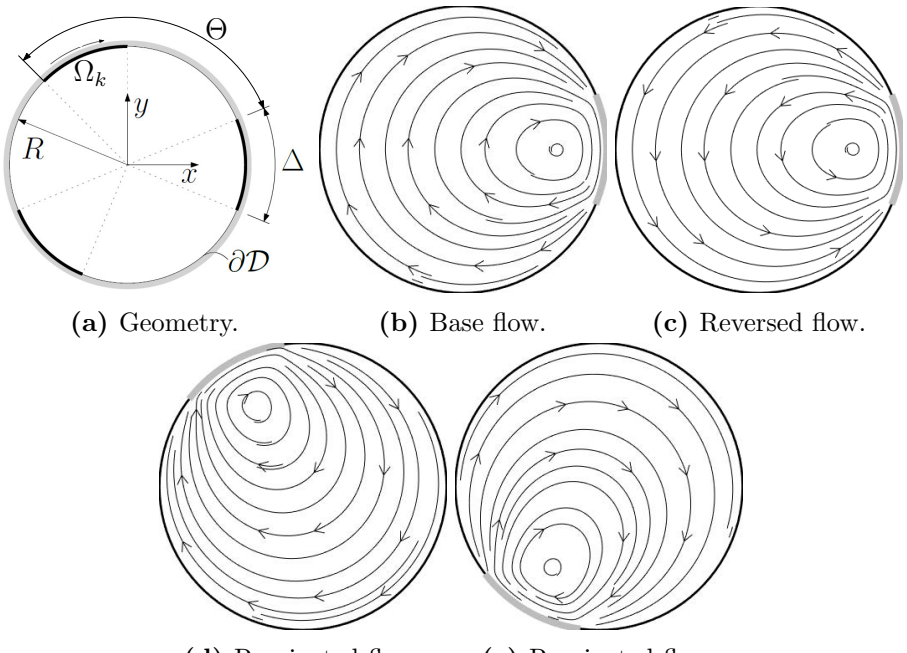

(a) Geometry. **(b)** Base flow. **(c)** Reversed flow.

(d) Reoriented flow. **(e)** Reoriented flow.

Figure 2.1: A schematic of the 2D Rotated Arc Mixer (RAM) with three apertures of arc length Δ: (a) geometry of the 2D RAM; (b) streamlines corresponding with the base flow; (c) reversed base flow; (d)-(e) reorientations of the base flow. Image taken from [14].

an analytical solution following [38]. As presented in [23], this simplifies (2.1) to

$$\boldsymbol{\nabla} \cdot \mathbf{v} = 0, \qquad -\boldsymbol{\nabla} P + \boldsymbol{\nabla}^2 \mathbf{v} = \mathbf{0}, \tag{2.2}$$

in case the fluid flow is driven by a single aperture. The corresponding initial and boundary conditions are given by

$$\mathbf{v}(\mathbf{x}, 0) = \mathbf{0}, \ \forall \ \mathbf{x} \in \mathcal{D}, \qquad \text{and} \qquad \mathbf{v}(\mathbf{x}, t) = \begin{cases} \omega \mathbf{e}_\theta & \text{if } \mathbf{x} \in \Gamma_k \\ \mathbf{0} & \text{if } \mathbf{x} \in \Gamma \setminus \Gamma_k \end{cases}, t > 0, \tag{2.3}$$

where $\Gamma_k = \{(r, \theta) \in \Gamma \mid -\Delta/2 \leq \theta - (k-1)\Theta \leq \Delta/2\}$ and $\mathbf{e}_\theta$ indicate aperture k and the unit vector in azimuthal direction, respectively. The coefficient $\omega = \pm 1$ determines the sense of circulation: clockwise (ω = -1) versus counter-clockwise (ω = 1).

The simplification to steady Stokes flow causes the aperture reorientations to carry over the flow, meaning that flow $\mathbf{v}_k$ driven by aperture k is just a reorientation of the base flow $\mathbf{v}_1$ as illustrated in Figure 2.1d-2.1e. Mathematically this can be written as

$$\mathbf{v}_k(\mathbf{x}) = \mathbf{v}_k(r, \theta) = \mathbf{v}_1(r, \theta + (k-1)\Theta) = \mathbf{v}_1(\mathcal{R}_k(\mathbf{x})), \tag{2.4}$$

where $\mathcal{R}_k$ is a rotation matrix. Moreover, it is possible to reverse the base flow by reversal of the motion of the first arc, as shown in Figure 2.1c. This yields a flow $\mathbf{v}(r, \theta) = -\mathbf{v}_1(r, \theta)$, while the streamline portrait is maintained (i.e., only the arrows change direction). For simplicity, only one aperture is activated at a time. In the case of N apertures, it means that N different flow fields can be created by activating an aperture without reversing the flows. When reversal of the flow fields is possible, $2N$ different flow fields can be created. At every time step, another aperture can be activated, resulting in another aperture-wise steady flow. As mentioned before, the strongly laminar conditions imply a rapid response of the fluid to changes in flow forcing by the apertures, meaning the acceleration stage can be neglected. So, we can assume the flow is in a piece-wise continuous steady state.

2.1.2 Thermal problem

The thermal problem can be described as heating an initially cold fluid at uniform temperature T_0 inside $\mathcal{D}$ via the hot boundary Γ with constant wall temperature $T_\infty > T_0$. The evolution of the temperature field from its non-uniform initial state towards the final homogeneous state is governed by the balance between advection and diffusion. The transport of a diffusing passive scalar field T in a velocity field $\mathbf{v}$ is described by the advection-diffusion equation (ADE):

$$\frac{\partial T}{\partial t} = -\mathbf{v} \cdot \boldsymbol{\nabla} T + \frac{1}{Pe} \boldsymbol{\nabla}^2 T, \tag{2.5}$$

where Pe is the Péclet number. The Péclet number is the ratio of timescales for diffusion and advection, $Pe = RU/\alpha$ with R the characteristic length, $U = \Omega R$ the flow velocity scale, and α the thermal diffusivity. A system with a high Péclet number indicates an advectively dominated distribution, whereas a system with a low Péclet number has a large amount of diffusion. The initial and boundary conditions corresponding with the above heating problem are $T(\mathbf{x}, 0) = T_0$ and $T(\mathbf{x}, t)|_\Gamma = T_\infty$ for all $x \in \mathcal{D}$ and $t \geq 0$. Relevant application areas typically have $Pe \sim \mathcal{O}(10^2 - 10^4)$, implying advection-dominated heat transfer yet with significant diffusion. Since diffusion is present, any initial temperature field $T(\mathbf{x}, 0)$ will eventually evolve towards the uniform final state $\lim_{t \to \infty} T(\mathbf{x}, t) = T_\infty$, even if the system is not regulated. So, $T(\mathbf{x}, t) = T_\infty$ is an asymptotically stable solution of (2.5) if diffusion

is present, as proven in [22]. Therefore, the principal goal is to find the fastest route to the uniform final state. As a result, the dynamic behavior can be entirely captured in the transient temperature

$$\tilde{T}(\mathbf{x},t) \equiv T(\mathbf{x},t) - T_\infty, \tag{2.6}$$

which is governed by the ADE

$$\frac{\partial \tilde{T}}{\partial t} = -\mathbf{v}\cdot\boldsymbol{\nabla}\tilde{T} + \frac{1}{Pe}\boldsymbol{\nabla}^2\tilde{T}, \quad \tilde{T}(\mathbf{x},0) = T_0 - T_\infty, \quad \tilde{T}(\mathbf{x},t)\mid_\Gamma = 0, \tag{2.7}$$

following from substitution of (2.6) into (2.5). The original problem is now translated into progression of the transient temperature towards the final state $\tilde{T}_\infty = 0$. Without loss of generality, the initial and boundary conditions can be set to $T_0 = 0$ and $T_\infty = 1$, which gives $\tilde{T}(\mathbf{x},0) = -1$ for the initial condition in (2.7). Using the transient temperature allows us to perform an error analysis encountered in control theory, where T_∞ is the reference signal and $\tilde{T}$ is the error signal [39].

To do fast predictions of the transient temperature, the compact model proposed in [14] has been used in this research. This compact model decomposes the temperature evolution into eigenmodes, which characterize the mixing dynamics of advected fields in flows [23]. Solutions of the ADE are expressed in terms of the exponentially decaying natural persistent patterns [26]. The temperature field for the base flow $\mathbf{v}_1$ can be decomposed into eigenmodes [23] according to

$$\tilde{T}(\mathbf{x},t) = \sum_{m=0}^{\infty} \alpha_m \phi_m(\mathbf{x}) \mathrm{e}^{\lambda_m t}, \qquad \tilde{T}(\mathbf{x},0) = \sum_{m=0}^{\infty} \alpha_m \phi_m(\mathbf{x}), \tag{2.8}$$

with $\{\phi_m, \lambda_m\}$ the eigenfunction-eigenvalue pairs defined by the eigenvalue problem

$$Pe^{-1}\boldsymbol{\nabla}^2\phi_m - \mathbf{v}_1\cdot\boldsymbol{\nabla}\phi_m = \lambda_m\phi_m, \tag{2.9}$$

corresponding with the advection-diffusion operator in (2.5) and α_m the expansion coefficients based on initial conditions [26]. The eigenvalue problem (2.9) is solved using the built-in function `eig` in MATLAB. The transient temperature $\tilde{T}(\mathbf{x},t_n)$ at the current time step t_n is the initial condition used for the determination of the expansion coefficients, and therefore changes each time an aperture is switched (i.e., at times $t_n = \tau n$). Progressive decay of transient temperatures implies stable eigenmodes that are ordered according to decay rate $\ldots \leq \mathrm{Re}(\lambda_1) \leq \mathrm{Re}(\lambda_0) < 0$, where $m = 0$ is the slowest-decaying mode. For $Pe \sim \mathcal{O}(10^2 - 10^4)$, the eigenvalues are complex with negative real part. This will be discussed in more detail in Section 2.1.3. The stability property follows from the second law of thermodynamics, which dictates that diffusive heat flux always acts against the temperature gradient [22]. This implies that any non-zero transient temperature, irrespective of the flow, always evolves towards the final equilibrium and the system is intrinsically stable. As mentioned before, flow $\mathbf{v}_k$ driven by aperture k is just a reorientation of the base flow $\mathbf{v}_1$ following

$$\tilde{T}(\mathbf{x},t) = \sum_{m=0}^{\infty} \alpha_m^{(k)} \phi_m\left(\mathcal{R}_k(\mathbf{x})\right) \mathrm{e}^{\lambda_m t}, \quad \tilde{T}(\mathbf{x},0) = \sum_{m=0}^{\infty} \alpha_m^{(k)} \phi_m\left(\mathcal{R}_k(\mathbf{x})\right). \tag{2.10}$$

Thus, spectral temperature evolution for the steady flow $\mathbf{v}_k$ implies an identical eigenvalue spectrum and a reorientation of the eigenfunctions related to the base flow $\mathbf{v}_1$.

2.1.3 Numerical method

In this section, two methods are discussed to simulate the 2D RAM numerically. First, the dedicated method proposed in [26] is discussed. Thereafter, it is shown that the method proposed in [14], which is based on the spectral temperature decomposition discussed in the previous section, results in the same structure as the semi-analytical solution obtained with the dedicated method proposed in [26].

The 2D RAM can be simulated numerically using the dedicated method proposed by Lester *et al.* [26]. Equation (2.7) is spatially discretized for each steady flow $\mathbf{v}_k$, from which a semi-discrete model is obtained, yielding

$$\frac{\mathrm{d}\tilde{\mathbf{T}}(t)}{\mathrm{d}t} = \mathbf{A}_k\tilde{\mathbf{T}}(t), \tag{2.11}$$

with $\tilde{\mathbf{T}}(t) = [\tilde{T}(\mathbf{x}_0, t), \ldots, \tilde{T}(\mathbf{x}_M, t)]^\top$ the nodal temperature value vector on computational grid $\mathbf{X} = [\mathbf{x}_0, \ldots, \mathbf{x}_M]^\top$ and $\mathbf{A}_k$ the discrete matrix approximation of the advection-diffusion operator. A cylindrical mesh with equidistant inter-nodal spacings should be chosen as computational grid to discretize the cost function, which will be needed for the control algorithm as discussed in Section 2.3.2. This computational grid is also used for the discretization of (2.11). Moreover, the number of elements should be chosen high enough to achieve convergence, which will be discussed in Chapter 3. Matrix $\mathbf{A}_k$ has complex eigenvalues with negative real parts. As $Pe \to \infty$, diffusion is negligible and transport becomes equal to pure advection. This corresponds with skew-symmetric $\mathbf{A}_k$ with purely imaginary eigenvalues [26]. As $Pe \to 0$, $\mathbf{A}_k$ becomes diagonal with purely real eigenvalues. This corresponds with diffusion dominated heat transfer; the effects of advection are negligible. Time-invariant $\mathbf{A}_k$ is implied by the time independence of $\mathbf{v}_k$, making it possible to write the transient temperature $\tilde{\mathbf{T}}$ as a function of the initial transient temperature $\tilde{\mathbf{T}}_0$ and the standard eigenvectors and eigenvalues of $\mathbf{A}_k$ according to

$$\tilde{\mathbf{T}}(t) = \mathbf{U}_k\tilde{\mathbf{T}}_0, \quad \mathbf{U}_k = \mathbf{V}_k\mathrm{e}^{\Lambda_k t}\mathbf{V}_k^{-1}, \tag{2.12}$$

using the spectral decomposition $\mathbf{A}_k = \mathbf{V}_k\mathbf{\Lambda}_k\mathbf{V}_k$, with $\mathbf{V}_k = [\boldsymbol{\phi}_0^{(k)}, \ldots, \boldsymbol{\phi}_M^{(k)}]$ and $\mathbf{\Lambda}_k = \mathrm{diag}(\lambda_0^{(k)}, \ldots, \lambda_M^{(k)})$ the standard eigenvector and eigenvalue matrices, respectively, of system matrix $\mathbf{A}_k$. Note that conventional finite volume method (FVM) discretizations [40] yield the same model structure as in (2.11).

The method in [22] is based on the spectral temperature decomposition discussed in Section 2.1.2. The spectral decompositions (2.8) and (2.10) given in Section 2.1.2 have the same structure as the semi-analytical solution (2.12), establishing

$$\tilde{\mathbf{T}}(t) = \mathbf{V}_k\mathrm{e}^{\mathbf{\Lambda}_k t}\mathbf{V}_k^{-1}\tilde{\mathbf{T}}_0 = \sum_{m=0}^{M}\alpha_m^{(k)}\boldsymbol{\phi}_m^{(k)}\mathrm{e}^{\lambda_m t}, \quad \boldsymbol{\alpha}^{(k)} = \mathbf{V}_k^{-1}\tilde{\mathbf{T}}_0 \tag{2.13}$$

with eigenvector $\boldsymbol{\phi}_m^{(k)}$ containing the nodal values of eigenfunction $\phi_m^{(k)}(\mathbf{x})$ and vector $\boldsymbol{\alpha}^{(k)}$ the discrete approximation of expansion coefficients $\alpha_m^{(k)}$ mapped on the computational grid. Using the rotation matrix $\mathbf{R}$, the discrete counterpart to operator $\mathcal{R}_k$ on the computational grid, the eigenvector bases $\mathbf{V}_k$ can be related to the base flow according to

$$\mathbf{V}_k = \mathbf{R}^{k-1}\mathbf{V}_1. \tag{2.14}$$

As explained by Lensvelt *et al.* [14], this affords two major reductions in computational effort compared to numerical treatment of (2.5) via conventional spatio-temporal discretizations.

Moreover, the computational effort is further reduced by neglecting the fastest-decaying eigenmodes. For sufficiently long times, only the most slowly decaying term present in the initial condition persists. Each eigenmode m has a characteristic time scale $\tau_m = -1/\operatorname{Re}(\lambda_m)$, which can be compared with the aperture activation time τ. The modes with $\tau_m/\tau \ll 1$ can then be neglected. Note that τ_v and τ_m are not related; $\tau_v/\tau \ll 1$ implies the transient effects of the velocity field associated with aperture reorientations may be ignored, whereas $\tau_m/\tau \ll 1$ implies the fastest-decaying eigenmodes in aperture activation time τ can be neglected. This results in a truncated expansion at $Q \ll M$ similar to (2.13):

$$\tilde{\mathbf{T}}(t) \approx \hat{\mathbf{T}}(t) = \sum_{m=0}^{Q} \hat{\alpha}_m^{(k)} \boldsymbol{\phi}_m^{(k)} \mathrm{e}^{\lambda_m t}, \quad \hat{\boldsymbol{\alpha}}^{(k)} = \mathbf{G}_k \tilde{\mathbf{T}}_0, \quad \mathbf{G}_k = (\hat{\mathbf{V}}_k^\top \hat{\mathbf{V}}_k)^{-1} \hat{\mathbf{V}}_k^\top, \tag{2.15}$$

with $\hat{\mathbf{V}}_k = [\boldsymbol{\phi}_0^{(k)}, \ldots, \boldsymbol{\phi}_Q^{(k)}]$ the reduced eigenvector basis and symbol $\hat{}$ indicating approximate quantities. This means that the vector $\hat{\mathbf{T}}(t) = [\hat{T}(\mathbf{x}_0, t), \ldots, \hat{T}(\mathbf{x}_m, t), \ldots, \hat{T}(\mathbf{x}_M, t)]^\top$ approximates of the nodal temperature value vector on the computational grid $\mathbf{X}$. Note that $\mathbf{G}_k$ is the Moore–Penrose inverse of matrix $\hat{\mathbf{V}}_k$ ($\hat{\mathbf{V}}_k$ is a $M \times Q$ matrix). Using this truncation, only the so-called "dominant eigenmodes" (slowest-decaying eigenmodes) remain. In Chapter 3, the number of modes Q is chosen large enough such that the simulation results are approximately the same as for using M modes. Next, this can be reformulated in an efficient matrix-vector operation, resulting in

$$\hat{\mathbf{T}}_k(t_{n+1}) = \hat{\mathbf{A}}_k \hat{\mathbf{T}}(t_n), \tag{2.16}$$

where $\hat{\mathbf{A}}_k$ can be found in [14] and the hat operator indicates approximate quantities.

2.2 Control of the 2D Rotated Arc Mixer

In this section, the control of the RAM is discussed. As discussed in Section 1.3, the goal is to find the fastest way to the final state by activating different apertures. Firstly, the system is discussed from a control perspective. Thereafter, different options of control will be treated.

2.2.1 Control strategy

The goal is to come up with a control strategy that determines the aperture sequence which minimizes the transient from the initial temperature to the target temperature. As can be seen in Figure 2.2, a feedback controller is incorporated into the system that determines this sequence, based on intermediate temperature fields. As discussed in [22], the flow $\mathbf{v}$ in the RAM is generated by switching between aperture-wise steady flows $\mathbf{v}_k$ (2.4) following

$$\mathbf{v}(\mathbf{x}, t) = \mathbf{v}_{u_n}(\mathbf{x}), \tag{2.17}$$

where u_n is the selected aperture, which is active on the time interval $[n\tau, (n+1)\tau)$. The selected aperture u_n activates the corresponding flow $\mathbf{v}_{u_n}$ according to Figure 2.1. The flow reorientation is described by a reorientation scheme $\mathcal{U} = \{u_0, u_1, \ldots, u_n, \ldots\}$ that determines the particular aperture sequence and thus the time signature of the flow; e.g., $\mathcal{U} = \{1, 3, 2\}$ subsequently activates apertures (1, 3, 2) each for a duration τ. The input set $\mathcal{W}$ contains the values that u can attain, which depends on the circulation possibilities in the RAM. When the RAM can only circulate the flow in one direction, $\mathcal{W} \in \{1, \ldots, N\}$. When the RAM can circulate the flow in two directions, $\mathcal{W} \in \{-N, \ldots, -1, 1, \ldots, N\}$. The number

of different switching inputs (i.e., the size of the input set) will be denoted with s. For the RAM, it follows that $s = N$ when the flow can circulate in one direction and $s = 2N$ when the flow can circulate in two directions.

2.2.2 Switched linear systems

This section describes some relevant material regarding switched linear systems. For a complete overview about switched system, see Liberzon [41].

Consider the following general switched linear discrete-time system

$$\mathbf{x}_{n+1} = \mathbf{F}_{u_n}\mathbf{x}_n + \mathbf{B}_{u_n}\mathbf{z}_n, \quad n \in \mathbb{N}_0, \tag{2.18}$$

where $\mathbf{x}_n \in \mathbb{R}^q$ is the state, $\mathbf{z}_n \in \mathbb{R}^{n_u}$ is the control input, $\mathbf{F}$ is the system matrix, $\mathbf{B}$ is the input matrix, and $u_n \in \{1, 2, \dots, s\}$ is the switching input at discrete time $n \in \mathbb{N}_0 := \{0, 1, 2, \dots\}$. The goal is to design a policy for the control and switching input that regulates the state to zero while minimizing a cost. It should be noted that the control input is absent ($\mathbf{z}_n = 0$ for all $n \in \mathbb{N}_0$) for the 2D RAM. This means that only the optimal switching input has to be found, i.e., the goal is to find the aperture sequence that results in the fastest way to the final uniform state. This is called an autonomous linear switched system since the control input is absent. The autonomous linear switched system is given as

$$\mathbf{x}_{n+1} = \mathbf{F}_{u_n}\mathbf{x}_n. \tag{2.19}$$

The semi-discrete model of the 2D RAM in (2.16) can be written in the same format as (2.19), where the state $\mathbf{x}_n$ is the temperature $\hat{\mathbf{T}}_n$ at discrete time step n.

It is desired to control the system optimally. However, it has to be defined what is optimal. This is usually done with a cost function [25]. Assuming that both the subsystems and the cost function are time invariant, it is possible to set the initial time to $t_0 = 0$ without loss of generality. Usually, the running cost function of the control problem is a quadratic cost function, which can be written as

$$J = \sum_{n=0}^{\infty} \left(\mathbf{x}_n^\top \mathbf{Q} \mathbf{x}_n \right), \tag{2.20}$$

where $\mathbf{Q} = \mathbf{Q}^\top \geq 0$ is the state cost matrix. In (2.20) an infinite horizon is considered. The computational burden for infinite horizon control problems is usually very large, so often

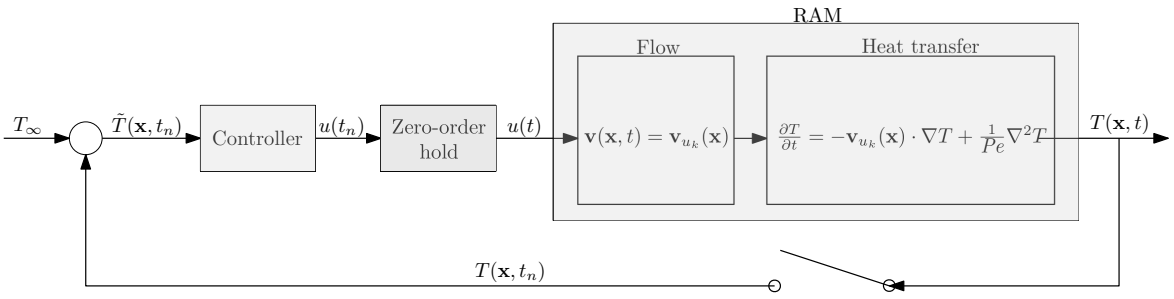

Figure 2.2: The closed-loop system for adaptive flow reorientation in the Rotated Arc Mixer. Since the feedback controller is not determined yet, the controller block is not specified.

finite horizon control problems are considered, giving

$$J = \sum_{n=0}^{H-1} \left(\mathbf{x}_n^\top \mathbf{Q} \mathbf{x}_n \right) + \mathbf{x}_H \mathbf{Q}_f \mathbf{x}_H, \tag{2.21}$$

where H is called the time horizon and $\mathbf{Q}_f = \mathbf{Q}_f^\top \geq 0$ is the final state cost matrix. For switched systems, also switching costs can be added in (2.21) as discussed in [42]. These switching costs account for the effort required to execute the control action [43]. In the RAM, the energy consumption to drive an arc is the same for all arcs. This means that switching costs are not relevant to the minimization procedure and therefore, switching costs are not considered in (2.21). However, when multiple arcs are activated at the same time, or arcs are activated at variable speeds, the energy consumption should be taken into account in (2.21). A more elaborate discussion about cost functions and performance indicators will be given in Section 2.3.

2.2.3 Optimal control

The problem of determining optimal control laws for hybrid and switched systems has been widely investigated in the last few years. In this section, different forms of (sub)optimal control are discussed. It is desired to develop a controller that can deal with noise, uncertainty, and disturbances, so that the controller can be used in practical applications. This excludes an open-loop controller that determines the entire aperture sequence before the start of the simulation.

Model predictive control

The certainty equivalent controller (CEC) is a suboptimal control scheme that is inspired by linear-quadratic control theory. The main attractive characteristic of CEC is its ability to deal with stochastic and even imperfect information problems by using the mature and effective methodology of deterministic optimal control. However, in CEC an infinite horizon is used. In most problems, these infinite horizon control problems cannot be solved due to their computational burden. This motivates a type of control with a finite horizon, called model predictive control (MPC). Model predictive control is a control scheme where a model is used for predicting the future behavior of the system in a finite time window. At each time step, an optimal control problem is solved over a fixed length horizon, starting from the current stage. The first component of the corresponding solution is then used as the control action for the current stage, while the remaining part of the solution is discarded. This process is then repeated at every time step. Compared to certainty equivalent control, in which a larger horizon is used, the MPC problem is simpler to solve and this makes it feasible to run the MPC algorithm online.

Essentially, the idea is that short-term optimization achieves optimality over a long time. However, the obtained policy using MPC is typically not optimal, even for problems without disturbances. One is tempted to conjecture that if the size of the horizon is larger, then the performance of the MPC algorithm is improved. This, however, need not be true as explained in [25]. Beyond the horizon H, the policy may be "blind" to the presence of particularly "favorable" or "unfavorable" states. Figure 2.3 shows an example from [44]. At the initial state, there are two possible controls, denoted u and u'. From the initial state, 2-step lookahead compares 0+1 with 0+2 and prefers the optimal control u, while 3-step lookahead compares 0+1+2 with 0+2+0 and prefers the suboptimal control u'. Thus, using a longer lookahead yields worse performance. Another example of reduced performance for

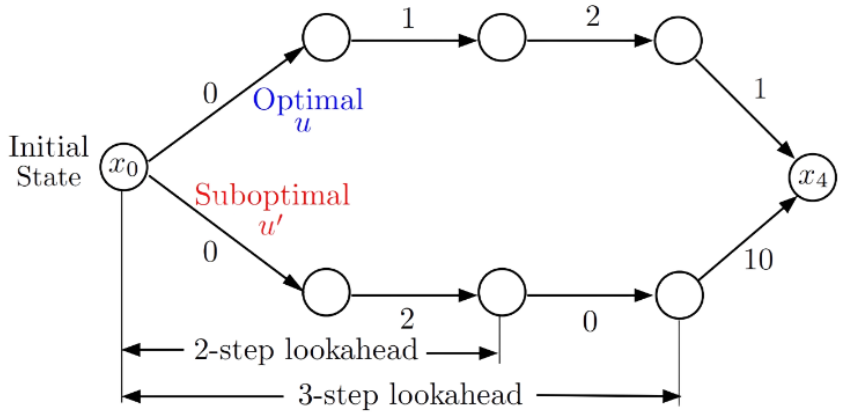

Figure 2.3: Example problem with costs for every transition, illustrating how using a longer lookahead (i.e., a larger horizon) may degrade the performance of the policy obtained. Image taken from [44].

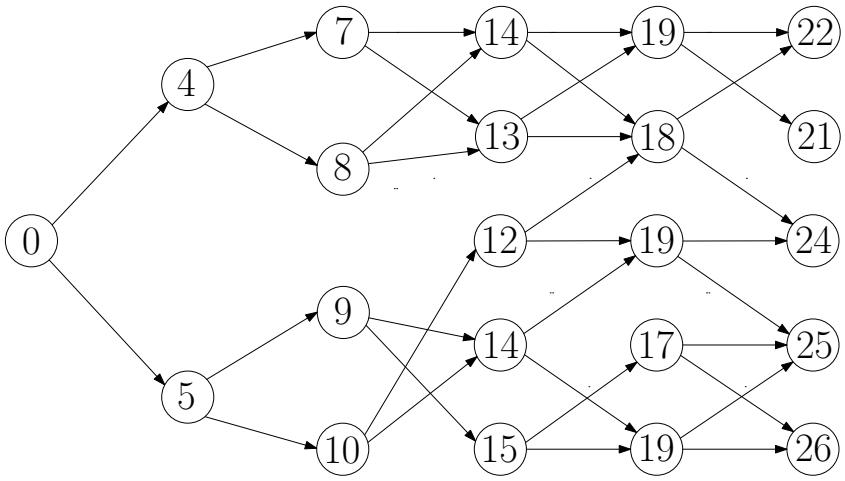

Figure 2.4: Example problem with total costs denoted at every note, illustrating how using a larger horizon may degrade the performance of the policy obtained.

a larger horizon is given in Figure 2.4. The total cost is indicated at every state. Both MPC controllers start with the same cost and should minimize the cost. Applying the MPC algorithm for the 1-step horizon controller results in a cost sequence 0 - 4 - 7 - 13 - 18 - 22. On the other hand, the cost sequence for the 3-step horizon controller is equal to 0 - 5 - 9 - 14 - 19 - 24, which is worse at every time step. The problem here has to do with large cost changes at the "edge" of the horizon (i.e., the cost changes from 12 to 18 and 17 to 25). Again, this example shows that the policy obtained with a larger horizon controller may be "blind" to the presence of particularly "favorable" and "unfavorable" states.

For system (2.19), the MPC algorithm can be represented by the following three steps:

1. At step n, compute all the possible control sequences in the horizon, i.e., $(u_n, u_{n+1}, \ldots, u_{H-1})$. This means that future temperatures are predicted in the 2D RAM for every possible combination in $\mathcal{U}$.
2. Compute the cost (2.21) for each of these control sequences and pick the sequence with minimum cost.

3. Apply the first element of this sequence, set $n = n + 1$, and go again to the first step.

In [14] the same approach has been used; however, the horizon in [14] is fixed at the duration of the control action (meaning a horizon of one discrete time step). In this research, larger horizons are considered as well. Note that the horizon keeps being shifted forward. For this reason, MPC is also called receding horizon control.

Rollout

A rollout algorithm is similar to the MPC algorithm, however, after the horizon a base policy is used. The base policy is fixed and determined before the start of the rollout algorithm. Assume the base policy is determined as $(\bar{u}_{n+H}, \bar{u}_{n+H+1}, \ldots, \bar{u}_{n_F-1})$. The rollout algorithm can then be written as:

1. At step n, compute all the possible control sequences, i.e., $(u_n, \ldots, u_{n+H-1}, \bar{u}_{n+H}, \ldots, \bar{u}_{n_F-1})$. Note that the base policy is fixed, i.e., only $(u_n, \ldots, u_{n+H-1})$ are free and can be optimized.
2. Compute the cost (2.21) for each of these control sequences and pick the sequence with minimum cost. Note that H should be replaced by n_F in (2.21) in case of the rollout policy.
3. Apply the first element of this sequence, set $n = n + 1$, and go again to the first step.

In Figure 2.5, the difference between MPC and rollout is visualized. By choosing the base policy $(\bar{u}_{n+H}, \bar{u}_{n+H+1}, \ldots, \bar{u}_{n_F-1})$, it is guaranteed that the rollout strategy will never perform worse than the base policy over an arbitrary finite horizon. However, choosing a well-performing base policy is required in this case. Note that this does not mean that rollout will perform better than an MPC controller.

Approach based on Pontryagin's maximum principle

The finite-time optimal control problem can also be solved using Pontryagin's maximum principle. Using this method, it is possible to optimize both the switching sequence and the aperture activation time. In order to obtain a more tractable optimal control problem, the switched system (2.19) is embedded [45, 46] into a larger family of systems. This is done by

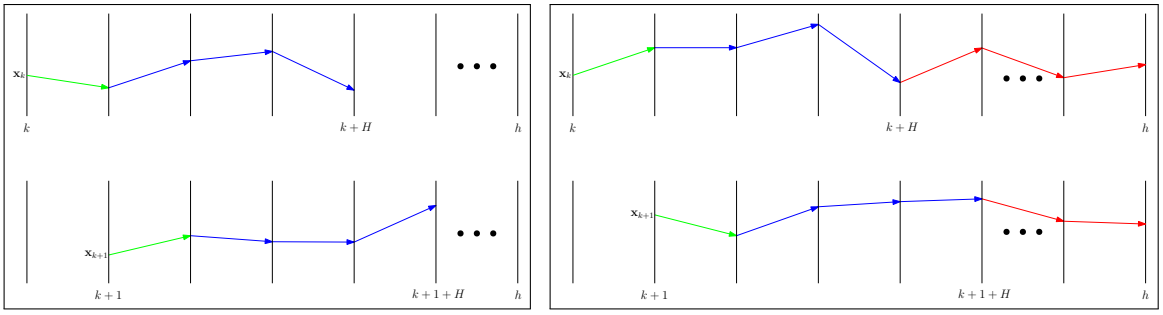

Figure 2.5: Different suboptimal approximate dynamic programming policies. On the left, model predictive control is shown. The calculated sequence is given in blue, from which the first decision is applied (green line). On the right, rollout is shown. The base policy is given in red.

defining a convex set W given as

$$W = \left\{ w \in \mathbb{R}^s : \sum_i^s w_i = 1, w_i \in [0,1] \right\}, \tag{2.22}$$

where $w(t_n) = \left[w_1(t_n), \ldots, w_s(t_n)\right]^\top \in \mathbb{R}^s$. The finite-time optimal control problem can now be transformed into the embedded finite-time optimal control problem as

$$\begin{aligned} \min_{(w(t_0),\ldots,w(t_{H-2}))} J &= \sum_{n=0}^{H-1} \mathbf{x}^\top(t_n)\mathbf{Q}\mathbf{x}(t_n) \\ \text{s.t. } \mathbf{x}(t_{n+1}) &= \sum_{i=1}^{s} w_i(t_n)\mathbf{F}_i\mathbf{x}(t_n). \end{aligned} \tag{2.23}$$

Note that the terminal costs are not present in (2.23) for the sake of simplicity. The representation in (2.23) allows the input $w_i(t_n)$ to vary continuously in the range $[0,1]$. However, as proven in [45], the optimal inputs for the larger family of systems belong to the set $\{0,1\}$. The optimal switching control law of problem (2.23) is then given as

$$u(t_n) = \underset{u(t_n)\in\{1,2,\ldots,s\}}{\operatorname{argmin}} \left[\boldsymbol{\xi}^\top(t_{n+1})\mathbf{F}_{u(t_n)}\mathbf{x}(t_n) \right], \tag{2.24}$$

where $\boldsymbol{\xi}(t_n) \in \mathbb{R}^q$, the co-states, are the solutions of

$$\boldsymbol{\xi}(t_n) = 2\mathbf{Q}\mathbf{x}(t_n) + \sum_{i=1}^{s} w_i(t_n)\mathbf{F}_i^\top \boldsymbol{\xi}(t_{n+1}), \tag{2.25}$$

satisfying $\xi(t_H) = 0$. Note that $u(t_n) = u_n$ is the selected aperture, which is active on the time interval $[n\tau, (n+1)\tau)$, and is part of the flow reorientation scheme $\mathcal{U} = \{u_0, u_1, \ldots, u_n, \ldots\}$ (indicating the time signature of the flow). Equation (2.24) thus gives the optimal switching input for (2.19). To determine the optimal solution, a two-point boundary value problem needs to be solved, as opposed to usual single-point boundary value problems. Two different ways to solve a two-point boundary value problem are the shooting method and the relaxation method [47]. In the shooting method the two-point boundary value problem is reduced to an initial (final) value problem with a random choice of the initial (final) conditions to satisfy the boundary conditions at one end of the time interval. The equations are then integrated with standard techniques and corrections are made for the initial guess; the process is repeated until convergence is reached. In the relaxation method, ordinary differential equations are approximated by finite difference equations on a mesh of points that span the domain of interest and the optimal solution is obtained iteratively, starting with a guess solution.

In Section 3.2, the discussed control strategies will be compared, after which one control strategy is implemented for the 2D RAM.

2.3 Performance indicators

2.3.1 Selection of performance indicators

An adequate description of the control target is essential. It is required to find the optimal balance between a fast increase in the total energy content and fast homogenization of the

internal temperature distribution. In [22], a start has been made on this subject, which will be partly repeated here. Relevant metrics are discussed for the global dynamics, which enables the formulation of the control problem as the minimization of a dedicated cost function that naturally emerges from the dynamic analyses and adequately incorporates both processes, i.e., increasing energy content and thermal homogenization. The transient temperature can be decomposed as

$$\tilde{T}(\mathbf{x},t) = \bar{T}(t) + T'(\mathbf{x},t), \quad \bar{T}(t) = \frac{1}{A}\int_{\mathcal{D}} \tilde{T}(\mathbf{x},t)\,\mathrm{d}\mathbf{x}, \quad T'(\mathbf{x},t) \equiv \tilde{T}(\mathbf{x},t) - \bar{T}(t), \tag{2.26}$$

where A is the area of the 2D RAM. Since $R = 1$ as described before, A can be replaced by π ($A = \pi R^2$). The decomposition above isolates the temperature distributions corresponding to these goals. The average temperature $\bar{T}(t)$ can be seen as an indicator of the total energy supplied to the fluid from time 0 to t:

$$\tilde{E}(t) = \int_{V_{\mathrm{RAM}}} \rho c_p \left(\tilde{T}(t) - \tilde{T}_0\right) \mathrm{d}V \tag{2.27}$$

$$= \rho c_p \int_{V_{\mathrm{RAM}}} \left(\tilde{T}(t)\,\mathrm{d}V - \tilde{T}_0 V_{\mathrm{RAM}}\right) \tag{2.28}$$

$$= \rho c_p V_{\mathrm{RAM}} \left(\bar{T}(t) - \tilde{T}_0\right), \tag{2.29}$$

where ρ is the fluid density, c_p the specific heat capacity, and V_{RAM} the volume of the RAM. Moreover, "heterogeneity" $T'(\mathbf{x},t)$ represents the (spatial) departure of $\tilde{T}$ from the momentary homogeneous state $\bar{T}$. As discussed in Chapter 1, most problems considered in the literature are homogenization problems, which in general concern adiabatic domains. This implies $\bar{T} = 0$, and therefore only the field $\tilde{T} = T'$ is important in these problems. The decomposition in (2.26) exposes the great dynamic complexity of the heating problem. For fluid heating both energizing and homogenization are important. Therefore, the total transient field $\tilde{T}$, as well as its components $\bar{T}$ and T', are relevant to its dynamics. This motivates the definition of three measures for the global dynamic behavior of the heating process [22]:

$$J_1(t) \equiv \frac{1}{\pi}\int_{\mathcal{D}} \tilde{T}(\mathbf{x},t)\,\mathrm{d}\mathbf{x}, \tag{2.30}$$

$$J_2(t) \equiv \frac{1}{\pi}\int_{\mathcal{D}} \tilde{T}^2(\mathbf{x},t)\,\mathrm{d}\mathbf{x}, \tag{2.31}$$

$$J_3(t) \equiv \frac{1}{\pi}\int_{\mathcal{D}} \left(T'\right)^2(\mathbf{x},t)\,\mathrm{d}\mathbf{x} \tag{2.32}$$

with $J_1 = \bar{T}$ the normalized energy content of the transient state, J_2 the global departure from the equilibrium, and J_3 the global heterogeneity. Note that $\tilde{T} \leq 0\ \forall \mathbf{x} \in \mathcal{D}$ and $t \geq t_0 = 0$ by the definition in (2.6), so the use of the absolute value sign in (2.30) is not necessary. To get the desired behavior, $J_1 = \bar{T}$ should be maximized since it represents the normalized energy content of the transient state. Measures J_2 and J_3, on the other hand, should be minimized to get the desired behavior. These measures relate via (2.26) and the property $\int_{\mathcal{D}} T'(\mathbf{x},t)\,\mathrm{d}\mathbf{x} = 0$ as

$$J_2(t) = J_1^2(t) + J_3(t), \tag{2.33}$$

and effectively represent two distinct degrees of freedom as shown in [22].

Following the procedure in [22], it is possible to derive the evolution of these measures. The resulting evolutions are given as

$$\frac{\mathrm{d}J_1}{\mathrm{d}t} = \frac{1}{\pi Pe}\int_\Gamma \mathbf{n}\cdot\boldsymbol{\nabla}\tilde{T}\,\mathrm{d}s, \tag{2.34a}$$

$$\frac{\mathrm{d}J_2}{\mathrm{d}t} = -\frac{2}{\pi Pe}\int_\mathcal{D} |\boldsymbol{\nabla}\tilde{T}|^2\,\mathrm{d}\mathbf{x}, \tag{2.34b}$$

where $\mathbf{n}$ is the normal vector to the surface of the 2D RAM. The evolution of J_3 follows from differentiating (2.33). Measure J_1 represents the energy content of the transient state, so $\mathrm{d}J_1/\,\mathrm{d}t$ represents the rate of change of the energy content. Equation (2.34a) shows that energy enters the 2D RAM via the diffusive flux normal to the boundary. From (2.30) it can be derived that $J_1(0) < 0$ due to the uniform initial condition $\tilde{T}(\mathbf{x},0) = -1$ and $\lim_{t\to\infty} J_2(t) = 0$ due to the final condition $\lim_{t\to\infty}\tilde{T}(\mathbf{x},(t)) = 0$, which is implied by the uniform boundary condition $\tilde{T}|_\Gamma = 0$. Since (2.34a) shows that $\mathrm{d}J_1/\,\mathrm{d}t > 0$), it follows that measure J_1 will increase monotonically. Moreover, (2.34b) via inequality $|\boldsymbol{\nabla}\tilde{T}|^2 > 0$ implies $\mathrm{d}J_2/\,\mathrm{d}t < 0$ in at least one non-zero subset $\mathbf{x}\in\mathcal{D}$ for any non-uniform $\tilde{T}$. It is known from (2.31) that $J_2(0) > 0$ and $\lim_{t\to\infty} J_2(t) = 0$, because $\tilde{T}(\mathbf{x},0) = -1$ and $\lim_{t\to\infty}\tilde{T}(\mathbf{x},(t)) = 0$ as explained before. This implies a monotonic decay for measure J_2. Since $\tilde{T}(\mathbf{x},0) = -1$ and $\lim_{t\to\infty}\tilde{T}(\mathbf{x},(t)) = 0$, the temperature fields are homogeneous at the start and the end of the process. This implies that $J_3(0) = \lim_{t\to\infty} J_3(t) = 0$. However, at the start, the heterogeneity will grow ($\mathrm{d}J_3/\,\mathrm{d}t|_{t=0} > 0$) because heat is transferred to the fluid close to the wall of the RAM. Eventually, the heterogeneity will decline ($\mathrm{d}J_3/\,\mathrm{d}t < 0$) towards the final state. This means that measure J_3 is non-monotonic.

In [21] similar efficiency indicators are used to characterize the efficiency of heat transfer by chaotic advection. The dimensionless fluid temperature defined in [21] is equal to $T(\mathbf{x},t)$, since $T_0 = 0$ and $T_\infty = 1$. The average dimensionless temperature $\bar{T}^*(t)$ and the standard deviation $\sigma(t)$ of the fluid are used as performance indicators. The average dimensionless temperature $\bar{T}^*(t)$ and the standard deviation $\sigma(t)$ of the fluid temperature are defined as

$$\bar{T}^*(t) = \bar{T}(t) + T_\infty, \quad \sigma(t) = \sqrt{\frac{1}{A}\int_\mathcal{D}\left(\tilde{T}(\mathbf{x},t) - \bar{T}(t)\right)^2\mathrm{d}\mathbf{x}} = \sqrt{J_3(t)}, \tag{2.35}$$

where A is the area of the domain. Since both indicators are important as described before, a new indicator is introduced that combines the two effects:

$$A_{T\sigma} = \frac{1}{t_{final}}\int_0^{t_{final}} \frac{\bar{T}^*(t)}{\sigma(t)}\,\mathrm{d}t, \tag{2.36}$$

where t_{final} indicates a certain time period. For an efficient stirring protocol, $A_{T\sigma}$ must tend toward a high value. The measure J_4 can now be defined as

$$J_4(t) \equiv \frac{\bar{T}^*(t)}{\sigma(t)} = \frac{J_1(t) + T_\infty}{\sqrt{J_3(t)}}, \tag{2.37}$$

which has to be maximized. It should be mentioned that $\sigma(t) = 0$ for a homogeneous temperature field. In this case, $J_4(t)$ is undefined (division by zero). When the simulation would start with a homogeneous temperature field, this yields an undefined value of J_4. However, in the spectral model the fluid temperature at the wall is higher due to the definition of $\tilde{T}(\mathbf{x},0)$ in (2.8) and the simulation does not start with a homogeneous field. When the temperature field is homogeneous at the start ($J(0) \to \infty$ because $\sigma(0) = 0$), measure J_4

will decay first, since σ increases. Eventually, measure J_4 will grow again towards its final value. This means measure J_4 is non-monotonic.

As the last performance indicator, it is chosen to maximize the lowest temperature present in the RAM according to (2.38). The idea behind this is to prevent the formation of (large) cold plumes. However, this approach does not say anything about global dynamic behavior.

$$J_5(t) \equiv \min_{\mathbf{x}\in\mathcal{D}} \tilde{T}(\mathbf{x}, t). \tag{2.38}$$

To visualize all performance indicators over time, the performance indicators can be normalized such that $\check{J}$ shows decaying behavior and $\check{J}(0) = 1$. The normalized performance indicators can be calculated as

$$\check{J}_p(t) = \frac{J_p(t)}{J_p(0)}, \quad p = [1, 2, 3, 5], \tag{2.39}$$

$$\check{J}_q(t) = \frac{J_q(0)}{J_q(t)}, \quad q = 4. \tag{2.40}$$

A measure should be used that captures both homogenization of the temperature field as well as energizing (related to the mean temperature of the fluid). Measures J_2 in (2.31) and J_4 in (2.37) are the most suitable candidates for this due to the combination of homogenization and energizing. J_2 incorporates both energizing (represented by J_1) and homogenization (represented by J_3) by virtue of relation (2.33) as discussed in [22]. J_4 also incorporates both energizing (represented by $\bar{T}^*(t)$) and homogenization (represented by $\sigma(t)$). The other measures do not capture both energizing and homogenization directly. In measure J_4, however, the balance between energizing and homogenization is not entirely clear; when the temperature field is homogeneous, J_4 will grow to infinity. This makes measure J_2 the best option to assess the performance of the control algorithm.

As described in Section 1.3, the main objective is to accomplish a homogeneous temperature field as fast as possible for the 2D RAM. Therefore, it is important to rewrite this requirement into a mathematical expression, making it possible to compare this requirement systematically. The requirement consists of two parts. First, it has to be defined how the desired homogeneous temperature field can be represented mathematically. Second, the time requirement (as fast as possible) should be defined mathematically. As discussed before, measure J_2 would be most suited to represent the desired homogeneous temperature field mathematically. The time requirement is translated into achieving a transient time t_ϵ as fast as possible [22], i.e., finding the smallest t_ϵ such that $J(t) \leq \epsilon \ \forall \ t \geq t_\epsilon$. Since the value of J is only known at some discrete time points n, the transient time is interpolated via [22]

$$t_{\epsilon,i} = t(n) + \tau \frac{\check{J}_i(n) - \epsilon_i}{\check{J}_i(n) - \check{J}_i(n+1)}, \quad i \in [1, 2, 3, 4, 5], \tag{2.41}$$

where n is the smallest integer such that $J(n+1) \leq \epsilon$. The values of ϵ_i are chosen such that the transient is captured well, i.e., $\epsilon_i = 10^{-2}$ for $i \in [2, 4]$ and $\epsilon_i = 10^{-1}$ for $i \in [1, 5]$. Since measures J_2 and J_4 capture both homogenization and energizing, it is desired that ϵ_i is relatively small for these measures to achieve the desired performance, therefore $\epsilon_i = 10^{-2}$ for $i \in [2, 4]$. Via relations (2.33) and (2.37) it is determined that $\epsilon_i = 10^{-1}$ for $i \in [1, 5]$ to have all the transient times $t_{\epsilon,i}$ in the same order of magnitude.

In the next chapter, different performance indicators (discussed in this section) will be used as cost functions. To compare the performance between these cost functions, the transient time in (2.41) will be used.

2.3.2 Discretization of performance measures

The cost functions given above should be discretized, since the approximated transient temperature $\hat{\mathbf{T}}$ is only known at discrete data points on the computational grid $\mathbf{X}$ as discussed in Section 2.1.3. As an example, $J_1(t)$ (2.30) is discretized [22] according to

$$\hat{J}_1(t) = \sum_{m=0}^{M} \gamma_m \hat{T}(\mathbf{x}_m, t), \tag{2.42}$$

where γ_m are weight factors incorporating area weighting of $\tilde{T}(\mathbf{x}_m, t)$. The discretizations of J_2, J_4, and J_5 are given in Appendix A. Note that other types of weighting are also possible, however, this results in a different (spatially weighted) measure. In case of area weighting, the discrete grid points are placed at the center of an element as can be seen in Figure 2.6. The area of such an element can be calculated as

$$\gamma_m = \pi \left(\left(r_m + \frac{\Delta r}{2} \right)^2 - \left(r_m - \frac{\Delta r}{2} \right)^2 \right) \frac{\Delta \theta}{2\pi} = r_m \Delta r \Delta \theta. \tag{2.43}$$

The area of the element in the center of the 2D RAM (with center point $x = y = 0$), is given as $(\Delta r)^2 \pi$. When the area of all elements is summed, it corresponds with the total area π of the 2D RAM.

2.4 Discussion

In this section, the main findings of this chapter are discussed.

Firstly, the numerical model of the 2D RAM was discussed in Section 2.1. This model will be used for the simulations in Chapter 3, using an efficient matrix-vector operation for the temperature predictions (2.16).

In Section 2.2.1, the control of the RAM was discussed. The goal is to determine the aperture sequence which minimizes the transient from the initial temperature to the target

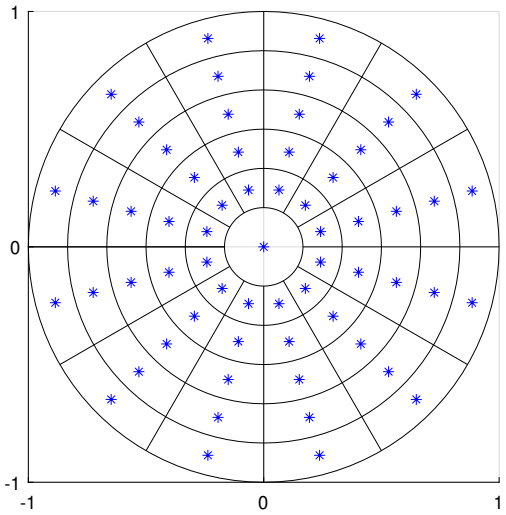

Figure 2.6: Area weighting in the 2D RAM.

temperature. The RAM can be seen as a switched linear system, which can be controlled in different ways. Model predictive control, rollout, and an approach based on Pontryagin's maximum principle are discussed as potential control options. In Chapter 3, one of these options will be selected, tested in simulations, and evaluated.

Finally, different performance indicators are discussed and analyzed in Section 2.3. Performance measures J_1, J_2, J_4, and J_5 will be compared in the next chapter. Furthermore, the transient time t_ϵ is defined in (2.41) to compare the performance of different performance measures. In addition, other parameters, such as the aperture activation time and the horizon, can be compared as well using the transient time.

Chapter 3

Computational performance analysis

In this chapter, the performance of the RAM is investigated for a RAM consisting of $N = 3$ apertures for different Péclet numbers and aperture activation times. The compact model described in Section 2.1.3 is used for the simulations. The simulation settings are discussed in Section 3.1. In Section 3.2, the used control strategy will be discussed, including the parameters that still need to be determined. This will be followed by Section 3.3, in which the effect of the horizon on performance is investigated for the values of Pe and τ given in Section 3.1. Thereafter, the influence of the aperture activation time τ on performance is analyzed in Section 3.4. In Section 3.5, a RAM with one circulation direction will be compared with a RAM with two circulation directions. Finally, a conclusion is given in Section 3.6.

3.1 Simulation settings

As discussed in Section 2.1.3, the number of elements should be chosen high enough to achieve convergence. In this research, the computational grid consists of a cylindrical mesh with equidistant inter-nodal spacings (Δr, $\Delta\theta$) and includes $N_r = 149$ and $N_\theta = 320$ elements in radial and angular direction, respectively. Truncation is at $Q = 1000$ modes according to (2.15). In [22], $N_r = 51$ and $N_\theta = 121$ elements are used with truncation at $Q = 500$ modes, which resulted in convergence (verified by mesh-refinement tests). Since the same model is used as in [22], using the same number of elements and modes should result in convergence. In this research, it is assumed the results are accurate when metric J_2 converges for a given aperture sequence. In Figure 3.1, the evolution of metric $\check{J}_2$ is shown for $Pe = 1000$, $\tau = 5$, $Q = 1000, \mathcal{U} = \{1, -3, -2\}$, and different numbers of elements as indicated. In this figure, no differences can be seen between simulations with different numbers of elements. In Table 3.1, $\check{J}_2$ is shown at $t = 15$ for the same settings. As $\check{J}_2$ does not change significantly for a finer mesh, it can be concluded that the used mesh ($N_r = 149$, $N_\theta = 320$, and $Q = 1000$) is fine enough for accurate results. Furthermore, metric J_2 is accurate within a range of 10^{-4}, i.e., $\check{J}_2|_{t=15} = 0.5390 \pm 0.0001$. This is verified with other Péclet numbers.

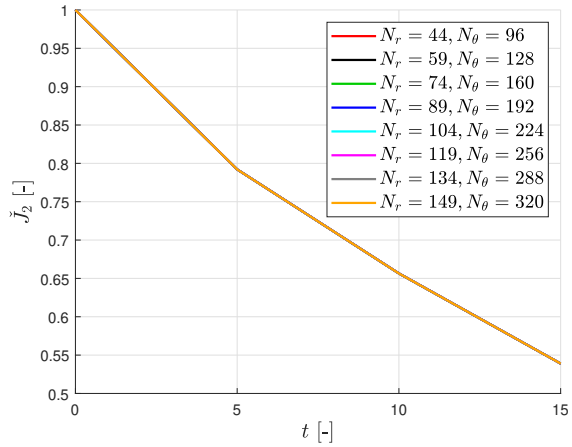

Figure 3.1: Evolution of $\check{J}_2$ for $Pe = 1000$, $\tau = 5$, $Q = 1000$, $\mathcal{U} = \{1, -3, -2\}$, and different numbers of elements.

N_r	N_θ	$\check{J}_2$
44	96	0.538994
59	128	0.538989
74	160	0.538973
89	192	0.538995
104	224	0.539010
119	256	0.539016
134	288	0.539017
149	320	0.538984

Table 3.1: $\check{J}_2$ at $t = 15$ for $Pe = 1000$, $\tau = 5$, $Q = 1000$, $\mathcal{U} = \{1, -3, -2\}$, and different numbers of elements.

The analysis is carried out for $5 \times 10^2 \leq Pe \leq 1.25 \times 10^3$ to encompass the values $Pe \sim \mathcal{O}(10^3)$ typical of practical systems within the present scope as described in Section 1.2. In addition, $3 \leq \tau \leq 7$ captures the transition from regular to chaotic advection with conventional periodic reorientation schemes [37].

3.2 Control strategy

In Section 2.2.3, different options of (sub)optimal control have been discussed, which are model predictive control, rollout, and an approach based on Pontryagin's maximum principle. In this chapter, the performance analysis will be done using an MPC controller. The main reasons for this choice are the ease of implementation and lower computational costs compared to the approach based on Pontryagin's maximum principle. Furthermore, it continues on the work done by Lensvelt *et al.* [14], where an MPC controller with a horizon of $H = 1$ is used. Another advantage is that the MPC controller can be easily extended to a rollout controller.

As discussed in Section 2.2.2, the heating problem considered in this report can be seen as an autonomous linear switched system (2.19) for which the optimal switching sequence is to be determined. To formulate a well-defined optimization problem, the cost function should be convex. This ensures convergence and regularity of the minimization procedure. The goal is to find the cost function that corresponds with the main goal, i.e., finding the fastest way to the homogeneous temperature field. In the MPC controller settings, the following three aspects should be addressed:

1. The type of costs (i.e., the cost function). Which performance indicator corresponds the most with the main goal? In Section 2.3.1, a selection will be made for the performance indicators.

2. Whether and how the costs are summed in intermediate prediction steps. For example, suppose an MPC controller with $H > 1$. It is possible to only look at the terminal cost (using only the terminal state x_H) and discard the costs at intermediate time steps. On the other hand, it is possible to sum the costs at intermediate time steps, where it

is even possible to weight the costs differently for each time step according to

$$J_{\text{total}} = \sum_{n=1}^{H} \mu(t_n) J(t_n), \tag{3.1}$$

where $\mu(t_n)$ is a weighting factor indicating the relative importance of a specific cost function J at time t_n. Note that using terminal costs is a special case of summing costs with $\mu(t_n) = 0 \; \forall \; n \in \mathbb{N}_0 \setminus H$. Furthermore, summing costs and terminal costs are the same in case $H = 1$. In this research, costs are summed equally, i.e., $\mu(t_n) = 1 \; \forall \; n \in \mathbb{N}_0$.

3. The horizon, i.e., the number of future samples over which the controller tries to minimize the cost defined in steps 1 and 2. A larger horizon does not necessarily result in improved performance of the MPC algorithm as discussed in Section 2.2.3, which will influence the choice of the optimal horizon. Besides the performance of the MPC algorithm, the horizon also correlates with the computational costs.

As discussed in Section 2.2.3, an optimization problem should be solved at every discrete time step i. In the optimization problem, the sequence with minimum cost ($\mathcal{U}^*$) is determined. Thereafter, the first element of the sequence (u_0^*) is applied and the procedure is repeated in the next step. At every time step i, the initial time of the optimization problem can be set to $t_i = t_0$ without loss of generality. The optimization problem is then given by

$$\begin{aligned}
\min_{\mathcal{U}} \quad & \sum_{n=1}^{H} \mu(t_n) J\left(\hat{\mathbf{T}}(t_n)\right), \\
\text{s.t.} \quad & \hat{\mathbf{T}}(t_0) = \hat{\mathbf{T}}(t_i), \\
& \mathcal{U} = \{u_0, u_1, \ldots, u_{H-1}\}, \\
& \hat{\mathbf{T}}(t_{n+1}) = \hat{\mathbf{A}}_{u_n} \hat{\mathbf{T}}(t_n), \qquad \forall \; n \; \in \{0, \ldots, H-1\}, \\
& u_n \in \mathcal{W}, \qquad\qquad\qquad\quad \forall \; n \; \in \{0, \ldots, H-1\}.
\end{aligned} \tag{3.2}$$

Note that cost function J is not specified in (3.2). Different cost functions will be compared in the next section.

3.2.1 Comparison of different performance indicators

As a first step, different performance indicators (J_1, J_2, J_4 and J_5) discussed in Section 2.3.1 are investigated for the 2D RAM consisting of 3 apertures at $Pe = 1000$ and $\tau = 5$. Only one direction of rotation ($\omega = -1$ in (2.3)) is considered here. The actual temperature evolution and the step-wise predictions are simulated using the numerical model (2.16). In every simulation, an MPC controller with horizon $H = 1$ is used. This controller determines the aperture sequence. Since four different performance indicators are considered, four simulations have been performed, each with a different cost function. After every simulation, it is possible to show the evolution of the four performance measures described above, although only one of them is used in determining the aperture sequence. After the simulations, the performance can be compared using the transient time according to (2.41). For a Péclet number of 1000, this gives the results in Table 3.2. Note that the transient times $t_{\epsilon,i}$ cannot be compared with each other, since they are defined differently. For an aperture activation time of $\tau = 5$, the evolution of the different normalized performance indicators $\check{J}$ is shown in Figure 3.2. The results for different Péclet numbers and aperture activation times are given in Table B.1. As can be seen in Table 3.2, the transient times differ relatively much for another aperture activation time and another cost function used in the MPC algorithm.

In particular, the transient times $t_{\epsilon,2}$ and $t_{\epsilon,4}$ are used to compare the different cost functions used in the MPC algorithm, since the measures J_2 and J_4 capture homogenization and energizing directly. However, this might favor cost functions J_2 and J_4 used in the MPC algorithm, since the performance of the algorithm is evaluated with the same indicator. As expected in Section 2.3.1, it turns out that measure J_5 is not suited as cost function when looking at the transient times. The transient times are relatively high compared to the other cost functions used in the MPC algorithm, regardless of which transient time is used for comparing the cost functions used in the MPC algorithm. Also, when looking at the transient time $t_{\epsilon,5}$, cost function J_5 performs poorly compared to other cost functions. Hence, J_5 is not suited as cost function. For measure J_1, it can be seen the transient time is high for $\tau = 3$ compared to the other measures. However, using measure J_1 as cost function for $\tau = 7$ results in the shortest transient time. Based on the transient times in Table B.1, it can be concluded that the difference between using J_1, J_2, and J_4 as cost functions is small. However, as discussed in the previous section, J_4 is non-monotonic, because in J_4 (2.37) the

Table 3.2: Transient times t_ϵ for different aperture activation times τ and different cost functions J used in the MPC algorithm. The Péclet number has a fixed value of 1000.

		Type of cost used to define transient time			
τ	Cost used in MPC	$t_{\epsilon,1}$	$t_{\epsilon,2}$	$t_{\epsilon,4}$	$t_{\epsilon,5}$
3	J_1	133.8	153.5	195.8	197.4
	J_2	104.7	112.7	119.8	124.4
	J_4	97.8	102.7	113.6	117.8
	J_5	117.9	126.3	145.9	136.0
5	J_1	105.0	110.0	117.3	121.6
	J_2	98.2	104.0	111.6	116.0
	J_4	112.9	116.8	124.1	130.9
	J_5	110.2	117.0	130.2	128.6
7	J_1	99.2	103.5	117.5	121.0
	J_2	109.9	115.0	124.1	128.7
	J_4	116.1	120.4	128.5	123.9
	J_5	116.1	120.4	128.5	123.9

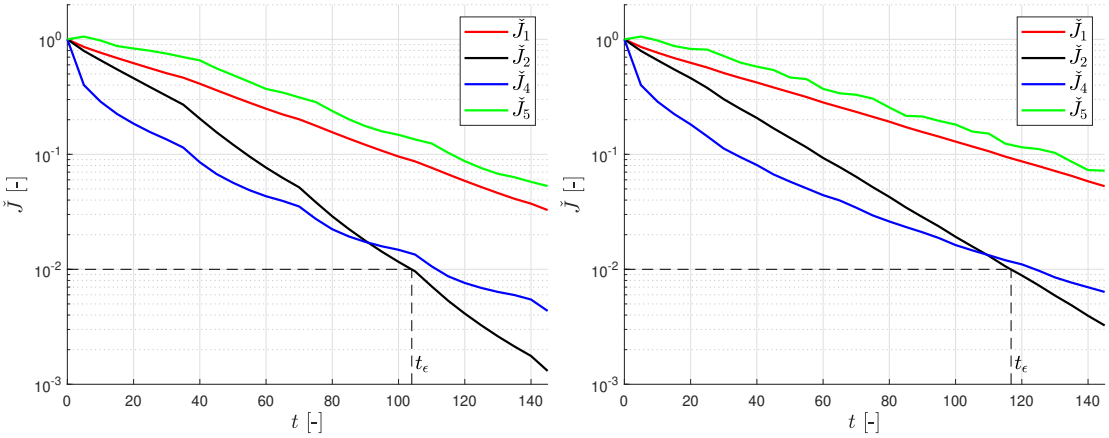

(a) Simulation with cost function J_2. **(b)** Simulation with cost function J_4.

Figure 3.2: Evolution of different normalized performance indicators for $Pe = 1000$ and $\tau = 5$.

average dimensionless temperature is divided by the standard deviation. This favors performance indicators J_1 and J_2 above J_4. At this point, it is decided to continue the analysis with both J_1 and J_2.

3.2.2 Summing of costs in intermediate prediction steps

As discussed in Section 3.2, it is important to determine whether and how costs are summed in intermediate prediction steps. The goal (accomplishing a homogeneous temperature field as fast as possible) suggests that only terminal costs would suffice. In Section 2.2.3, the conclusion was drawn that a larger horizon does not necessarily result in a better performance. Therefore, simulations have been performed in which both situations (i.e., summing costs and terminal costs) are compared. In the simulations, a horizon $H = 3$ has been used. This horizon should be large enough to see differences in both situations. To compare both situations, the performance indicator β is defined as

$$\beta(Pe, \tau) = \frac{t_{\epsilon,s}}{t_{\epsilon,t}}, \tag{3.3}$$

where subscripts "s" and "t" denote summing and terminal costs, respectively. The performance can be quantified as follows: $\beta > 1$ indicates a shorter transient - and thus better performance - of using terminal costs compared to summing costs at intermediate prediction steps; $\beta < 1$ indicates a relatively better performance of summing the costs at intermediate steps. The results are shown in Table 3.3 for J_1 and J_2, using transient times $t_{\epsilon,1}$ and $t_{\epsilon,2}$, respectively. The transient times $t_{\epsilon,s}$ are given as well to be able to make a comparison between different values of τ and J. Subsequently, the transient times $t_{\epsilon,t}$ can be computed using relation (3.3). For most values of τ and J the difference between both situations is small (i.e., $\beta \approx 1$). Some differences can be seen for $\tau = 3$ and $J = J_2$, for both $Pe = 750$ and $Pe = 1000$. In case of a small aperture activation time ($\tau = 3$), it is more beneficial to sum the costs. Since $\beta < 1$ in most cases, the costs will be summed in intermediate steps from now on. Different options of summing are possible by adding weights according to (3.1). In this report, however, the costs are summed equally, i.e., the weighting factor is equal to 1 for every step.

Moreover, it is interesting to see what happens when other area weighting factors γ (2.43) are used in this comparison. As explained before, this corresponds to another cost function (i.e., a spatially weighted L1-norm). According to Figure 2.6, there are comparatively more discrete data points in the RAM's center than there are at the wall. This enables us to emphasize the temperature at the RAM's center more strongly by not using area weighting (i.e., $\gamma_m = 1 \; \forall \; m \; \in \{1, \ldots, M\}$). The rationale for this is that heat, coming from the walls, will be faster at the center of the RAM, resulting in faster energizing and homogenization. Figure 3.3 shows the costs $\check{J}_1$, the adaptive reorientation scheme, and the temperature field

Table 3.3: Comparison of simulations where only terminal costs are considered with simulations where the costs are summed at intermediate steps using performance indicator β.

(a) $Pe = 750$.

τ [-]	J [-]	$t_{\epsilon,s}$ [-]	β [-]
3	J_1	85.1	0.992
3	J_2	87.1	0.903
5	J_1	84.5	0.988
5	J_2	93.3	0.977

(b) $Pe = 1000$.

τ [-]	J [-]	$t_{\epsilon,s}$ [-]	β [-]
3	J_1	102.9	1.004
3	J_2	105.7	0.897
5	J_1	102.7	1.007
5	J_2	111.6	0.963

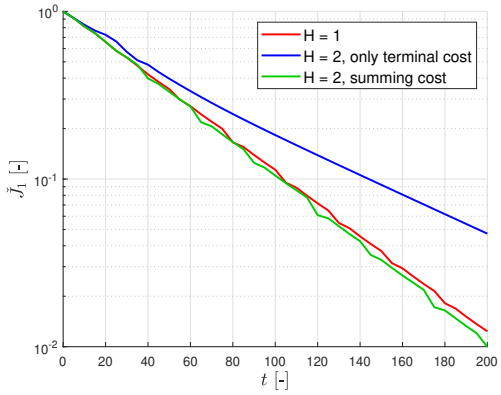

(a) Cost function $\check{J}_1$.

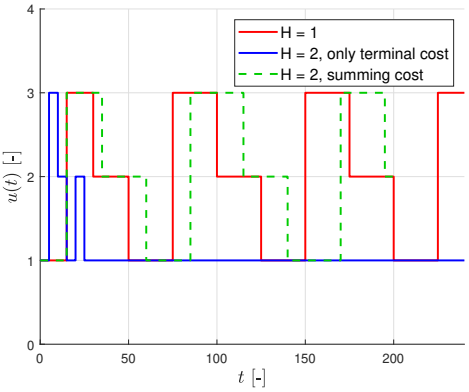

(b) Adaptive reorientation scheme $\mathcal{U}$.

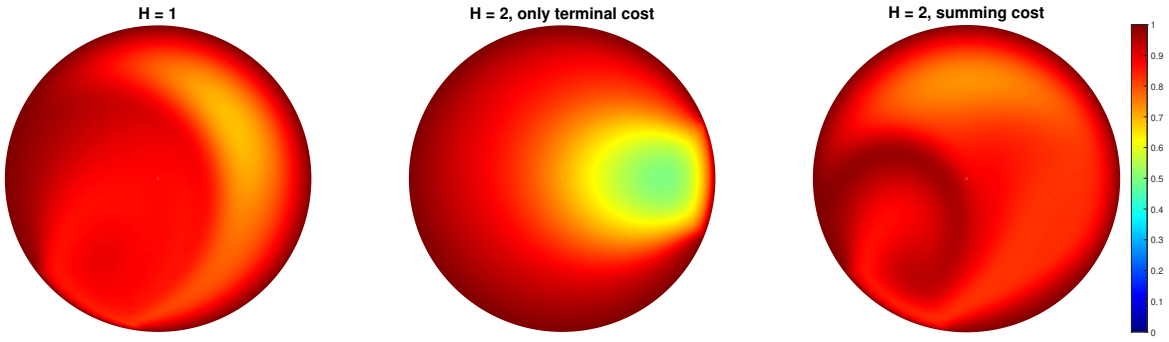

(c) Temperature field in RAM for $t = 90$.

Figure 3.3: Comparison between MPC with only terminal cost with MPC with summing cost for $\gamma = 1$, $J = J_1$, $\tau = 5$ and $Pe = 1000$.

in the RAM for $t = 90$ using area weighting factors $\gamma_m = 1$. Again, MPC with terminal cost is compared with MPC with summing cost. It follows that the MPC controller with $H = 2$ and terminal costs performs poorly. The controller only switches at the start of the simulation, after which aperture 2 is selected for the remaining time. Therefore, only area weighting will be used in this research.

3.2.3 Comparison of L1-norm and L2-norm of temperature as cost function

In Section 3.2.1, it was concluded that J_1 and J_2 would be the best options to use as cost function in the MPC algorithm. In this section, the performance of both metrics is evaluated. The performance is again determined using the transient time (2.41). To make a fair comparison between both cost functions, the same transient time $t_{\epsilon,2}$ is used. To compare both cost functions, the performance indicator ζ is defined as

$$\zeta(Pe, \tau) = \frac{t_{\epsilon,2,J1}}{t_{\epsilon,2,J2}}, \tag{3.4}$$

where subscripts "J1" and "J2" denote simulations with J_1 and J_2 as cost functions used in the MPC algorithm, respectively. The performance can be quantified as follows: $\zeta > 1$ indicates better performance for using J_2 as cost function compared to using J_1 as cost function. Note that in both situations an MPC controller is used with a horizon $H = 3$.

The results are given in Table 3.4. When only clockwise rotation is possible in the RAM, J_1 would be the best option for the cost function for all combinations of Pe and τ, because $\zeta \leq 1$ for all combinations considered in Table 3.4a. In case rotation is possible in both directions, the differences between both cost functions are much smaller. Although in Table 3.4b $\zeta \geq 1$ for all combinations of Pe and τ, the difference in performance is neglectable. This can also be seen when looking at the aperture sequences shown in Figure 3.4. In Figure 3.4b it can be seen that the number of switches is approximately the same; the simulation in which J_1 is used has two fewer switches in the considered time interval. Another thing that stands out is that the controller with J_1 switches between 1 and -2, whereas the controller with J_2 switches between 1 and -3. This, however, does not significantly affect the performance (which is confirmed by ζ, since $\zeta \approx 1$). On the other hand, the performance is different when only clockwise rotation is possible in the RAM as shown in Figure 3.4a. The number of switches differs significantly: using the controller with J_1 as cost function results in three switches, and the controller with J_2 as cost function results in eleven switches. This pattern is also present at other values of Pe and τ, which can be seen in Table B.2. It seems like the many number of switches has a negative impact on the performance. The many number of switches is only present when J_2 is used as the cost function. To find out why this happens, the temperature fields are compared for J_1 and J_2 in Figure 3.5. The MPC controller with $J = J_2$ results in more switches, which can also be seen in Figure 3.4a. In the first few time steps, this results in better performance. However, when looking at the controller with $J = J_1$, it can be seen that a hot plume is spread into the cold part from $t \geq 25$. This results in a fast decay of measure J_2 in the time interval $25 \leq t \leq 35$. On the other hand,

Table 3.4: Comparison of an MPC controller with $J = J_1$ with an MPC controller with $J = J_2$ using ζ as performance indicator. A horizon $H = 3$ is used.

(a) Only clockwise rotation.

ζ		τ		
		3	5	7
Pe	500	0.936	0.919	0.904
	750	0.977	0.906	0.898
	1000	0.973	0.920	0.903
	1250	1.000	0.898	0.892

(b) Rotation in both directions.

ζ		τ		
		3	5	7
Pe	500	1	1	1
	750	1.005	1.005	1.014
	1000	1.015	1	1
	1250	1.012	1.008	1.020

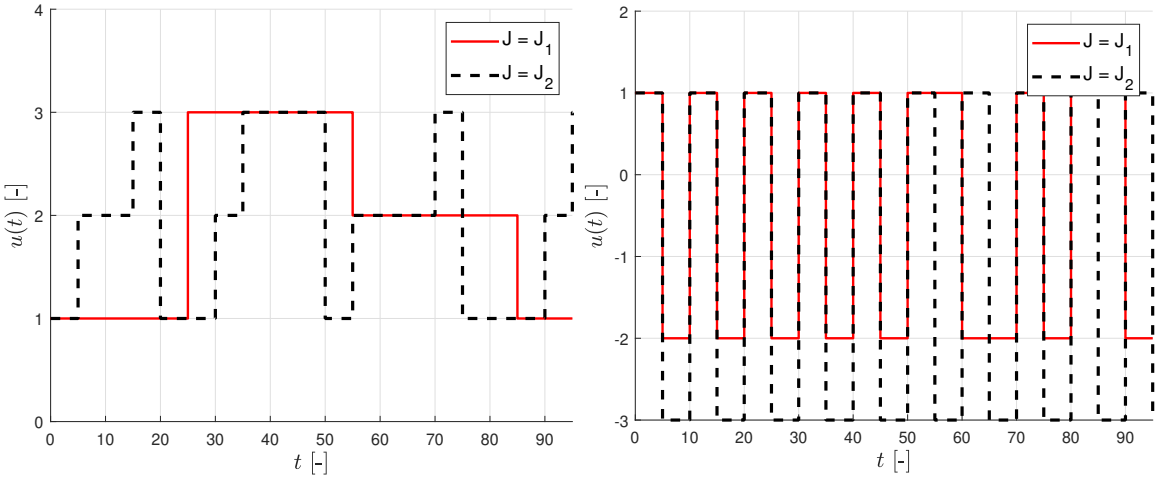

(a) Only clockwise rotation. **(b)** Rotation in both directions.

Figure 3.4: Adaptive reorientation schemes for $Pe = 750$, $\tau = 5$ and using a horizon $H = 3$.

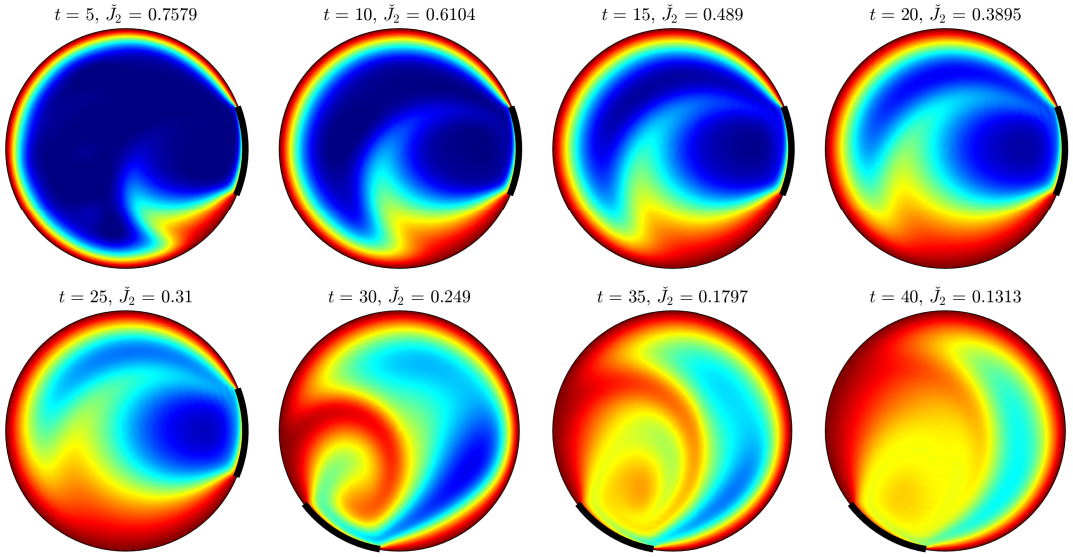

(a) Using an MPC controller with $J = J_1$.

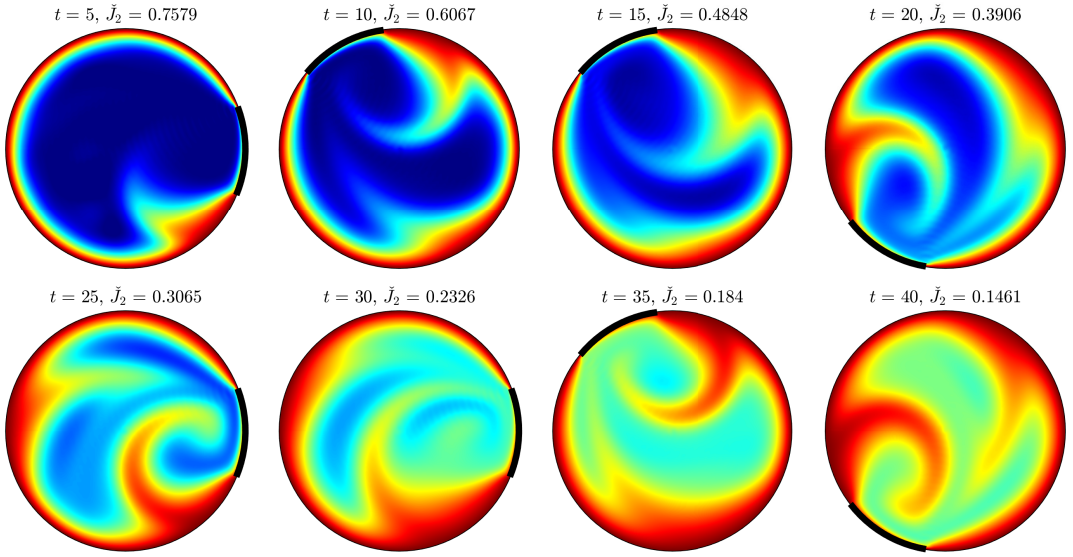

(b) Using an MPC controller with $J = J_2$.

Figure 3.5: Temperature evolution for MPC controllers with different cost functions using $Pe = 750$, $\tau = 5$, $H = 3$, and only clockwise rotation.

the controller with $J = J_2$ forms two smaller plumes, as can be seen from $t \geq 20$. These plumes do not get the time to grow, because the controller switches to another aperture. When comparing the situation at $t = 25$, one large plume can be seen at the bottom for the controller with $J = J_1$. On the other hand, for the controller with $J = J_2$ two plumes can be seen at $t = 25$; one plume at the left side of the RAM and one plume at the bottom right of the RAM. When comparing the situation at $t = 40$, it turns out that forming a large hot plume is more beneficial. This can be seen in the temperature field and the value of $\check{J}_2$ at $t = 40$. Again, it can be seen that the many number of switches does have a negative impact (after some time steps) on the performance. The reason the controller with $J = J_2$ has more

switches than the controller with $J = J_1$ seems to be in the definition of the cost function and relation (2.33). Measure J_2 covers both the energizing (via J_1) and the homogenization (via J_3), whereas J_1 only covers the energizing. From the results in Table 3.4a, it follows that J_1 performs better than J_2. When comparing the temperature fields and the costs, it appears that the difference in performance is made at the start of the simulation. Therefore, it can be concluded that energizing is the most important process at the start of the simulation. This result is intuitive, since it is important to refresh the fluid near the boundaries; otherwise, the temperature gradient at these boundaries lessens and heat transfer slows [13]. On the other hand, when using J_2 as cost function, also the homogenization process is considered at the start of a simulation and this results in more switches. This is verified using Figure 3.6, in which it can be seen that the global heterogeneity (indicated with J_3 on the y-axis) is lower for $J = J_2$ compared to $J = J_1$ in the first 40 time units. Moreover, the normalized energy content J_1 is lower for $J = J_1$ compared to $J = J_2$ in the considered time interval. In short, the emphasis of controller $J = J_1$ is on energizing, whereas the emphasis of controller $J = J_2$ is on both energizing and homogenization. It follows, however, that emphasizing energizing at the start of the simulation ultimately also leads to better homogenization.

3.3 Larger horizon

An important parameter in the MPC algorithm is the horizon. In general, it is expected that a larger horizon results in better performance. Suppose only clockwise rotation is possible in the RAM. With N apertures, N different control actions are possible at each discrete time step. Suppose an MPC controller with a horizon of $H = 3$ is compared with an MPC controller with a horizon of $H = 1$. At each iteration, N^H different options are considered in the MPC algorithm. The solution of the controller with $H = 1$ is always present in the solution set of the controller with $H = 3$, which suggests that a controller with a larger horizon will never perform worse than a controller with a smaller horizon. However, as discussed in Section 2.2.3, this is not always the case. Therefore, it is important to investigate the influence of the horizon on the performance of the 2D RAM. Another essential aspect related to the horizon is the computation time. In Figure 1.3 it was shown that the computation time increases exponentially with a larger horizon. When dealing with real-time systems, it is desired that the MPC algorithm can run fast, so the algorithm can do its predictions on time and can use the latest temperature measurement. In short, if a

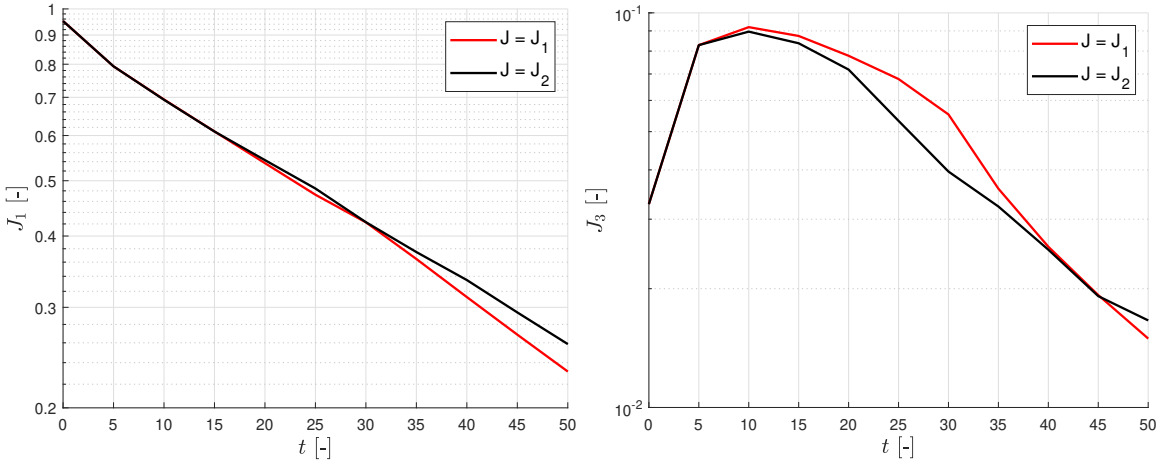

Figure 3.6: Comparison of performance measures J_1 and J_3 for the simulations with $J = J_1$ and $J = J_2$ for $Pe = 750$, $\tau = 5$ and only clockwise rotation.

larger horizon results in better performance, does this outweigh the computational costs? In this section, only the performance part is considered. The comparison will be made between using $H = 1$ and $H = 3$. When it proves beneficial to use a larger horizon (i.e., $H = 3$), it is worth investigating the effect of even larger horizons as well. For these situations, the importance of computational costs is more important.

Furthermore, no perturbations are acting on the system in the following simulations. When using a horizon $H = 1$, $N = 3$ temperature fields are predicted using the spectral model. One of these predicted temperature fields (determined by the cost function J_i) is the temperature field in the next time step. For a larger horizon (i.e., $H > 1$), an optimal aperture sequence is determined at each time step, from which only the first decision is implemented. Although there are no perturbations, it is still possible that the optimal sequence changes in the next step of the algorithm.

3.3.1 Rotation in one direction

To compare the performance of controllers with different horizons, again the transient time (2.41) is used. This enables us to define the performance indicator χ as

$$\chi(Pe, \tau) = \frac{t_{\epsilon,2,H1}}{t_{\epsilon,2,H3}}, \tag{3.5}$$

where subscripts "H1" and "H3" denote simulations with a horizon of $H = 1$ and $H = 3$, respectively. Note that the transient time $t_{\epsilon,2}$ (based on J_2) is used to compare the performance. In the simulations, both J_1 and J_2 will be used as cost functions. When $\chi > 1$, the transient time for the MPC controller with $H = 3$ is shorter than the transient time for the MPC controller with $H = 1$, i.e., the performance is better for the larger horizon controller. In the considered parameter range, an MPC controller with $H = 1$ is better than a conventional periodic scheme as shown in Lensvelt *et al.* [14]. This allows us to compare the performance of a larger horizon controller (in this case, $H = 3$) with a controller with $H = 1$. The results are given in Table 3.5 in case only clockwise rotation is possible. It has to be mentioned that no conclusions can be drawn over which cost function is better. Table 3.5 shows only the performance indicator χ (3.5) and does not compare J_1 and J_2. When J_1 is used as cost function, a larger horizon is better for all the combinations of τ and Pe considered. Furthermore, the performance increases the most for small values of τ. When J_2 is used as cost function in simulations, it turns out that an MPC controller with a horizon $H = 1$ is better for $\tau = 5$. It is interesting to see that for this value of the aperture activation time, a controller with a larger horizon performs worse. This motivates a more in-depth analysis of such a case, in which the parameters $Pe = 1000$, $\tau = 5$, and $J = J_2$ will be used. To this end, the temperature evolution, the performance indicator $\check{J}_2$,

Table 3.5: Comparison of an MPC controller with $H = 1$ with an MPC controller with $H = 3$ using χ as performance indicator. Only clockwise circulations are considered here.

(a) $J = J_1$.

χ		τ		
		3	5	7
Pe	500	1.164	1.028	1.027
	750	1.382	1.092	1.011
	1000	1.492	1.071	1.012
	1250	1.283	1.059	1.036

(b) $J = J_2$.

χ		τ		
		3	5	7
Pe	500	1.113	1.000	1
	750	1.053	0.911	1.028
	1000	1.065	0.932	1.015
	1250	1.024	0.910	1.005

and the switching sequence are shown in Figure 3.7 and Figure 3.8. When comparing both situations, one can observe that the MPC controller with $H = 3$ performs better on the time interval $25 \leq t \leq 35$. However, from $t \geq 40$ the MPC controller with $H = 1$ performs better. Another interesting observation is the number of aperture switches in the considered time interval; the larger horizon controller has more switches, which results in the forming of different thermal plumes. In this case, however, it seems more beneficial to form one large thermal plume (from $t = 10$ until $t = 30$ for the MPC controller with $H = 1$) and subsequently send this plume into the cold region ($t \geq 35$). Moreover, it turns out that the MPC controller with $H = 3$ puts more emphasis on homogenization compared to the MPC

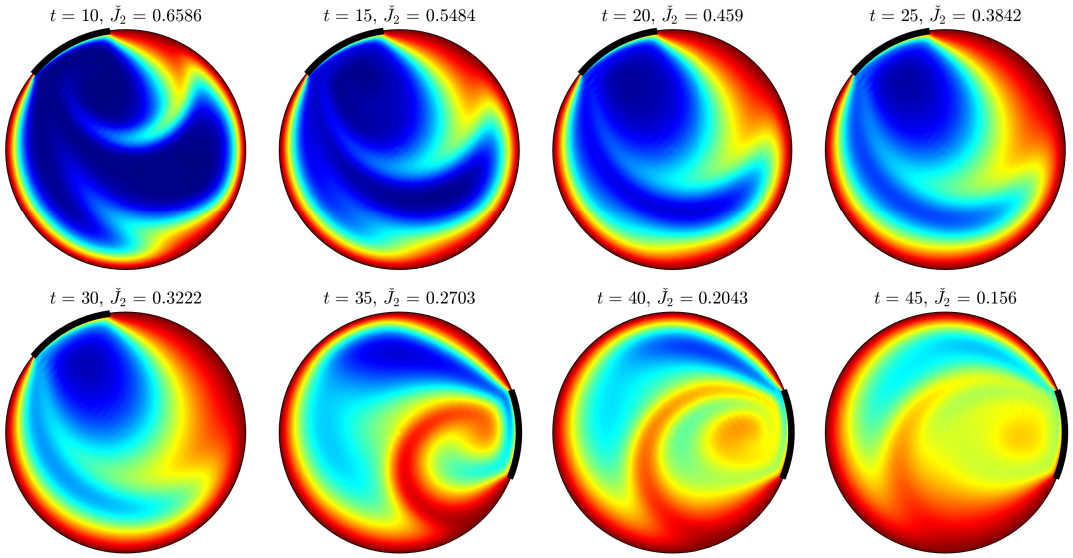

(a) Using an MPC controller with a horizon $H = 1$.

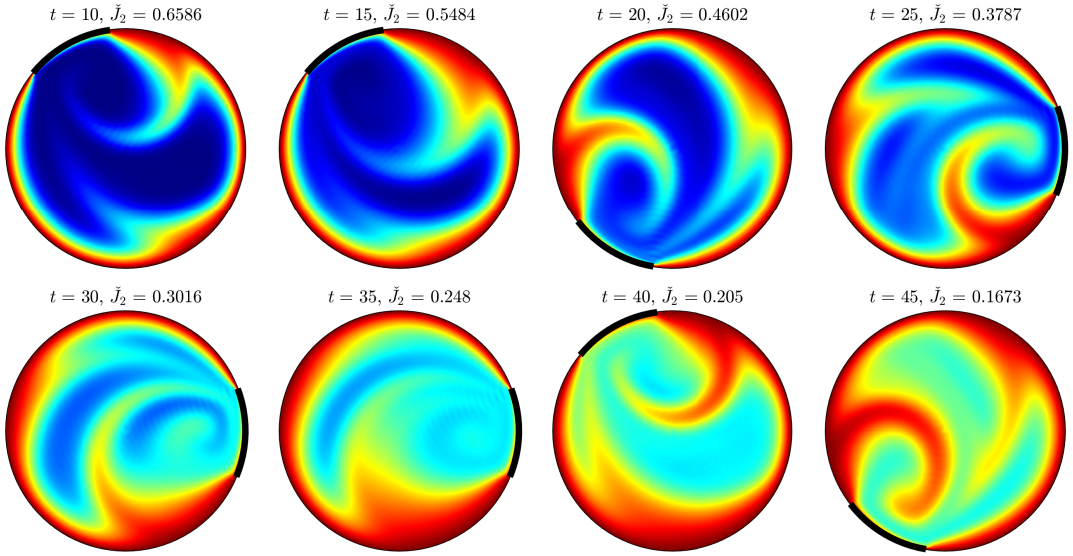

(b) Using an MPC controller with a horizon $H = 3$.

Figure 3.7: Temperature evolution for MPC controllers with different horizon lengths using $Pe = 1000$, $\tau = 5$, $J = J_2$, and only clockwise rotation.

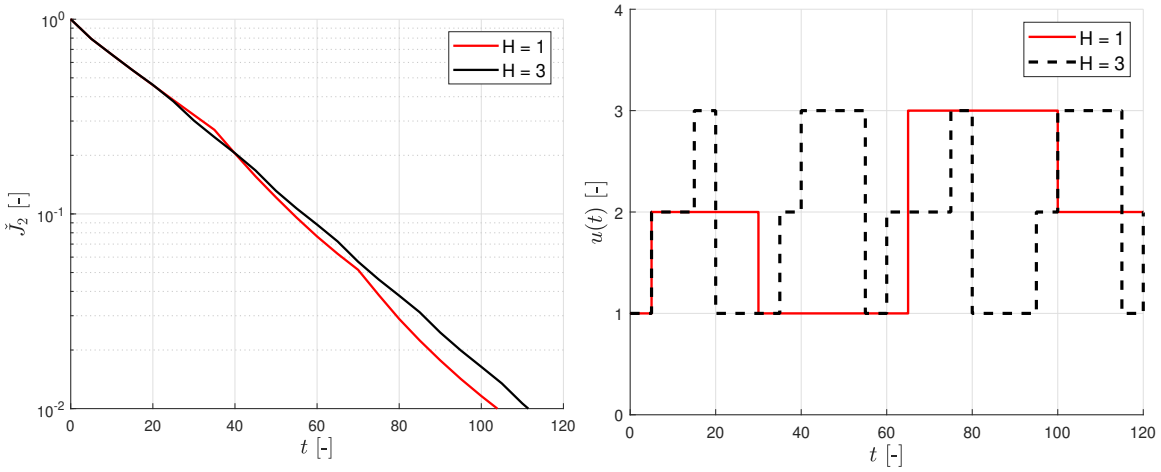

(a) $\check{J}_2$ **(b)** Adaptive reorientation scheme $\mathcal{U}$.

Figure 3.8: Performance for MPC controllers with different horizon length using $Pe = 1000$, $\tau = 5$, $J = J_2$ and only clockwise rotation.

controller with $H = 1$ when analyzing the global heterogeneity J_3. In short, it would be better to activate the same aperture for a longer time, instead of switching between different apertures. This is the same observation as done in Section 3.2.3. The fact that this only applies to this set of parameters ($Pe = 1000$, $\tau = 5$, and $J = J_2$) is crucial to remember. For the other cases in Table 3.5b where $\chi < 1$, however, the same observations are made. The transient times and the number of switches are shown in Table B.2. When comparing the transient times t_ϵ for a certain Peclet number, it turns out that a relatively high transient time corresponds with a high number of switches. This is the same as seen before in the specific situation in Figure 3.7. While for J_1 no problems occur for a larger horizon, for J_2 the number of switches increases in some situations for a larger horizon resulting in a worse performance. When using a controller with $H = 1$, the system only switches when it has an immediate increase in performance. For $H = 3$, however, the system switches to increase the performance after 3 steps. This results in more switches which has a negative influence on performance. Possible solutions to reduce the number of switches are discussed in Chapter 4.

In Figure 3.9, χ is plotted over the aperture activation time τ for $Pe = 750$. These results correspond with the results in Table 3.5. For J_1, $\chi > 1 \; \forall \; \tau$ and χ decreases when τ increases. This result is intuitive; the larger the activation time τ, the lesser the improvement of increasing H will be. On the other hand, no correlation is present between χ and τ for J_2. This again shows that only for MPC using $J = J_1$ it is beneficial to use a larger horizon for rotation in one direction. It is not possible to find the optimal aperture activation time using Figure 3.9, since χ is shown, which compares the performance of an MPC controller with $H = 1$ with an MPC controller with $H = 3$. The influence of the aperture activation time on performance will be discussed in Section 3.4.

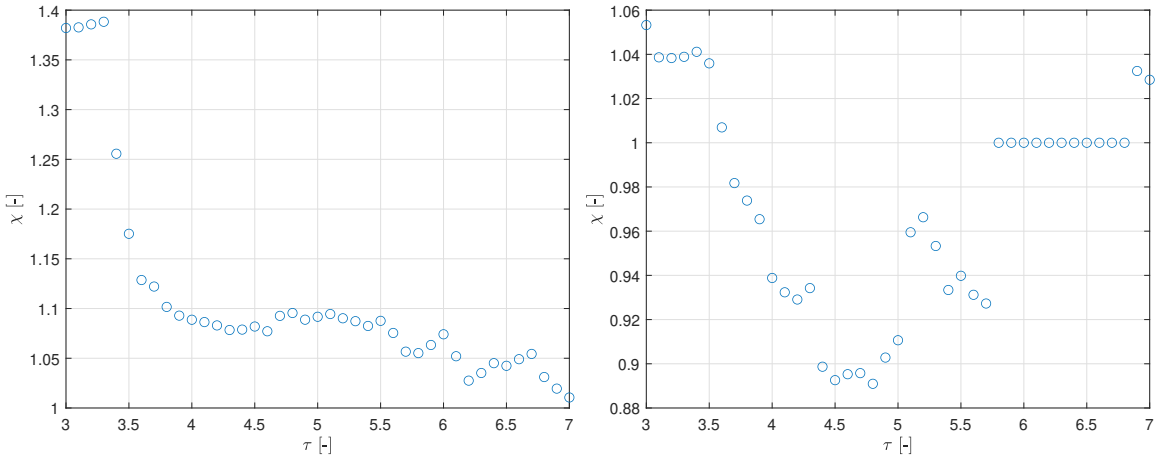

(a) $J = J_1$. **(b)** $J = J_2$.

Figure 3.9: Comparison of an MPC controller with $H = 1$ with an MPC controller with $H = 3$ using χ as performance indicator for $Pe = 750$. This is done for both an MPC controller with $J = J_1$ and an MPC controller with $J = J_2$. Only clockwise circulations are considered here.

3.3.2 Rotation in two directions

The same procedure can be followed as done for rotation in one direction. This gives us the results in Table 3.6. The first noticeable thing is that $\chi \geq 1 \ \forall(Pe, \tau)$. In particular for an aperture activation time $\tau = 3$ the performance increases. Moreover, some combinations of Pe and τ result in the same performance for the two different controllers (i.e., $\chi = 1$). To understand this, it is important to see the aperture sequence when two rotation directions are allowed. In Figure 3.10 and Figure 3.11 the temperature evolution and the adaptive reorientation schemes are given, respectively, for two different situations, both for $J = J_2$. Both situations show a way to increase performance. In Figure 3.11a the controller with $H = 1$ determines to change the arcs moving in opposite directions, while it is better to keep the same arcs moving in the opposite direction. In Figure 3.11b, the controller with $H = 3$ sometimes chooses to move one certain arc longer than the activation time τ, while the controller with $H = 1$ continuously keeps switching. In particular, the last part (holding one aperture for a longer time) happens significantly more for the cases where $\zeta > 1$. To investigate what is happening here, the temperature fields are plotted for the situation with $Pe = 1250$ and $\tau = 3$ in Figure 3.10. The MPC controller with a horizon $H = 1$ results in switching between arcs 1 and 3 at every time step τ, whereas the MPC controller with a horizon $H = 3$ results in switching between arcs 1 and 3 at every two time steps (2τ).

Table 3.6: Comparison of an MPC controller with $H = 1$ with an MPC controller with $H = 3$ using χ as performance indicator. Two rotation directions are possible.

(a) $J = J_1$.

χ		τ		
		3	5	7
Pe	500	1.034	1	1
	750	1.044	1.015	1
	1000	1.083	1	1
	1250	1.169	1.018	1

(b) $J = J_2$.

χ		τ		
		3	5	7
Pe	500	1.041	1	1
	750	1.049	1.020	1.014
	1000	1.116	1	1
	1250	1.183	1.012	1.020

Holding the arcs for a longer time results in faster homogenization (i.e., the cold islands are destroyed faster) and therefore in a better performance. Besides the temperature fields in Figure 3.10, this also follows from the values of $\check{J}_2$, which are lower in case the arcs are held for a longer period of time, resulting in better performance. The conclusion that can be drawn from these simulations is that a larger horizon results in better performance when rotation is possible in two directions. Although this has only been tested for $H = 2$ and $H = 3$, the expectation is that an even larger horizon will perform better for small τ.

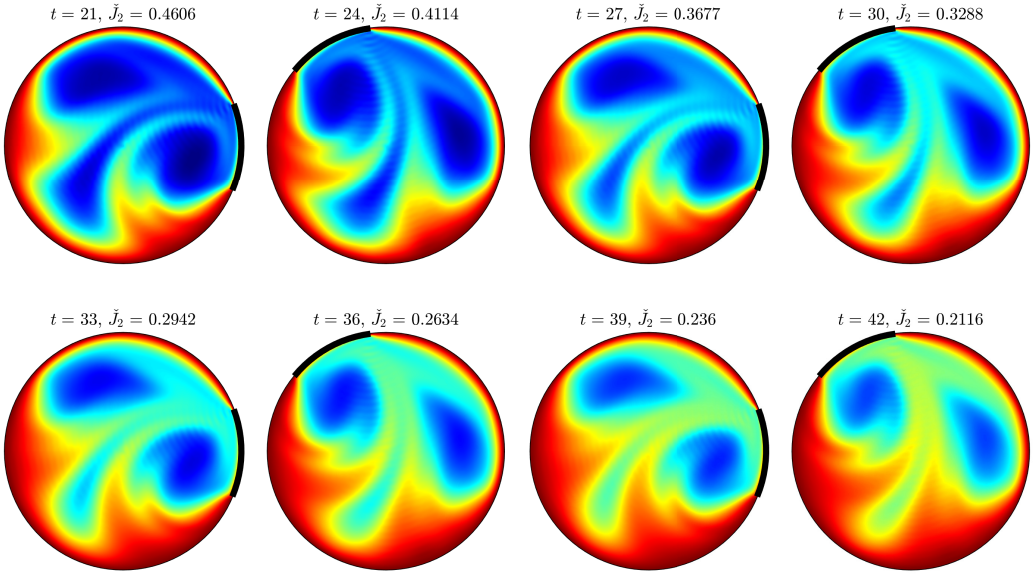

(a) Using an MPC controller with a horizon $H = 1$.

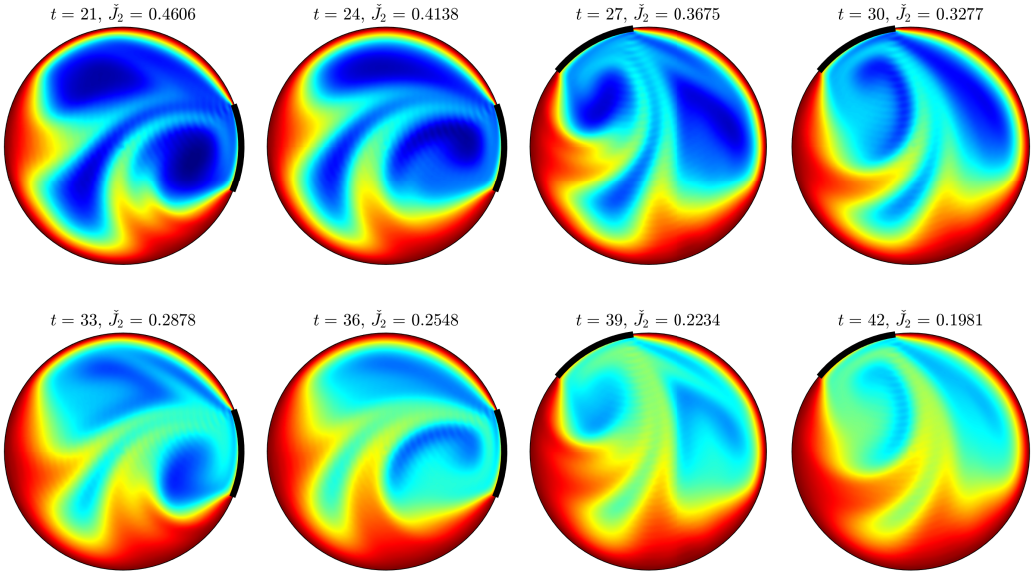

(b) Using an MPC controller with a horizon $H = 3$.

Figure 3.10: Temperature evolution for MPC controllers with different horizon lengths using $Pe = 1250$, $\tau = 3$, $J = J_2$, and both directions of rotation.

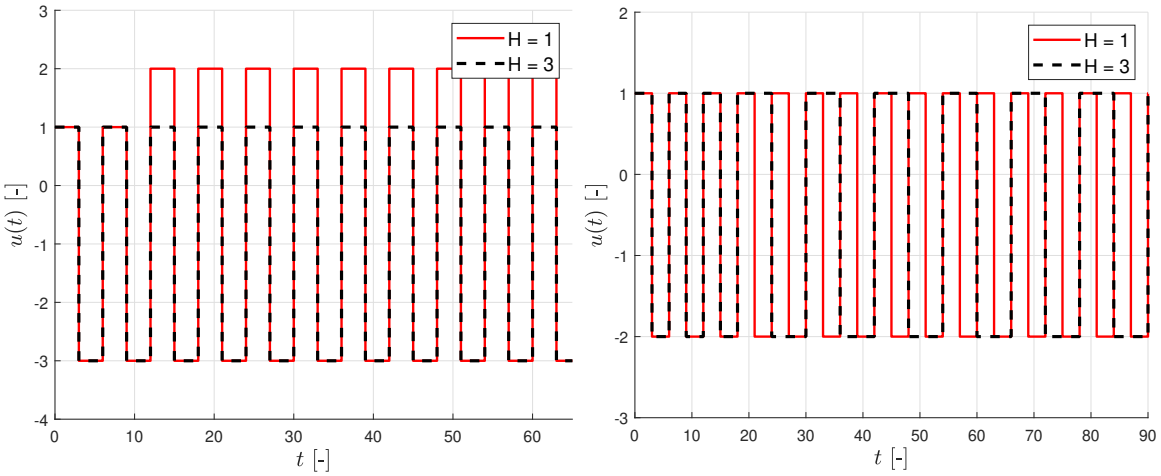

(a) $Pe = 500$. **(b)** $Pe = 1250$.

Figure 3.11: Adaptive reorientation schemes for $\tau = 3$, $J = J_2$ and two rotation directions.

3.4 Influence of aperture activation time

As already seen before, the aperture activation time does have a relatively large influence on performance. This is, for example, shown in Figure 3.9 and Table B.2. However, it is hard to draw conclusions based on Figure 3.9, since two controllers with different horizons are compared here. Given the fact that more control actions are possible with a smaller activation time, the hypothesis is that in general a smaller activation time results in better performance provided the horizon is large enough. As an example, consider a horizon $H = 1$ and an activation time $\tau = 5$. It is expected that a controller with a horizon $H = 2$ and an activation time $\tau = 2.5$ will at least achieve the same performance as the first controller, because the same prediction time is considered in both controllers. However, since the second controller allows the aperture to change one more time, it is expected this controller will perform better (or at least not perform worse since the solution of the first controller is also present in the solution set of the second controller). However, choosing the aperture activation time too small results in poor performance [37]. As discussed before, a lower bound $\tau \geq 3$ is used in this research.

3.4.1 Rotation in one direction

To compare the performance for different values of the aperture activation time, the transient time is determined using (2.41). In Section 3.2.3 it was concluded that for clockwise rotation of the RAM J_1 would be the best option as cost function. In this section, the performance is investigated with respect to the aperture activation time. However, both cost functions J_1 and J_2 used in the MPC algorithm are considered in this aspect. Moreover, in Section 3.3.1 it was concluded that a larger horizon does not necessarily lead to better performance. Therefore, it is chosen to determine a minimum transient time $t_{\min}$, which is defined as

$$t_{\min} = \min(t_{\epsilon,2,H1}, t_{\epsilon,2,H3}), \tag{3.6}$$

where $t_{\epsilon,H1}$ and $t_{\epsilon,H3}$ are the transient times t_ϵ using an MPC controller with a horizon of $H = 1$ and $H = 3$, respectively. In Figure 3.12 the minimum transient times are shown for different values of the aperture activation time. Since $\chi > 1 \ \forall \ \tau$ when $J = J_1$, it follows that $t_{\epsilon_2,H1} > t_{\epsilon_2,H3}$. This means that $t_{\min} = t_{\epsilon_2,H3}$ if J_1 is used as cost function in the MPC algorithm. When looking at Figure 3.12a, it can be concluded that the aperture activation

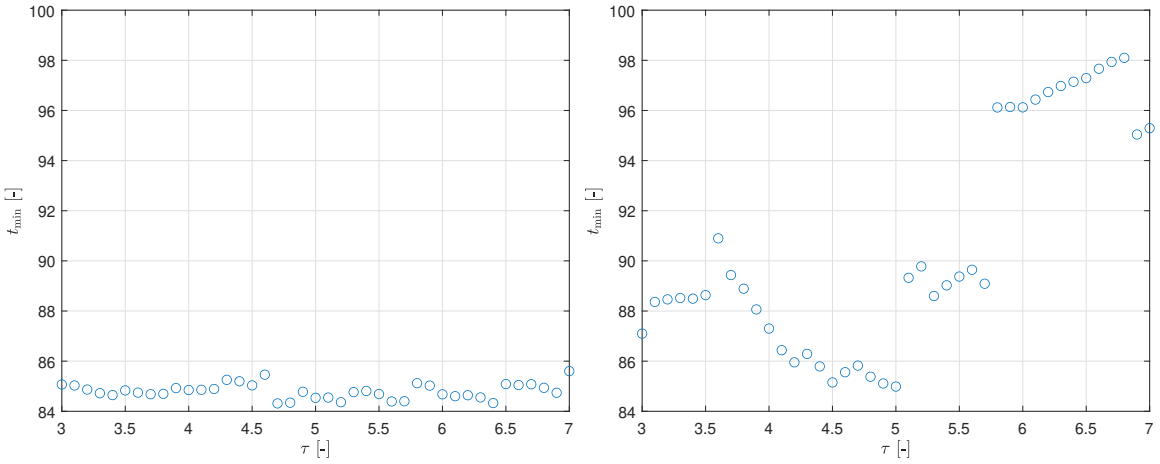

(a) J_1. **(b)** J_2.

Figure 3.12: Transient times for MPC controllers with different aperture activation times $Pe = 750$ and only clockwise rotation.

time does not have a large influence on the transient time (i.e., on performance) in case J_1 is used as cost function. Any aperture activation time between the values considered would be a good option. Also for other Péclet numbers, the influence of the aperture activation time on performance is small. See Table B.2b for more results. On the other hand, when J_2 is used as cost function as shown in Figure 3.12b, it can be concluded that the aperture activation time has a large influence on the performance. For $Pe = 750$, it seems an aperture activation time of $\tau \approx 4.5$ is optimal. Also for other Pe, shown in Table B.2, an activation time of $\tau \approx 5$ seems to be optimal. Unfortunately, the relation between the aperture activation time and the performance is unclear and therefore, the optimal aperture activation time $\tau \approx 5$ cannot be motivated. The jumps in $t_{\min}$ illustrated in Figure 3.12b at $\tau = 5$ and $\tau = 5.7$ cannot be explained. These jumps in $t_{\min}$ occur both by jumps in $t_{\epsilon,2,H1}$ and jumps in $t_{\epsilon,2,H3}$ In conclusion, it can be stated that an aperture activation time $\tau \approx 5$ in general results in a good performance for the RAM when only clockwise rotation is possible.

3.4.2 Rotation in two directions

When the RAM is able to move the fluid in both directions (i.e., clockwise and counterclockwise), the transient time is smaller for all combinations of Pe and τ. Furthermore, as shown in Section 3.3.2, a larger horizon will result in a better (or at least not worse) performance, since $\chi \geq 1 \forall (Pe, \tau)$ for rotation in two directions. To compare the performance for different values of τ, the transient time is used, which is determined using the MPC controller with a horizon $H = 3$. In Figure 3.13, the transient times are plotted for both J_1 and J_2 as cost functions. For both cost functions, using an aperture activation time of $\tau \approx 6.5$ would result in the best performance in case $Pe = 750$. When looking at the transient times for other Pe in Table B.3, it is concluded that $\tau = 7$ performs the best. As already seen before, for two circulation directions the adaptive reorientation scheme almost always consists of switching between two arcs that move in opposite directions (Figures 3.4b and 3.11). This implies that the difference in performance is not always the cause of the control algorithm. As an example, observe the transient times in Figure 3.13b for $4.1 \leq \tau \leq 7.0$. The transient times show a declining trend for a larger τ. However, for all these values of τ, the aperture sequence is the same (i.e., switching between arcs 1 and 3). This shows an optimum aperture activation time exists, which is independent of the control algorithm for $Pe = 750$.

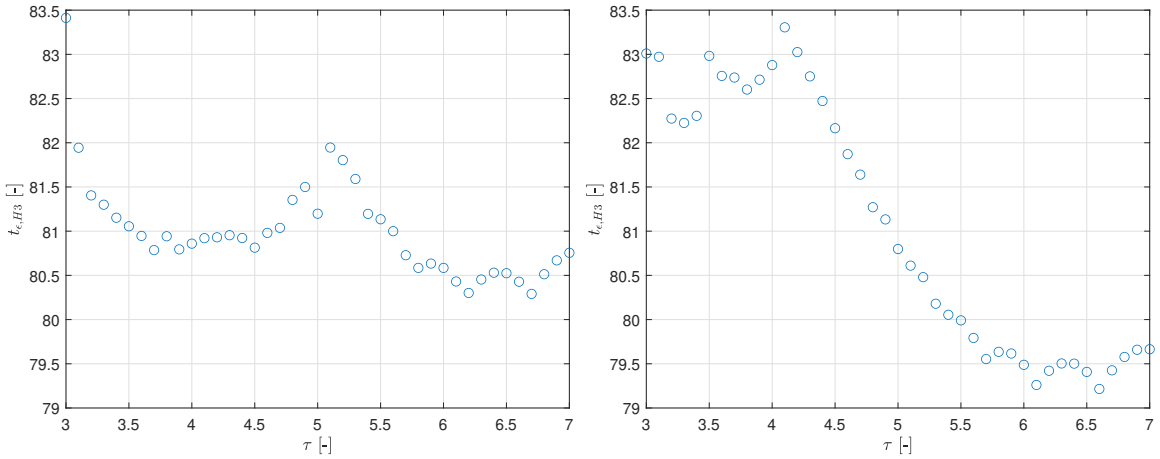

(a) J_1. **(b)** J_2.

Figure 3.13: Transient times for MPC controllers with different aperture activation times $Pe = 750$ and both rotation directions.

3.5 Comparing rotation in one and two directions

In this section, the performance of a 2D RAM that can rotate in one direction is compared with a 2D RAM that can rotate in two directions. To compare this properly, the performance indicator κ is defined as

$$\kappa(Pe, \tau) = \frac{t_{\epsilon,\omega 1}}{t_{\epsilon,\omega 2}}, \tag{3.7}$$

where subscripts "ω1" and "ω2" denote simulations with one circulation direction and two circulation directions, respectively. When $\kappa > 1$, the performance is better for the RAM with two circulation directions. The indicator κ is shown in Table 3.7 for the considered parameter range of Pe and τ. From these results, it can be concluded that rotation in two directions is guaranteed to lead to better performance. This is the expected result, since the number of different control actions is higher for the RAM with two circulation directions. In the sections before, however, it is shown that the optimal cost function, aperture activation time, and horizon depend on the rotations possible in the RAM.

Table 3.7: Comparison of one circulation direction with two circulation directions in the RAM using κ as performance indicator. an MPC controller with $H = 3$ is used.

(a) $J = J_1$.

κ		τ		
		3	5	7
Pe	500	1.066	1.038	1.053
	750	1.020	1.041	1.060
	1000	1.047	1.068	1.082
	1250	1.107	1.054	1.058

(b) $J = J_2$.

κ		τ		
		3	5	7
Pe	500	1.138	1.131	1.165
	750	1.049	1.155	1.196
	1000	1.091	1.161	1.198
	1250	1.121	1.182	1.209

3.6 Conclusion

This section repeats and combines the results from Sections 3.2 - 3.5 to achieve the best performance for the RAM.

A general conclusion that can be drawn is that rotation in two directions significantly improves the temperature homogenization in the RAM compared to only one rotation direction. This is independent of the used cost function, horizon, and aperture activation time.

In Section 3.2.1 it was concluded that the performance indicators J_1 and J_2 would be the most suited candidates as cost functions. The difference in performance for these norms is in general small, which motivated a more elaborate investigation of these cost functions in Section 3.2.3. Moreover, as discussed in Section 3.2.2, it is more beneficial to sum the costs in the cost function than to take the terminal cost. However, a few things about this conclusion have to be noted. The conclusion is based on simulations with an MPC controller with a horizon $H = 3$. For a larger horizon, it could be the case that the difference between summing and terminal costs is negligible, or even that a terminal cost would be better. In addition, the costs can be summed in different ways, but in this report, the costs are summed equally.

When only one circulation direction is possible in the RAM, J_1 would be the best option for the cost function, because $\zeta \leq 1$ for all combinations considered in Table 3.4a. The controller with $J = J_1$ results in significantly fewer switches than the controller with $J = J_2$, which has a positive effect on the performance. Moreover, a larger horizon (i.e., $H = 3$) also results in a shorter transient time as shown in Table 3.5a. Furthermore, it can be concluded that the influence of the aperture activation time is small when J_1 is used as cost function in the MPC controller with $H = 3$. An activation time of $\tau \approx 5$ is recommended.

When two directions of rotations are possible, the switching sequence is often periodic, regardless of the cost function. Because of this, the difference in performance is small for J_1 and J_2. However, since $\zeta \geq 1$ for all combinations of Pe and τ as shown in Table 3.4b, it is recommended to use J_2 as cost function. Furthermore, it is better to use a larger horizon since $\chi \geq 1$ in the considered parameter range of Pe and τ. The performance improvement is the highest for a small activation time τ. Finding the optimal aperture activation time is more difficult. It is recommended to analyze the influence of the aperture activation time for the Péclet number used in the application. As a guideline, an aperture activation time of $\tau \approx 6.5$ seems a good starting point.

From the conclusions above, it follows that a larger horizon proves to be beneficial in most cases. Note that the maximum horizon considered in this chapter is $H = 3$. It is interesting to investigate whether an even larger horizon increases the performance even more. A reduced model is required for this analysis, since the number of predictions grows exponentially with the horizon as shown in Figure 1.3. This subject is discussed in Chapter 4.

In some cases (e.g., using $J = J_2$, $\tau = 5$, and one circulation direction), using a larger horizon has a negative influence on the performance. As discussed, this is due to the many aperture switches in the process. In Chapter 4, some options are discussed to reduce the number of switches and thus improve the performance.

Chapter 4

Outlook and further possible improvements

In this chapter, further possible improvements are discussed based on the results from Chapter 3. In the previous chapter, the maximum horizon considered was $H = 3$. It is interesting to investigate whether a larger horizon increases the performance even more, however, a larger horizon increases the computation time enormously. Using a RAM that can circulate the flow in two directions and an MPC controller with $H = 5$, 9.330 temperature predictions are needed as shown in Figure 1.3. This corresponds with $\mathcal{O}(10^{11} - 10^{12})$ flops for the temperature predictions when using the spectral model (calculations are discussed in Section 4.1). A modern computer processor can operate in the range of $\mathcal{O}(10^9 - 10^{10})$ flops. For practical applications, however, it is preferred to do the temperature predictions just before the calculation of the new control action. This allows the last temperature measurement to be included in the control algorithm. Therefore, a larger horizon (i.e., $H \geq 5$) is not possible using the spectral model given in Section 2.1.3. This motivates the study of a reduced model, which will be discussed in this chapter. Furthermore, in Chapter 3 it was concluded that in general many aperture switches affect the performance negatively, in particular in the case of one rotation direction. In this chapter, some ideas will be presented to increase the performance of the system, with some methods based on limiting the number of switches.

4.1 Reduced model

As discussed in [14], the compact model involves $2QM$ flops per prediction, where $Q = 1.000$ and $M = N_r \times N_\theta + 1 = 47.681$. The conventional method (i.e., FVM method), on the other hand, involves $2NM^2$ flops, where $N = \tau/\Delta t \sim \mathcal{O}(10^2 - 10^3)$ is the number of steps for time interval τ. In Figure 1.3 it is shown that the number of predictions increase exponentially for a larger horizon. 9.330 predictions are needed when using an MPC controller with $H = 5$ and a RAM with two circulation directions, resulting in $9.330 \times 2 \times 1.000 \times 47.681 = \mathcal{O}(10^{11} - 10^{12})$ flops. To make the control strategy also viable for larger horizons, a reduced-order model of the RAM is required. In [22], it was shown that the reorientation scheme obtained with a FVM-based method coincides with the reorientation scheme found via the compact model, which is based on the spectral method. In this section, the FVM model will be used for model reduction. There are two main reasons to use the FVM model over the spectral method for model reduction. First, the eigenvalues from the FVM model have a clear physical meaning,

since they are determined using the system matrix $\mathbf{A}_k$ in (2.11). These eigenvectors and eigenvalues provide dynamic properties such as natural modes and natural periods. The eigenvalues determined in the spectral method, on the other hand, are determined using the approach in [26] and are based on diffusion eigenfunctions. However, it is desired to keep the slowest-decaying eigenmodes of the advection-diffusion operator during model reduction, since they best capture the thermal behavior. This favors model reduction based on the FVM model over the spectral model. Second, the system matrix $\mathbf{A}_k$ can be determined easily using FVM schemes for other applications than the RAM, whereas the spectral method is designed for the RAM.

4.1.1 Eigenmode analysis

The system matrix $\mathbf{A}_1$ of the base flow (2.11) is obtained by spatial discretization of (2.5) using a conventional FVM scheme. As a next step, the dominant eigenvalue-eigenvector pairs of system matrix $\mathbf{A}_1$ are determined using the built-in function `eigs` in MATLAB, as already done in [22]. The function `eigs` is used instead of the function `eig`, since $\mathbf{A}_1$ is a large $(M \times M)$, sparse matrix. The real part $\mathrm{Re}(\lambda_m)$ of the eigenvalues are shown in Figure 4.1 for $Pe = 1000$. As discussed in Section 2.1.3, each eigenmode m has a characteristic time scale $\tau_m = -1/\,\mathrm{Re}(\lambda_m)$. For the case in Figure 4.1 with $Pe = 1000$, the slowest-decaying mode has a characteristic time scale $\tau_0 = 75.0$. To reduce the computation time, the number of eigenvalue-eigenvector pairs should be reduced to save computation time. In this report, this is done by considering all eigenvalue-eigenvector pairs satisfying $\tau_m \geq 0.01\tau_0$, i.e., the eigenvalue-eigenvector pairs with $\tau_m < 0.01\tau_0$ will be neglected. The value 0.01 is based on Figure 4.1; using this value will result in a shorter computation time (as discussed below), without losing too much accuracy. In this method, the truncation is based on the intrinsic time-scale of the RAM dynamics, whereas the truncation for the approach described in Section 2.1.3 is based on the time-scale of activation (the modes with $\tau_m/\tau \ll 1$ are neglected in Section 2.1.3). Using $\tau_m \geq 0.01\tau_0$ results in $m \approx 167$ modes for $Pe = 1000$. For other Péclet numbers (i.e., $Pe = 500, 750, 1250$), approximately the same number of modes is found.

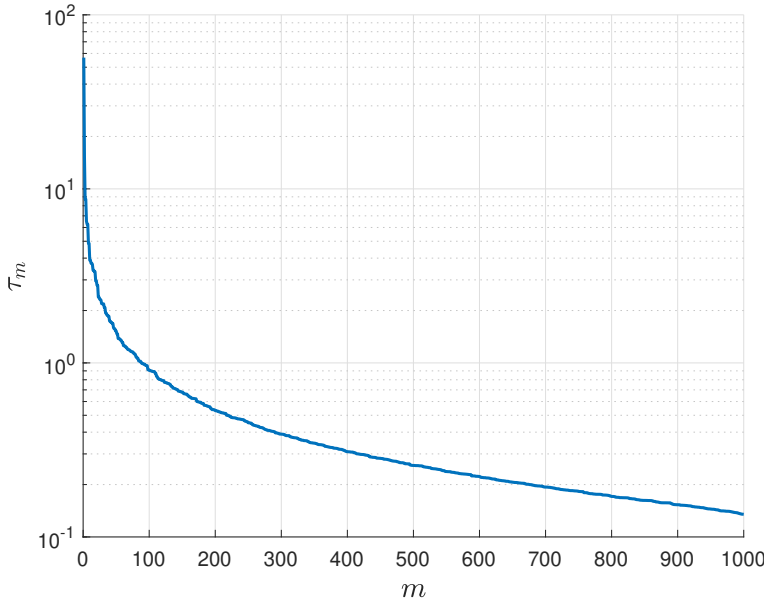

Figure 4.1: Characteristic time τ_m corresponding to eigenvalue λ_m using a FVM scheme for $Pe = 1000$.

Therefore, it is decided to take $S = 200$ modes from now on. Eigendecomposition of matrix $\mathbf{A_1}$ results in eigenvector matrix $\mathbf{V}$ and diagonal eigenvalue matrix Λ. The temperature can now be approximated as

$$\hat{\mathbf{T}}_k(t_{n+1}) = \hat{\mathbf{V}}_k \mathrm{e}^{\hat{\mathbf{\Lambda}}_k \tau} \mathbf{G}_k \mathbf{T}(t_n), \quad \mathbf{G}_k = (\hat{\mathbf{V}}_k^\top \hat{\mathbf{V}}_k)^{-1} \hat{\mathbf{V}}_k^\top, \quad \hat{\mathbf{\Lambda}}_k = \mathrm{diag}(\lambda_0, \ldots, \lambda_S), \tag{4.1}$$

where symbol $\hat{\cdot}$ indicates approximate quantities based on the truncation with $S = 200$ modes. The computational costs of the predictions are determined by the number of elements and the number of modes (Q is the number of modes in the compact model and S is the number of modes in the reduced model). For the same number of elements M as in the spectral model, the reduced model involves $2SM$ flops per prediction, yielding $Q/S = 1000/200 = 5$ as relative computational effort compared to the compact model.

4.1.2 Performance of the reduced model

In this section, the performance of the reduced model is compared with the spectral model used for the simulations in Chapter 3. In the previous chapter, the spectral model was used for both the actual temperature evolution and the temperature predictions. In this section, the temperature predictions are done using the reduced model described in Section 4.1.1. The actual temperature evolution, however, is simulated using a full FVM model, not with the reduced model. In short, the following situations are compared:

- Using the spectral model (2.16) for both the actual temperature evolution and the temperature predictions (as done in Chapter 3);
- Using a full FVM model for the actual temperature evolution and using the reduced model for the temperature predictions. The reduced model is never used to simulate the actual temperature evolution.

To make a fair comparison between both situations, the actual temperature evolution should be approximately the same for the spectral model and the full FVM model, which is investigated in [22]. As discussed in [22], the evolution of J_2 determined with the spectral method slightly deviates from the full FVM-based model, which need to be attributed to different characteristics of the numerical schemes (e.g., FVMs are known to suffer from numerical diffusion [40], which increases the homogenization rate in the simulations artificially). This is confirmed in this study, since measure $\check{J}_2$ obtained with the full FVM model is slightly below $\check{J}_2$ of the spectral model (the maximum difference is 1.5%) for the same aperture sequence. Figure 4.2 shows that $\check{J}_2$ are not exactly the same for the full FVM model and the spectral model. As discussed in [22], attainment of identical $\mathcal{U}$ (for the spectral model and the full FVM model) implies that the controller is insensitive to (at least) disturbances of this magnitude, caused by numerical effects or otherwise. As a next step, the spectral model will be compared with the reduced prediction model. From now on, the term "reduced model" means that only the temperature predictions (in the MPC algorithm) are done using the reduced model as discussed in Section 4.1.1; the actual temperature evolution is simulated using the full FVM model.

To make a good comparison between both models, the reduced model is simulated for different values of Pe, τ, and J as also done in the previous chapter. This enables us to compare the transient times, switching sequence and costs. The transient times and the number of switches for different parameter settings can be found in Table C.1 and Table C.2. When comparing this with the results for the spectral method in Appendix B.2, it follows that the results (i.e., aperture sequence) differ significantly for one circulation direction. In most

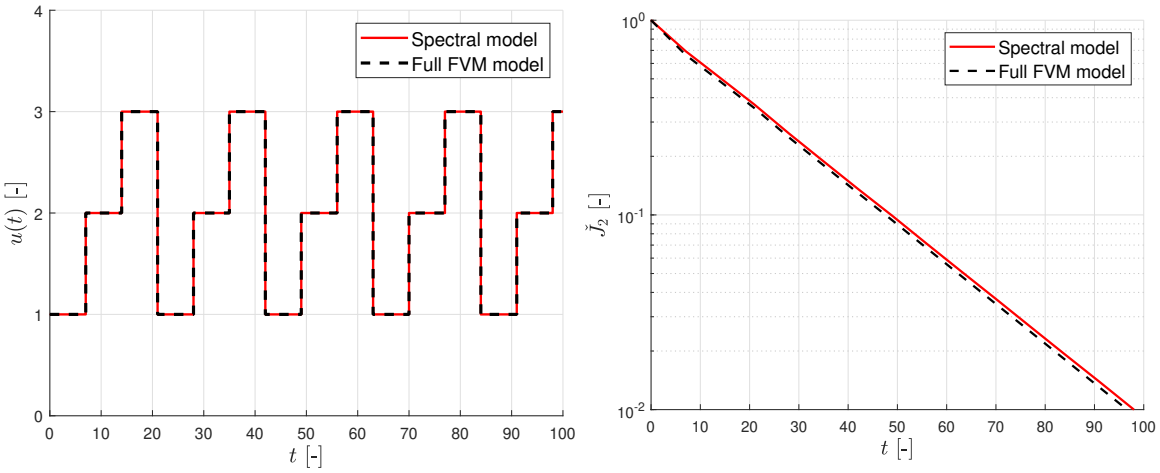

(a) Adaptive reorientation scheme $\mathcal{U}$. **(b)** Performance metric $\check{J}_2$.

Figure 4.2: Comparison of spectral model with full FVM model for $Pe = 750$, $\tau = 7$, $J = J_2$, $H = 1$, and only clockwise rotation.

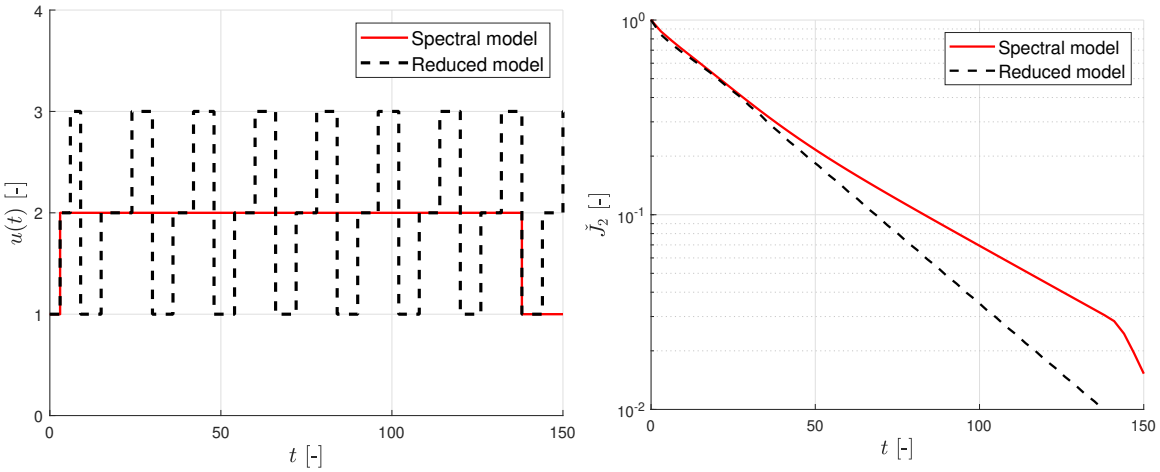

(a) Adaptive reorientation scheme $\mathcal{U}$. **(b)** Performance metric $\check{J}_2$.

Figure 4.3: Comparison of spectral model with reduced model for $Pe = 1250$, $\tau = 3$, $J = J_1$, $H = 1$, and only clockwise rotation.

cases, the performance is worse for the reduced model; only in a few special cases the performance of the reduced model is better, as shown in Figures 4.3 and 4.4. These figures show the aperture sequence and performance metric $\check{J}_2$ (note that J_1 is used as cost function in the MPC algorithm) for various simulation and MPC settings. From this, the conclusion can be drawn that the reduced model with $S = 200$ modes does not predict the future temperature as well as the spectral model. However, still it might be beneficial to use the reduced model in combination with a larger horizon. This will be discussed in more detail in Section 4.2.

For two circulation directions, the performance of the reduced model and the spectral model is almost the same. For both the reduced model and the spectral model, the aperture sequence almost always consists of switching between two arcs in opposite direction. When analyzing the costs at each iteration step, it follows that this switching signal is significantly better than switching to another aperture. This is different than the situation with one circulation direction; the costs for different apertures are closer to the same value for one

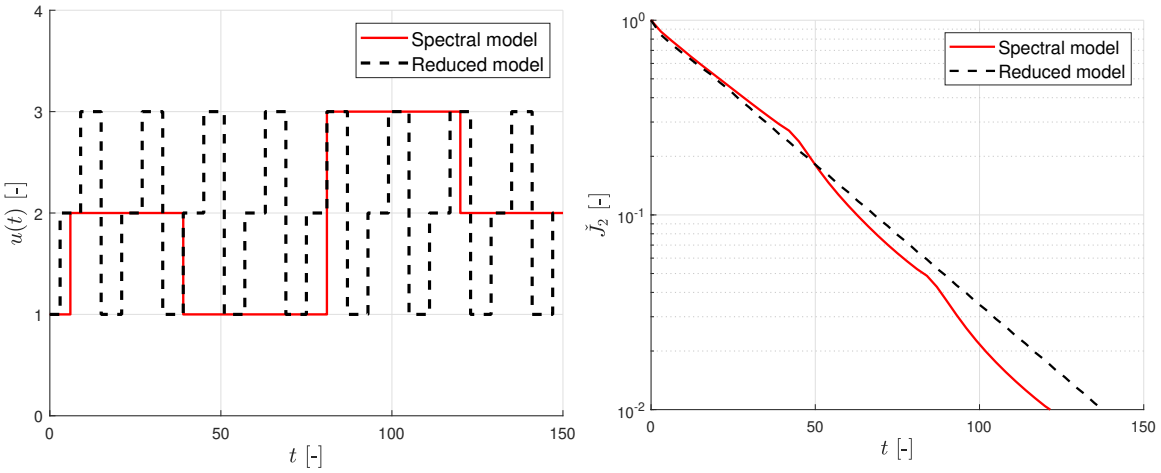

(a) Adaptive reorientation scheme $\mathcal{U}$.

(b) Performance metric $\check{J}_2$.

Figure 4.4: Comparison of spectral model with reduced model for $Pe = 1250$, $\tau = 3$, $J = J_1$, $H = 3$, and only clockwise rotation.

circulation direction. When a less accurate model (e.g., the reduced model) is used in this case, it is more likely another aperture is selected. This behavior is also observed for the compact model with fewer elements ($N_r = 50, N_\theta = 120$) and fewer modes ($Q = 500$).

Most of the differences found for two circulation directions are distinct apertures between which is switched; for example, using the spectral model results in switching between arc 1 and -2, whereas using the reduced model results in switching between arc 1 and -3. As already stated in Section 3.2.3, this hardly affects the performance. This allows for further investigation of the reduced model to use larger horizons.

4.2 Reducing the number of switches

In Chapter 3 and Section 4.1.2 it was concluded that a high number of switches often has a negative influence on the performance. In Section 3.3.1, it turned out that a larger horizon does not necessarily increases the performance, which was due to the high number of switches present in the controller with a larger horizon ($H = 3$). In this section, four ideas are presented which limit the number of switches in order to increase the performance.

The first idea is to increase the horizon further. In Chapter 3 the largest horizon that has been used is $H = 3$. When a larger horizon is used, the system is given more time to form a large thermal plume and subsequently extend it into the colder interior by activating another arc. When a horizon of $H = 3$ is used, on the other hand, multiple smaller plumes are formed by multiple switches as shown in Figure 3.7. To use a larger horizon, a reduced prediction model has to be used as described in Section 4.1.2. One simulation with a significant larger horizon ($H = 8$) has been performed to test this hypothesis. The results are shown in Figure 4.5 and Figure 4.6. In this scenario, the larger horizon controller ($H = 8$) results in less switches and in a better performance. From the temperature evolution illustrated in Figure 4.5, it can be seen that forming one large hot plume (the controller with $H = 8$) is more beneficial than forming two smaller plumes (the controller with $H = 3$). Even though this is one specific situation with certain parameters, it shows the potential of using a significant larger horizon. Note that the transient times $t_{\epsilon,2}$ can be derived from Figure 4.6b and are $t_{\epsilon,2} = 94.2$ and $t_{\epsilon,2} = 85.0$ for the controllers with $H = 3$ and $H = 8$, respectively.

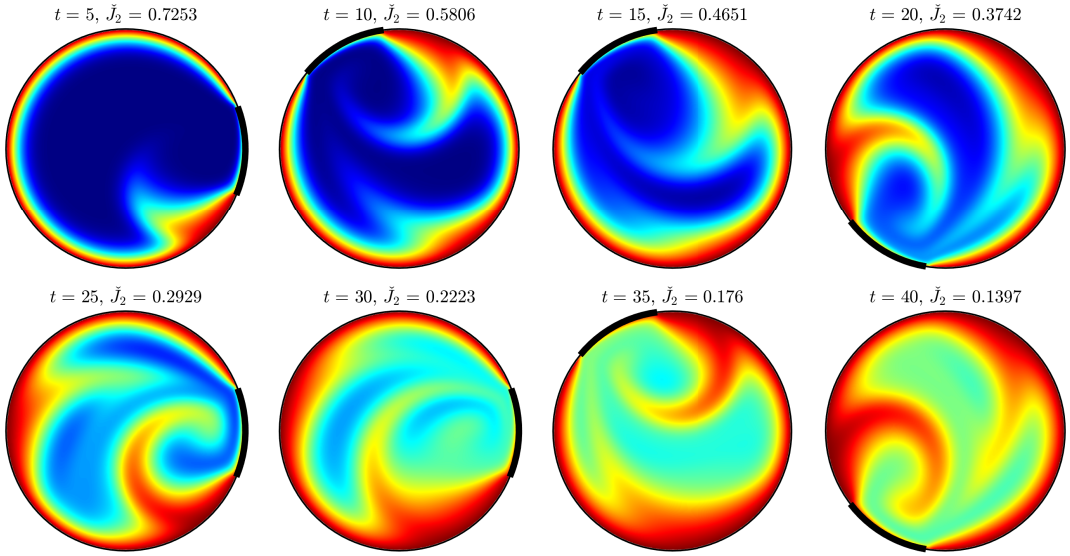

(a) Using an MPC controller with $H = 3$.

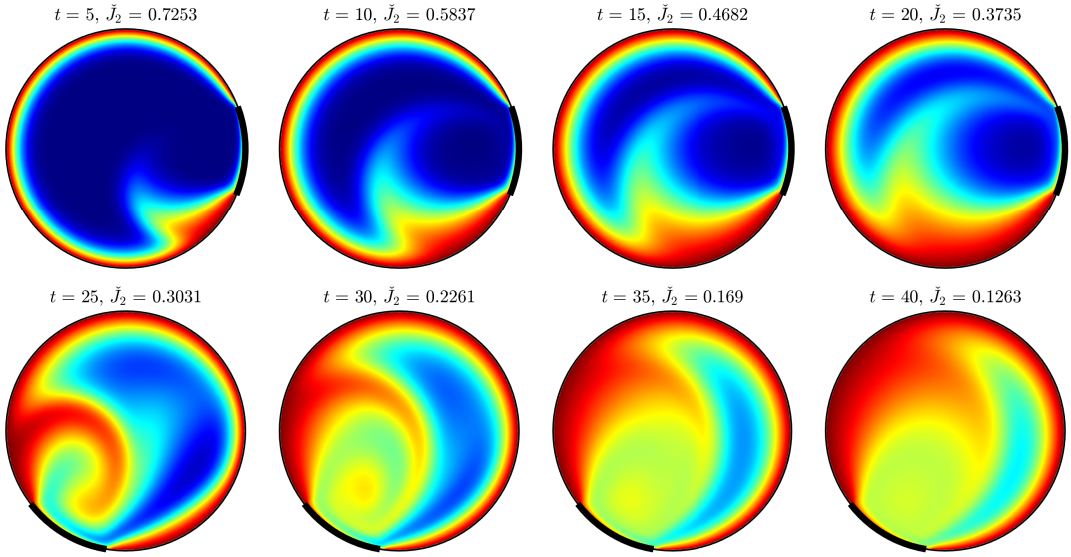

(b) Using an MPC controller with $H = 8$.

Figure 4.5: Temperature evolution for MPC controllers using the reduced model with different horizons for $Pe = 750$, $\tau = 5$, $J = J_2$, and only clockwise rotation.

The full evolution of $\check{J}_2$ is shown to judge the performance of the different controllers over time. To be able to draw conclusions from using larger horizons (i.e., $H > 3$), it is necessary to do more simulations.

Another suggestion to reduce the number of switches is using more advanced cost functions. As discussed in Section 3.2.3, using J_2 as cost function results in more switches than using J_1 as cost function, since J_2 covers both the energizing (via J_1) and the homogenization (via J_3). At the start of the process, energizing is the most important part, whereas at the end of the process, homogenization is more important. It might, therefore, be beneficial to combine

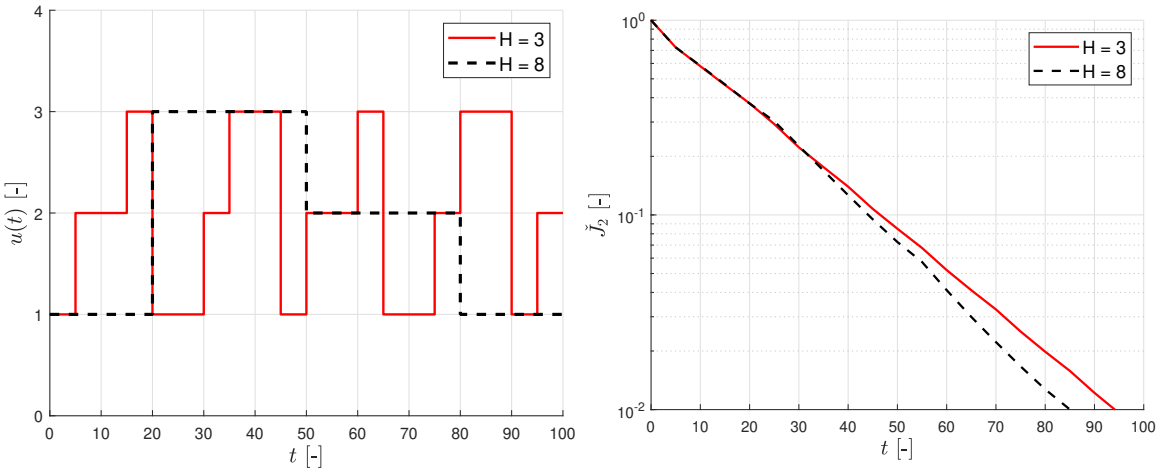

(a) Adaptive reorientation scheme $\mathcal{U}$.

(b) Performance metric $\check{J}_2$.

Figure 4.6: Comparison of reduced model with different horizons for $Pe = 750$, $\tau = 5$, $J = J_2$, and only clockwise rotation.

J_1 and J_2 is a new cost function J_a, which could, for example, be defined as

$$J_a = \begin{cases} J_1 & \text{if } J_1 > \epsilon_J, \\ J_2 & \text{otherwise,} \end{cases} \tag{4.2}$$

where ϵ_J is a certain threshold value defining when to switch from cost function. The condition $J_1 > \epsilon_J$ can easily be evaluated at every control iteration, making (4.2) easy to implement in the MPC algorithm. It is essential to define the threshold value ϵ_J properly, since it plays an important role in the performance of the advanced cost function. Therefore, more research is needed to find the optimal balance between J_1 (energizing) and J_2 (homogenization and energizing). Note that other conditions (e.g., with another performance metric) are also possible. One simulation has been performed with $\epsilon_J = 0.5$, i.e., when the average transient temperature is half of its final value, the cost function will switch from J_1 to J_2. This is only an educated guess, more research should be done to select a value of ϵ_J with a good motivation. The aperture sequence and performance indicator $\check{J}_2$ are shown in Figure 4.7 for $Pe = 1000$, $\tau = 5$, $H = 3$, and only clockwise rotation. The advanced cost function J_a performs better than cost function J_2 when the performance is evaluated with metric $\check{J}_2$. However, J_1 outperforms J_a for this case. At $t = 40$, the advanced cost function switches from J_1 to J_2. As a result, the MPC controller with J_a as cost function starts switching, since homogenization is important as well for $t \geq 40$. In Figure 4.7b, it can be seen that this results in a better performance (based on metric $\check{J}_2$) for $55 \leq t \leq 70$. When $t \geq 70$, however, the MPC controller with cost function J_1 performs better than the MPC controller with cost function J_a. When comparing the aperture sequence and metric $\check{J}_2$ for the cost functions J_1 and J_a, it can be concluded that aperture switching has a positive effect on performance in the short term, but a negative effect on performance in the long term. From this the conclusion can be drawn that ϵ_J is too small for this specific case. As mentioned before, more research should be done regarding this subject.

Another possibility is to use the rollout strategy as discussed in Section 2.2.3. The disadvantage of using a rollout strategy is that a base policy should be determined in advance. Although the rollout strategy will never perform worse than the base policy, it is required to find a well performing base policy. From the simulations done in Chapter 3, it followed that many aperture sequences are aperiodic in case the RAM is only able to move the fluid in one

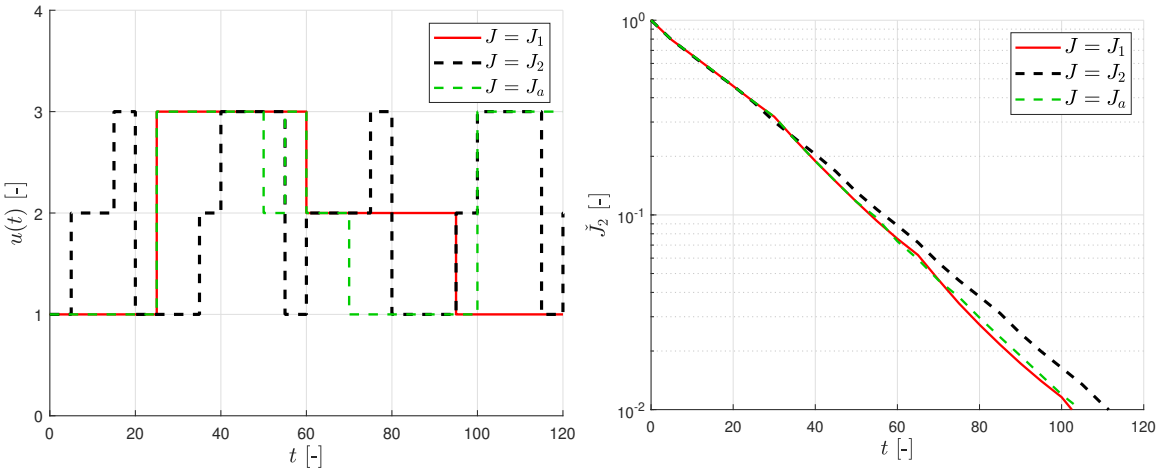

(a) Adaptive reorientation scheme $\mathcal{U}$.

(b) Performance metric $\check{J}_2$.

Figure 4.7: Comparison of different cost functions using the spectral model for $Pe = 1000$, $\tau = 5$, $H = 3$, and only clockwise rotation.

direction. On the other hand, for two rotation directions the aperture reorientation scheme is often periodic (sometimes after a short transient) and consists of switching between two arcs in opposite direction. This would be a good option to use as base policy in a rollout controller. Simulations should be performed to test the rollout algorithm.

The last option is based on the rollout strategy, but without a base policy. In this option, a distinction is made between the prediction and the control horizon as shown in Figure 4.8. Before, the control horizon and prediction horizon were the same (i.e., $H = c = p$). In this case, temperature predictions for all possible sequences are performed in the control horizon c as before. After that, the last input of the sequence stays constant in the prediction horizon p as shown in Figure 4.8, while the temperature predictions continue for the constant input. In other words, the control horizon is the part of the time horizon in which changes in the input are allowed. The prediction horizon extends past the control horizon to predict the output, but without changes of input.

As seen in Chapter 3, it is often beneficial to hold one arc for a longer time instead of extensively switching between different arcs. By making this distinction between prediction horizon and control horizon and using $p > c$, the controller is forced to keep its input constant in the last steps of the time window. The intention is to reduce the number of aperture switches. This method is not effective if the prediction horizon is too small. For example, when using $c = 1$ and $p = 4$, only one aperture is free in the optimization algorithm. This results in three possible sequences, the same arc for a duration of four time steps. However, only one step is implemented. Since in the calculation it is assumed the arc will stay active for a duration of four time steps, this might result in many switches. For a larger horizon (i.e., $H \gtrsim 3$), this problem will not occur.

The above concept has been tested for the specific situation with $Pe = 1000$, $\tau = 5$, $J = J_2$, and only clockwise rotation. The comparison is done for a control horizon $c = 3$ and the prediction horizons $h = 3$ and $h = 7$. The results are shown in Figure 4.9. For this specific case, it proves advantageous to use $p = 7$ instead of $p = 3$. Furthermore, it turns out that the adaptive reorientation scheme for the MPC controller with $c = 3$ and $p = 7$ (see Figure 4.9) is the same as for the MPC controller with $H = 8$ (see Figure 4.6) for $0 \leq t \leq 80$. Moreover, the same observations are done as in Figure 4.5: forming one large hot plume (the

controller with $p = 7$) is more beneficial than forming two smaller plumes (the controller with $p = 3$). Although for this specific case it proves advantageous to use $p = 7$ instead of $p = 3$, more simulations should be performed with varying control and prediction horizon to draw conclusions.

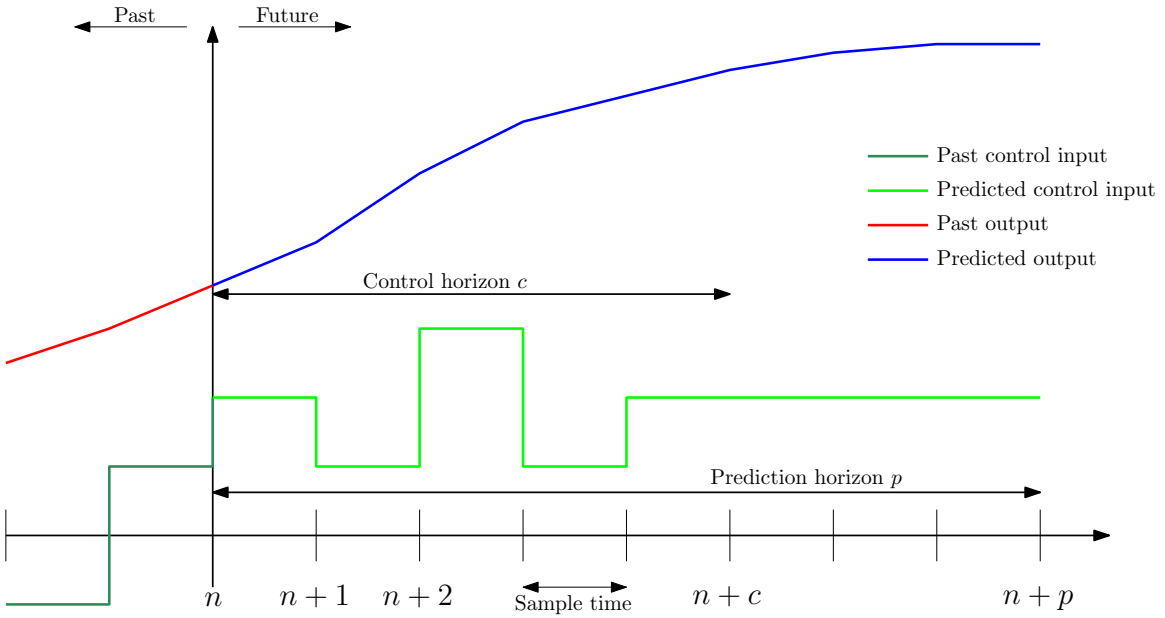

Figure 4.8: Concept of MPC controller with control horizon c and prediction horizon p, based on [48].

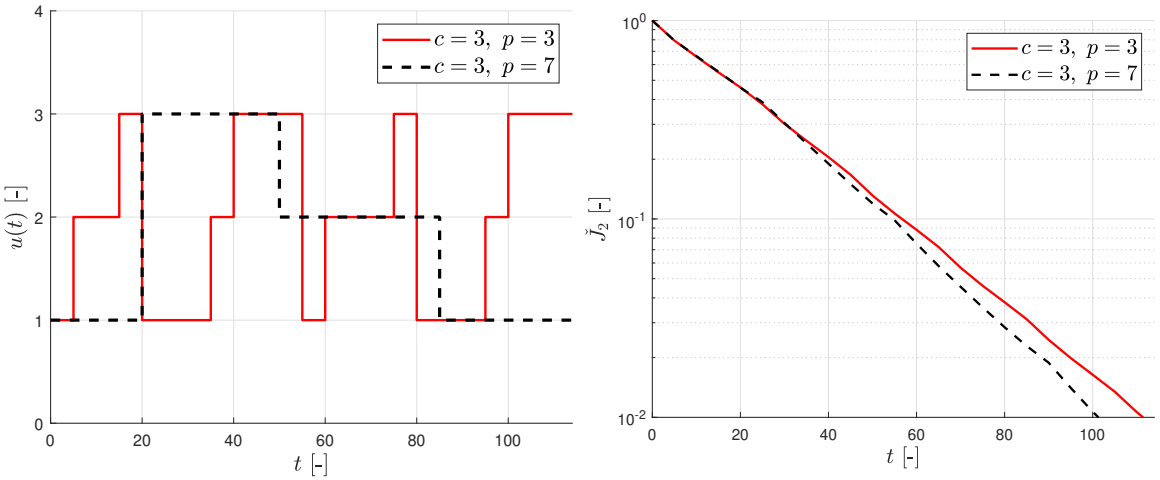

(a) Adaptive reorientation scheme $\mathcal{U}$.

(b) Performance metric $\check{J}_2$.

Figure 4.9: Comparison of spectral model with different prediction horizons for $Pe = 1000$, $\tau = 5$, $J = J_2$, and only clockwise rotation.

4.3 Discussion

In this chapter, a reduced model of the RAM has been discussed and the performance of the reduced model has been compared with the spectral model given in Section 2.1.3. For the reduced model, the 200 slowest-decaying eigenmodes of the state matrix $\mathbf{A}_1$ are used. It turned out that the temperature predictions are less accurate than the spectral model, in particular when only one circulation direction is possible in the RAM. Although the temperature predictions are less accurate, it was shown in Section 4.2 that using a significant larger horizon (i.e., $H = 8$) might be effective, since it prevents the system from having many aperture switches.

Moreover, in Section 4.2 several other methods were discussed to improve the performance. Besides using a larger horizon, more-advanced cost functions, a rollout strategy and using a larger prediction horizon ($p > c$) are potential methods to increase the performance further. In particular the last method looks promising, because the performance will not be worse than the usual MPC controller with $p = c$. Furthermore, almost no additional computation power is needed, in contrast to using a larger horizon.

Chapter 5

Conclusion and recommendations

In this chapter, the conclusions that can be drawn from this project are discussed. A reflection on the main goal and the subgoals stated in Section 1.3 is given. Additionally, recommendations regarding the project and future work are given.

5.1 Conclusion

The goal of the project was to develop a full-state feedback control strategy to accomplish a homogeneous temperature field as fast as possible for the 2D RAM. It followed that using two circulation directions significantly improves the temperature homogenization in the RAM compared to using only one rotation direction. Despite this difference in performance, it turned out that the optimal cost function, aperture activation time, and horizon depend on the rotations (one circulation direction versus two circulation directions).

Firstly, it was shown in Section 3.2.2 that it is more beneficial to sum the costs in the cost function than to take the terminal cost. However, this conclusion is based on simulations with an MPC controller with a horizon of three discrete time steps. For a larger horizon, it could be the case that the difference between summing and terminal costs is negligible, or even that a terminal cost would be better.

One subgoal was to design a performance indicator that reflects attaining a homogeneous temperature field as fast as possible for the 2D RAM. The L2-norm of the temperature is most suited as performance indicator from a theoretical point of view, since it incorporates both energizing and homogenization . However, this does not mean that the L2-norm is also the best option for the cost function. When only one circulation direction is possible in the RAM, the L1-norm of the temperature would be the best option for the cost function, whereas the L2-norm of the temperature would be the best cost function when two directions of rotation are possible. It appears that the controller using the L2-norm as cost function is more aggressive, which is due to the fact that the L2-norm coves both energizing and homogenization.

Finding the optimal aperture activation time is more difficult, since it depends on several parameters such as the Péclet number and the horizon. It is recommended to analyze the influence of the aperture activation for the Péclet number used in the application. Using

the results from this report, it is recommended to use an aperture activation time between 5 and 6.5.

Furthermore, in Chapter 3 the benefits of using a larger horizon than one discrete time step are discussed. In almost all cases, it is beneficial to use a larger horizon. In this research, however, the maximum horizon used is three steps because of computational costs. More research should be done regarding the performance for horizons larger than three steps. In Chapter 4, a start has been made with a reduced model. Although the reduced FVM model is less accurate than the spectral model, it was shown in Section 4.2 that using a significant larger horizon (e.g., a horizon of 8 steps) has potential.

Additionally, in Chapter 4 some other methods are described to increase the performance by limiting the number of switches. Besides using a larger horizon and more-advanced cost functions, potential methods to increase the performance are using a rollout strategy and using a larger prediction horizon (e.g., a prediction horizon that is larger than the control horizon). The last method seems most promising, since not much additional computation power is required and the performance will not be worse than the MPC controller with the same prediction and control horizon.

Finally, it can be concluded that in this research a start has been made with the development of a full-state feedback control strategy to accomplish a homogeneous temperature field as fast as possible for the 2D RAM. However, more research is needed to further elaborate some findings (e.g., the influence of a larger horizon and varying the control and prediction horizon) and draw conclusions from them. Lastly, the control strategy could be developed further by testing it experimentally.

5.2 Recommendations

The designed control strategy is able to accomplish a homogeneous temperature field fast, but there are some recommendations to continue on this work.

In Chapter 4, some methods are discussed to improve the performance of the control strategy. Firstly, it is recommended to look at controllers with a larger horizon. To use a control strategy with a larger horizon in practical applications, the computation costs should be reduced which can be done using a reduced model. In this research, it followed that using the 200 slowest-decaying eigenmodes in the reduced model is not enough to obtain the same results as the spectral model. This leads to two questions. First, how accurate should the reduced model be to do reliable temperature predictions? Second, how much does the performance increase when using larger horizons?

When using a larger horizon, it is recommended to reconsider some of the decisions taken in this project, the structure of the cost function in the MPC controller settings in particular. In Section 3.2.2 it was concluded that it is more beneficial to sum the costs in the cost function than to take the terminal cost. However, for a larger horizon it could be the case that the difference between summing and terminal costs is negligible, or even that a terminal cost would be better. It is suggested to do more research into this area. Furthermore, the use of more advanced cost function is also a possibility as discussed in Section 4.2.

In addition, it is suggested to gain more physical insight into the cost functions. For a certain set of parameters, a certain cost function works well, while for another set of parameters the cost function does not work well. It is advised to look for an explanation for this, because physical understanding is instrumental for defining a proper cost function.

Moreover, in this research only one aperture of the RAM is activated at a time. However, it is possible to activate two (or more) arcs at the same time, resulting in more possible flow fields. In general, more options will increase the performance of the control algorithm.

Besides possible improvements in the control strategy, there are several other recommendations. Most important is to test the control strategy experimentally. In this research, only simulations have been used to evaluate the performance of the control strategy. These simulations are approximate imitations of the real 2D RAM and they never exactly imitate the RAM. Therefore, the control strategy should be experimentally investigated and validated using a laboratory set-up. Experiments can provide us with new empirical data, resulting in new insights and conclusions.

In this project, it was assumed that the complete temperature vector is known at any time exactly. In applications, this is not possible and information can only be collected by sensors, forcing us to create a framework for partial-state information. This can, for example, be solved by development of observers, which estimate the full state from discrete sensor data. In [49], an initial observer model is presented which estimates the temperature field in the fluid domain based on a discrete-point temperature measurement.

Another suggestion is to do the simulations with more variations in the parameters. In this research, only the RAM with three apertures is considered. Moreover, a finer (and possibly a larger) range in Péclet numbers and aperture activation times gives a better view in the performance of the control strategy. Furthermore, it might be interesting to find out why the performance changes so much for different values of the Péclet number and the aperture activation time and link this to system parameters.

Finally, it is recommended to test the control strategy on other applications than the 2D RAM. Although the 2D RAM is well suited for the development of the control strategy because it is experimentally realizable, it is important to test the control strategy also on other applications. To apply the control strategy on other applications, compact models of these applications are needed. One way to construct these compact models would be data-based, for example by so-called “Dynamic Mode Decomposition” (DMD), which enables determination of the dominant eigenmodes directly from temperature time series [14]. To assess whether DMD is an appropriate method for the construction of the compact models, more research is required.

References

[1] H. Aref, J.R. Blake, M. Budišić, S.S.S. Cardoso, J.H.E. Cartwright, H.J.H Clercx, K. El Omari, U. Feudel, R. Golestanian, E. Gouillart, G.F. van Heijst, T.S. Krasnopolskaya, Y. Le Guer, R.S. Mackay, V.V. Meleshko, G. Metcalfe, I. Mezić, A.P.S. Moura, O. Piro, M.F.M. Speetjens, R. Sturman, J.-L. Thiffeault, and I. Tuval, "Frontiers of chaotic advection," *Reviews of Modern Physics*, vol. 89, 025007, 2017.

[2] C. Isci, A. Buyuktosunoglu, C.Y. Cher, P. Bose, and M. Martonosi, "An analysis of efficient multi-core global power management policies: Maximizing performance for a given power budget," in *2006 39th Annual IEEE/ACM International Symposium on Microarchitecture (MICRO'06)*, 2006, pp. 347–358.

[3] A.L. Moore and L. Shi, "Emerging challenges and materials for thermal management of electronics," *Materials Today*, vol. 17, no. 4, pp. 163–174, 2014.

[4] C.Y. Lee, W.T. Wang, C.C. Liu, and L.M. Fu, "Passive mixers in microfluidic systems: A review," *Chemical Engineering Journal*, vol. 288, pp. 146–160, 2016.

[5] G. Metcalfe and D.R. Lester, "Mixing and heat transfer of highly viscous food products with a continuous chaotic duct flow," *Journal of Food Engineering*, vol. 95, no. 1, pp. 21–29, 2009.

[6] M.F.M. Speetjens, S. Varghese, and R.R. Trieling, "Lagrangian approach to analysis and engineering of two generic transport problems in enhanced subsurface flows," *Journal of Contaminant Hydrology*, vol. 224, 103482, 2019.

[7] A.N. Piscopo, R.M. Neupauer, and D.C. Mays, "Engineered injection and extraction to enhance reaction for improved in situ remediation," *Water Resources Research*, vol. 49, no. 6, pp. 3618–3625, 2013.

[8] M.G. Trefry, D.R. Lester, G. Metcalfe, A. Ord, and K. Regenauer-Lieb, "Toward enhanced subsurface intervention methods using chaotic advection," *Journal of Contaminant Hydrology*, vol. 127, no. 1, pp. 15–29, 2012.

[9] A. Costine, P. Fawell, A. Chryss, S. Dahl, and J. Bellwood, "Development of test procedures based on chaotic advection for assessing polymer performance in high-solids tailings applications," *Processes*, vol. 8, no. 6, 731, 2020.

[10] J. Subedi, S. Rajendran, and R.M. Manglik, "Laminar forced convection in viscous shear-thinning liquid flows inside circular pipes: Case for a modified power-law rheology," *Journal of Heat Transfer*, vol. 142, no. 12, 121802, 2020.

[11] J. Gollub, H. Fernando, M. Gharib, J. Kim, S. Pope, A. Smits, and H. Stone, *Research in fluid dynamics: Meeting national needs*, A Report of the U.S. National Committee on Theoretical and Applied Mechanics, 2006.

[12] J.M. Ottino, *The Kinematics of Mixing: Stretching, Chaos, and Transport*. Cambridge University Press, 1989.

[13] Y. Le Guer and K. El Omari, "Chaotic advection for thermal mixing," *Advances in Applied Mechanics*, vol. 45, pp. 189–237, 2012.

[14] R. Lensvelt, M.F.M. Speetjens, and H. Nijmeijer, "Heat-transfer enhancement by adaptive reorientation of flow fields," in *5th Thermal and Fluids Engineering Conference (TFEC)*, 2020, pp. 411–420.

[15] M.F. Eggl and P.J. Schmid, "Mixing enhancement in binary fluids using optimised stirring strategies," *Journal of Fluid Mechanics*, vol. 899, 2020.

[16] J.G. Franjione and J.M. Ottino, "Symmetry concepts for the geometric analysis of mixing flows," *Philosophical Transactions: Physical Sciences and Engineering*, vol. 338, no. 1650, pp. 301–323, 1992.

[17] M. Liu, F.J. Muzzio, and R.L. Peskin, "Quantification of mixing in aperiodic chaotic flows," *Chaos, Solitons & Fractals*, vol. 4, no. 6, pp. 869–893, 1994.

[18] V.S. Dolk, M. Lauret, D.J. Antunes, P.D. Anderson, and W.P.M.H. Heemels, "A switched system approach to optimize mixing of fluids," in *6th IFAC Conference on Analysis and Design of Hybrid Systems (ADHS)*, vol. 51, 2018, pp. 31–36.

[19] L. Cortelezzi, A. Adrover, and M. Giona, "Feasibility, efficiency and transportability of short-horizon optimal mixing protocols," *Journal of Fluid Mechanics*, vol. 597, pp. 199–231, 2008.

[20] D.P.G. Foures, C.P. Caulfield, and P.J. Schmid, "Optimal mixing in two-dimensional plane poiseuille flow at finite peclet number," *Journal of Fluid Mechanics*, vol. 748, pp. 241–277, 2014.

[21] K. El Omari and Y. Le Guer, "Alternate rotating walls for thermal chaotic mixing," *International Journal of Heat and Mass Transfer*, vol. 53, pp. 123–134, 1-3 2010.

[22] R. Lensvelt, M.F.M. Speetjens, and H. Nijmeijer, "Fast fluid heating by adaptive flow reorientation," *International Journal of Thermal Sciences*, vol. 180, 107720, 2022.

[23] O. Baskan, M.F.M. Speetjens, G. Metcalfe, and H.J.H. Clercx, "Experimental and computational study of scalar modes in a periodic laminar flow," *International Journal of Thermal Sciences*, vol. 96, pp. 102–118, 2015.

[24] D. Antunes and W.P.M.H. Heemels, "Linear quadratic regulation of switched systems using informed policies," *IEEE Transactions on Automatic Control*, vol. 62, no. 6, pp. 2675–2688, 2017.

[25] D.P. Bertsekas, *Dynamic Programming & Optimal Control*, 3rd. Athena Scientific, 2005.

[26] D.R. Lester, M. Rudman, G. Metcalfe, and H.M. Blackburn, "Global parametric solutions of scalar transport," *Journal of Computational Physics*, vol. 227, pp. 3032–3057, 6 2008.

[27] A.C. Antoulas, *Approximation of Large-Scale Dynamical Systems*. Society for Industrial and Applied Mathematics, 2005.

[28] H. Gao, J. Lam, and C. Wang, "Model simplification for switched hybrid systems.," *Systems and Control Letters*, vol. 55, no. 12, pp. 1015–1021, 2006.

[29] L. Zhang, P. Shi, E.-K. Boukas, and C. Wang, "H-infinity model reduction for uncertain switched linear discrete-time systems," *Automatica*, vol. 44, no. 11, pp. 2944–2949, 2008.

[30] A. Birouche, J. Guillet, B. Mourllion, and M. Basset, "Gramian based approach to model order-reduction for discrete-time switched linear systems," in *18th Mediterranean Conference on Control and Automation*, 2010, pp. 1224–1229.

[31] A. Birouche, B. Mourllion, and M. Basset, "Model order-reduction for discrete-time switched linear systems," *International Journal of Systems Science*, vol. 43, no. 9, pp. 1753–1763, 2012.

[32] I.V. Gosea, M. Petreczky, A.C. Antoulas, and C. Fiter, "Balanced truncation for linear switched systems," *Advances in Computational Mathematics*, vol. 44, pp. 1845–1886, 2018.

[33] N. Monshizadeh, H.L. Trentelman, and M.K. Camlibel, "A simultaneous balanced truncation approach to model reduction of switched linear systems," *IEEE Transactions on Automatic Control*, vol. 57, no. 12, pp. 3118–3131, 2012.

[34] I. Pontes Duff, S. Grundel, and P. Benner, "New gramians for switched linear systems: Reachability, observability, and model reduction," *IEEE Transactions on Automatic Control*, vol. 65, no. 6, pp. 2526–2535, 2020.

[35] M. Bastug, "Model Reduction of Linear Switched Systems and LPV State-Space Models," Ph.D. thesis, Aalborg University, 2016.

[36] M. Bastug, M. Petreczky, R. Wisniewski, and J. Leth, "Model reduction by moment matching for linear switched systems," in *2014 American Control Conference*, 2014, pp. 3942–3947.

[37] O. Baskan, M.F.M. Speetjens, G. Metcalfe, and H.J.H. Clercx, "Experimental and numerical parametric analysis of a reoriented duct flow," *European Journal of Mechanics - B/Fluids*, vol. 57, pp. 1–14, 2016.

[38] T.-Y. Hwu, D.-L. Young, and Y.-Y. Chen, "Chaotic advections for stokes flows in circular cavity," *Journal of Engineering Mechanics*, vol. 123, no. 8, pp. 774–782, 1997.

[39] H.K. Khalil, *Nonlinear systems*, third. Prentice-Hall, 2002.

[40] J.W. Thomas, *Numerical Partial Differential Equations: Finite Difference Methods*. Springer, 1995.

[41] D Liberzon, *Switching in Systems and Control*. Birkhäuser, 2003.

[42] J. Gao and D. Li, "Linear–quadratic switching control with switching cost," *Automatica*, vol. 48, no. 6, pp. 1138–1143, 2012.

[43] J.-P. Corriou, *Process Control: Theory and Applications*, second. Springer, 2018.

[44] D.P. Bertsekas, *Reinforcement Learning and Optimal Control*. Athena Scientific, 2019.

[45] T. Das and R. Mukherjee, "Optimally switched linear systems," *Automatica*, vol. 44, no. 5, pp. 1437–1441, 2008.

[46] G. Wu, J. Sun, and J. Chen, "Optimal linear quadratic regulator of switched systems," *IEEE Transactions on Automatic Control*, vol. 64, no. 7, pp. 2898–2904, 2019.

[47] W.H. Press, S.A. Teukolsky, W.T. Vetterling, and B.P. Flannery, *Numerical Recipes in C: The Art of Scientific Computing*, second. Cambridge University Press, 1992.

[48] X. Yang, G. Liu, A. Li, and L. Van Dai, "A Predictive Power Control Strategy for DFIGs Based on a Wind Energy Converter System," *Energies*, vol. 10, 1098, 2017.

[49] R.P.C. van Eert, "Observer-based heat transfer prediction to enable heat transfer enhancement by adaptive flow field reorientation: An experimental analysis," Master thesis, Eindhoven University of Technology, 2022.

Appendix A

Discretization of performance indicators

The performance indicators J_2 (2.31), J_4 (2.37) and J_5 (2.38) can be discretized as

$$\hat{J}_2(t) = \sum_{m=1}^{M} \gamma_m \hat{T}^2(\mathbf{x}_m, t), \tag{A.1}$$

$$\hat{J}_4(t) = \frac{\sum_{m=1}^{M} \gamma_m \hat{T}(\mathbf{x}_m, t) + T_\infty}{\sqrt{\sum_{m=1}^{M} \gamma_m \left(\hat{T}(\mathbf{x}_m, t) - \sum_{m=1}^{M} \gamma_m \hat{T}(\mathbf{x}_m, t)\right)^2}}, \tag{A.2}$$

$$\hat{J}_5(t) = \min_{m \in [1,2,\ldots,M]} \gamma_m \hat{T}(\mathbf{x}_m, t). \tag{A.3}$$

Appendix B

Simulation results spectral model

This appendix shows the simulation results obtained with the spectral model. In Section B.1, the results are given for different cost functions. In Section B.2, the elaborate results are given for different parameter settings.

B.1 Different cost functions

In Table B.1, the transient times are given for different Péclet numbers, aperture activation times, and cost functions.

Table B.1: Transient times t_ϵ for different values of Pe, τ and J.

(a) $Pe = 500$.

		Type of cost used to define transient time			
τ	Cost used in MPC	$t_{\epsilon,1}$	$t_{\epsilon,2}$	$t_{\epsilon,4}$	$t_{\epsilon,5}$
3	J_1	73.0	77.4	83.3	85.1
	J_2	73.3	79.0	85.1	87.0
	J_4	64.7	68.0	79.8	78.9
	J_5	69.0	73.7	85.9	78.9
5	J_1	62.4	66.7	82.2	82.6
	J_2	67.4	70.6	76.6	77.8
	J_4	68.2	70.9	76.9	79.9
	J_5	69.5	74.8	86.2	80.1
7	J_1	62.2	67.0	74.4	75.4
	J_2	69.0	72.2	78.8	76.5
	J_4	69.0	72.2	78.8	76.5
	J_5	69.0	72.2	78.8	76.5

Table B.1: Transient times t_ϵ for different values of Pe, τ and J, continued.

(b) $Pe = 750$.

		Type of cost used to define transient time			
τ	Cost used in MPC	$t_{\epsilon,1}$	$t_{\epsilon,2}$	$t_{\epsilon,4}$	$t_{\epsilon,5}$
5	J_1	103.5	117.6	148.5	150.1
	J_2	85.6	91.7	113.5	114.7
	J_4	82.1	85.2	93.7	93.9
	J_5	96.0	101.9	118.3	110.3
5	J_1	84.8	92.3	104.5	107.8
	J_2	81.9	85.0	96.5	95.3
	J_4	92.4	95.4	102.6	107.3
	J_5	90.4	94.4	107.1	100.6
7	J_1	83.1	86.5	95.1	95.5
	J_2	94.5	98.0	105.7	102.5
	J_4	94.5	98.0	105.7	102.5
	J_5	94.5	98.0	105.7	102.5

(c) $Pe = 1000$.

		Type of cost used to define transient time			
τ	Cost used in MPC	$t_{\epsilon,1}$	$t_{\epsilon,2}$	$t_{\epsilon,4}$	$t_{\epsilon,5}$
3	J_1	133.8	153.5	195.8	197.4
	J_2	104.7	112.7	119.8	124.4
	J_4	97.8	102.7	113.6	117.8
	J_5	117.9	126.3	145.9	136.0
5	J_1	105.0	110.0	117.3	121.6
	J_2	98.2	104.0	111.6	116.0
	J_4	112.9	116.8	124.1	130.9
	J_5	110.2	117.0	130.2	128.6
7	J_1	99.2	103.5	117.5	121.0
	J_2	109.9	115.0	124.1	128.7
	J_4	116.1	120.4	128.5	123.9
	J_5	116.1	120.4	128.5	123.9

Table B.1: Transient times t_ϵ for different values of Pe, τ and J, continued.

(d) $Pe = 1250$.

		Type of cost used to define transient time			
τ	Cost used in MPC	$t_{\epsilon,1}$	$t_{\epsilon,2}$	$t_{\epsilon,4}$	$t_{\epsilon,5}$
3	J_1	151.5	155.9	173.7	177.6
	J_2	120.3	124.5	134.9	143.7
	J_4	127.0	131.4	138.7	140.6
	J_5	139.3	147.3	169.6	158.4
5	J_1	119.4	123.5	137.3	144.3
	J_2	114.2	118.1	124.9	132.1
	J_4	132.6	136.5	143.1	149.8
	J_5	128.6	134.8	143.4	147.2
7	J_1	115.0	121.2	135.5	141.4
	J_2	127.2	131.8	139.7	142.3
	J_4	136.2	140.8	149.1	145.4
	J_5	136.2	140.8	149.1	145.4

B.2 Elaborate results for different parameter settings

In Table B.2, the transient times and number of switches are given for different Péclet numbers, aperture activation times, and cost functions for one circulation direction. In Table B.3, the transient times and number of switches are given for different Péclet numbers, aperture activation times, and cost functions for two circulation directions.

Table B.2: Comparison of a MPC controller with $H = 1$ with a MPC controller with $H = 3$ using χ as performance indicator. Only clockwise circulations are considered here.

(a) MPC controller with $H = 1$.

Pe	J	τ	$t_{\epsilon,2}$	Number of switches
500	1	3	77.4	3
		5	66.7	1
		7	67.0	2
	2	3	79.0	3
		5	70.6	10
		7	72.2	11
750	1	3	117.6	1
		5	92.3	3
		7	86.5	3
	2	3	91.7	2
		5	85.0	3
		7	98.0	15
1000	1	3	153.5	1
		5	110.0	3
		7	103.5	3
	2	3	112.7	3
		5	104.0	4
		7	115.0	11
1250	1	3	155.9	2
		5	123.5	3
		7	121.2	4
	2	3	124.5	3
		5	118.1	4
		7	131.8	13

(b) MPC controller with $H = 3$.

Pe	J	τ	$t_{\epsilon,2}$	Number of switches
500	1	3	66.5	2
		5	64.9	2
		7	65.2	2
	2	3	71.0	12
		5	70.6	12
		7	72.2	11
750	1	3	85.1	3
		5	84.5	3
		7	85.6	3
	2	3	87.1	5
		5	93.3	11
		7	95.3	10
1000	1	3	102.9	3
		5	102.7	3
		7	102.3	3
	2	3	105.7	7
		5	111.6	12
		7	113.3	12
1250	1	3	121.5	4
		5	116.6	3
		7	117.0	3
	2	3	121.6	7
		5	129.8	13
		7	131.1	13

Table B.3: Comparison of a MPC controller with $H = 1$ with a MPC controller with $H = 3$ using χ as performance indicator. Both directions of rotation are considered here.

(a) MPC controller with $H = 1$.

Pe	J	τ	$t_{\epsilon,2}$	Number of switches
500	1	3	64.5	22
		5	62.5	13
		7	62.0	9
	2	3	64.9	22
		5	62.5	13
		7	62.0	9
750	1	3	87.1	30
		5	82.4	17
		7	80.8	12
	2	3	87.1	30
		5	82.4	17
		7	80.8	12
1000	1	3	106.5	35
		5	96.1	20
		7	94.6	14
	2	3	108.2	37
		5	96.1	20
		7	94.6	14
1250	1	3	128.3	43
		5	112.6	23
		7	110.5	16
	2	3	128.3	43
		5	111.1	19
		7	110.5	16

(b) MPC controller with $H = 3$.

Pe	J	τ	$t_{\epsilon,2}$	Number of switches
500	1	3	62.4	21
		5	62.5	13
		7	62.0	9
	2	3	62.4	21
		5	62.5	13
		7	62.0	9
750	1	3	83.4	24
		5	81.2	14
		7	80.8	12
	2	3	83.0	22
		5	80.8	17
		7	79.7	12
1000	1	3	98.3	26
		5	96.1	20
		7	94.6	14
	2	3	96.9	22
		5	96.1	20
		7	94.6	14
1250	1	3	109.8	25
		5	110.7	17
		7	110.5	16
	2	3	108.5	21
		5	109.8	22
		7	108.4	16

Appendix C

Simulation results reduced model

In Table C.1, the transient times and number of switches are given for different Péclet numbers, aperture activation times, and cost functions for one circulation direction. In Table C.2, the transient times and number of switches are given for different Péclet numbers, aperture activation times, and cost functions for two circulation directions.

Table C.1: Comparison of a MPC controller with $H = 1$ with a MPC controller with $H = 3$ using χ as performance indicator. Only clockwise circulations are considered here.

(a) MPC controller with $H = 1$.

Pe	J	τ	$t_{\epsilon,2}$	Number of switches
500	1	3	80.6	1
		5	67.8	2
		7	68.8	4
	2	3	80.6	2
		5	70.7	10
		7	72.2	11
750	1	3	116.5	1
		5	91.4	3
		7	86.0	3
	2	3	90.9	2
		5	94.2	13
		7	96.8	14
1000	1	3	152.1	2
		5	109.7	3
		7	103.1	3
	2	3	111.5	13
		5	114.2	14
		7	119.0	18
1250	1	3	137.7	24
		5	123.1	3
		7	121.7	4
	2	3	137.6	23
		5	132.9	16
		7	139.7	20

(b) MPC controller with $H = 3$.

Pe	J	τ	$t_{\epsilon,2}$	Number of switches
500	1	3	67.3	3
		5	65.2	2
		7	65.1	2
	2	3	71.2	12
		5	70.7	10
		7	72.2	11
750	1	3	84.6	3
		5	87.5	5
		7	85.0	3
	2	3	87.3	6
		5	94.2	13
		7	96.8	14
1000	1	3	101.8	3
		5	107.6	7
		7	113.0	12
	2	3	107.9	11
		5	115.8	18
		7	119.0	18
1250	1	3	137.5	23
		5	127.8	11
		7	131.1	13
	2	3	125.5	12
		5	135.7	22
		7	139.7	20

Table C.2: Comparison of a MPC controller with $H = 1$ with a MPC controller with $H = 3$ using χ as performance indicator. Both directions of rotation are considered here.

(a) MPC controller with $H = 1$.

Pe	J	τ	$t_{\epsilon,2}$	Number of switches
500	1	3	61.9	21
		5	62.0	13
		7	61.6	9
	2	3	64.0	22
		5	63.2	13
		7	61.6	9
750	1	3	86.1	29
		5	79.9	16
		7	79.0	12
	2	3	86.4	29
		5	79.9	16
		7	79.0	12
1000	1	3	107.0	36
		5	98.1	20
		7	96.0	14
	2	3	106.5	36
		5	98.1	20
		7	94.3	14
1250	1	3	127.1	43
		5	112.7	23
		7	110.4	16
	2	3	126.4	43
		5	112.7	23
		7	108.3	16

(b) MPC controller with $H = 3$.

Pe	J	τ	$t_{\epsilon,2}$	Number of switches
500	1	3	61.9	21
		5	62.0	13
		7	61.6	9
	2	3	61.9	21
		5	62.0	13
		7	61.6	9
750	1	3	83.5	28
		5	79.9	16
		7	79.0	12
	2	3	81.6	22
		5	79.9	16
		7	79.0	12
1000	1	3	97.7	26
		5	96.0	16
		7	94.3	14
	2	3	95.9	20
		5	95.7	20
		7	94.3	14
1250	1	3	111.1	28
		5	110.3	17
		7	108.3	16
	2	3	109.5	22
		5	109.6	22
		7	108.3	16